DISSERTATION

submitted to the
Combined Faculties for the Natural Sciences and for Mathematics
of the Ruperto-Carola University of Heidelberg, Germany

for the degree of
Doctor of Natural Sciences

Presented by
Graduate Engineer in Biotechnology **Caroline Ronzaud**
born in Echirolles, France

Oral-examination: 19th of March 2007

Analysis of the role of the mineralocorticoid receptor in renal principal cell sodium reabsorption *in vivo*

Referees: Prof. Dr. med. Günther Schütz

Prof. Dr. Blanche Schwappach

TABLE OF CONTENTS

1. SUMMARY

Germline inactivation of the mineralocorticoid receptor (MR) gene in mice results in early postnatal lethality due to massive loss of sodium and water associated with impaired epithelial sodium channel (ENaC) activity in kidney and colon. The aim of the present study was the analysis of the role of renal principal cell MR, which is activated by aldosterone, in ENaC-mediated sodium reabsorption. For this purpose, mice deficient for MR in ENaC-expressing renal principal cells were generated using the Cre-loxP recombination system. A large fragment of genomic mouse DNA harbouring 156 kb of the aquaporin 2 (AQP2) gene was used to drive the expression of Cre recombinase in principal cells (AQP2Cre mice). Mice carrying a conditional MR allele were crossed with AQP2Cre mice to obtain mutant ($MR^{AQP2Cre}$) mice. $MR^{AQP2Cre}$ mice developped normally under standard diet and exhibited unaltered renal sodium excretion, but strongly elevated plasma aldosterone levels. When challenged with a low-sodium diet, $MR^{AQP2Cre}$ mice showed increased renal sodium and water excretion resulting in a continuous loss of bodyweight. Immunofluorescence for MR and αENaC staining revealed that the loss of MR expression is restricted to principal cells of the collecting duct (CD) and late connecting tubule (CNT), and that MR is crucial for apical αENaC trafficking to the apical membrane. The early CNT that accounts for about 30% of the CNT was not targeted. Determination of the fractional excretion of sodium before and after treatment with the ENaC blocker amiloride showed that renal ENaC activity in the mutant mice was preserved. These data demonstrate that the late distal convoluted tubule (DCT) and early CNT, which were not targeted in $MR^{AQP2Cre}$ mice, can compensate to a large extent impaired ENaC-mediated sodium reabsorption in the late CNT and CD.

To overcome a possible postnatal lethality of the $MR^{AQP2Cre}$ mice, an inducible principal cell-specific gene inactivation system was established in parallel to induce MR inactivation in adult mice. The large genomic DNA fragment harbouring the AQP2 gene, used for the generation of the constitutive AQP2Cre transgene, was also used to drive the expression of the tamoxifen-inducible $CreER^{T2}$ fusion protein ($AQP2CreER^{T2}$ mice). Three $AQP2CreER^{T2}$ transgenic lines containing 1, 4 and 9 copies of the transgene respectively were established and showed tamoxifen-induced recombination in most of the renal principal cells, but leakiness of the fusion protein in the papilla region of the kidney.

To identify aldosterone-regulated genes potentially involved in the control of ENaC-mediated renal sodium reabsorption, gene expression profiling using microarrays was performed on a mouse renal cortical CD principal cell line ($mpkCCD_{c14}$) in the presence or absence of aldosterone. Quantitative RT-PCR for the identified candidates on microdissected CDs from control mice fed with standard or low-sodium diet confirmed the induction by aldosterone of the genes encoding the serum- and glucocorticoid-regulated kinase 1 (Sgk1) and the ubiquitin-specific protease 2 (Usp2). Quantitative RT-PCR on microdissected CDs from control mice and principal cell MR-deficient ($MR^{AQP2Cre}$) mice under low-sodium diet showed that the gene expression levels of Sgk1 and the serine/threonine protein kinase 3 (Pim3) were reduced in the mutant mice. Thus, these data identified Pim3 as a new MR-regulated gene involved in the control of ENaC-mediated sodium reabsorption.

1. ZUSAMMENFASSUNG

Die Keimbahninaktivierung des Mineralokortikoidrezeptor-(MR)-Gens in Mäusen führt infolge eines massiven Verlusts von Natrium und Wasser zu Lethalität in der zweiten Woche nach der Geburt. Der Natrium/Wasser-Verlust geht einher mit einer gestörten Aktivität des epithelialen Natriumkanals (ENaC) in der Niere und im Kolon. Ziel der vorliegenden Arbeit ist es, die Rolle des MR in Aldosteron-aktivierten Hauptzellen des distalen Nierenepithels bei der Natrium-Rückresorption durch ENaC zu klären. Dazu wurden mit Hilfe des Cre-loxP-Rekombinationssystems Mäuse hergestellt, bei denen der MR in den Hauptzellen der Niere inaktiviert ist. Zur Expression der Cre-Rekombinase in Hauptzellen wurde ein 156 kB-großes Fragment genomischer Maus-DNA, das die regulatorischen Elemente des Aquaporin 2-Gens enthält, verwendet (AQP2Cre Mäuse). Zur Erzeugung von MR-defizienten Mäusen ($MR^{AQP2Cre}$), wurden Mäuse mit einem konditionalen MR-Allel und AQP2Cre-Mäuse gekreuzt. Unter Standarddiät entwickelten sich $MR^{AQP2Cre}$-Mäuse normal, ihre Natrium-Ausscheidung war nicht verändert, aber sie hatten stark erhöhte Aldosteron-Spiegel im Plasma. Bei Gabe vom Natrium-armen Futter zeigten $MR^{AQP2Cre}$-Mäuse eine erhöhte renale Natriumausscheidung einhergehend mit erhöhter Urinproduktion, was zu einem kontinuierlichen Gewichtsverlust führte. Färbungen für MR und αENaC mittels Immunfluoreszenz zeigte einen Verlust des MR und der apikalen ENaC Expression selektiv in den Hauptzellen der Sammelrohre (CD) und den distalen Bereich der Verbindungsstücke (CNT). Der proximale Bereich des CNT, der etwa 30% der gesamten CNT ausmacht, war nicht von der Germinaktivierung betroffen. Eine Bestimmung der fraktionellen Natriumausscheidung vor und nach Behandlung mit dem ENaC-Blocker Amilorid ergab, dass die ENaC-Aktivität in der Niere insgesamt unverändert war. Diese Daten zeigen, dass in $MR^{AQP2Cre}$ Mäusen der Verlust des MR im distalen CNT und CD weitgehend kompensiert werden kann durch den distalen Konvolut (DCT) und den proximalen CNT, welche den MR weiterhin exprimieren.

Um eine mögliche Lethalität der konstitutiven Inaktivierung des MR-Gens in den Hauptzellen des distalen Nierenepithels umgehen zu können, wurden parallel Mäuse mit einer induzierbaren MR-Inaktivierung hergestellt. Das selbe genomische Fragment, das für die Herstellung der AQP2Cre-Mäuse verwendet worden war, wurde zur Expression eines durch Tamoxifen-induzierbaren $CreER^{T2}$-Fusionsproteins und zur Herstellung von $AQP2CreER^{T2}$-Mäusen benutzt. Es wurden drei $AQP2CreER^{T2}$-transgene Linien mit 1, 4 oder 9 Kopien erzeugt. Alle zeigten Tamoxifen-abhängige Rekombination, aber das Fusionsprotein wurde auch ohne Tamoxifen-Gabe in der Nierenpapille aktiviert.

Zur Identifizierung von Aldosteron-regulierten Genen, die an der Kontrolle der Natrium-Rückresorption durch ENaC beteiligt sind, wurde eine Expressionsanalyse durch Hybridisierung von RNA aus einer Maus-Hauptzelllinie ($mpkCCD_{c14}$) an DNA-Mikroarrays durchgeführt. Die $mpkCCD_{c14}$-Zellen waren mit Aldosteron bzw. Vehikel behandelt. Die auf diese Weise gefundenen Kandidatengene wurden mittels quantitativer RT-PCR von RNA, die aus mikrodissezierten CD von Kontroll-Mäusen nach Standard- oder Natrium-armen Futter isoliert worden war, verifiziert. Auf diese Weise wurde die Induzierbarkeit der Serum- und Glukokortikoid-regulierten Kinase 1 (Sgk1) und der Ubiquitin-spezifische Protease 2 (Usp2)

durch Aldosteron *in vivo* nachgewiesen. Quantitative RT-PCR von RNA am mikrodissezierten CD von Kontrollmäusen und von Mäusen mit einer selektiven MR-Mutation in Hauptzellen des distalen Nierenepithels ($MR^{AQP2Cre}$), die unter Natrium-armen Futter gehalten wurden, zeigte eine verringerte Expression von Sgk1 und der Serine/Threonine Protein Kinase 3 (Pim3). Diese Expressionsdaten identifizieren Pim3 als neues MR-reguliertes Gen, das möglicherweise an der Kontrolle der ENaC-abhängigen Natrium-Rückresorption beteiligt ist.

2. INTRODUCTION

2.1. The mineralocorticoid aldosterone

Fluid and electrolyte regulation is essential for homeostasis. If water or electrolyte levels rise or fall beyond normal limits, many functions of the body fail to proceed at their normal rates. The mineralocorticoids are so named for their role in the regulation of minerals, sodium and potassium metabolism. Aldosterone is the principal physiological mineralocorticoid and plays a major role in the control of sodium balance, fluid homeostasis and blood pressure by regulation of transepithelial sodium transport.

Aldosterone is a steroid hormone and is synthesized from cholesterol in the zona glomerulosa of the adrenal cortex by a series of enzymatic reactions catalyzed by dehydrogenases and mixed-function oxidases, many of which belonging to the cytochrome P450 enzyme superfamily (1). Aldosterone biosynthesis is regulated principally by extracellular potassium concentration and plasma angiotensin II levels. Small increase in extracellular potassium concentration acutely induces the production of aldosterone (2). The action of angiotensin II on aldosterone involves a negative-feedback loop, called the renin-angiotensin-aldosterone system (RAAS) that also includes sodium delivery and extracellular fluid volume. The major function of this feedback loop is to modify sodium homeostasis and, secondarily, to regulate arterial pressure (3, 4). Thus, sodium restriction sensed by the macula densa, a specialized group of renal cells that function as chemoreceptors for monitoring tubular sodium concentration, and low blood pressure both activate the synthesis of the renin enzyme by the juxtaglomerular cells of the renal cortex. Renin is secreted into the blood and cleaves its substrate, angiotensinogen, which is synthesized by the liver, to produce the decapeptide angiotensin I. Angiotensin I is rapidly cleaved by the angiotensin-converting enzyme (ACE) in the lung and other tissues to form the octapeptide angiotensin II that leads to vasoconstriction and aldosterone secretion **(Figure 1)**. The effects of angiotensin II on both the adrenal cortex and the renal vasculature promote renal conservation. Conversely, with suppression of renin release and suppression of the level of circulating angiotensin II, aldosterone secretion is reduced, and renal blood flow is increased, thereby promoting reduced sodium reabsorption.

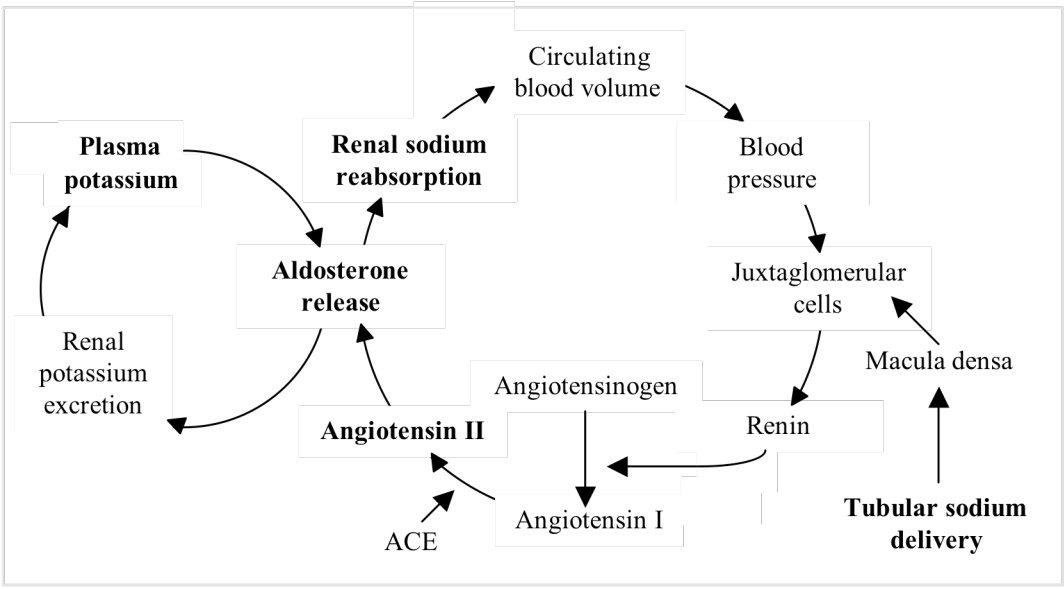

Figure 1. Renin-angiotensin-aldosterone and potassium-aldosterone negative-feedback loops. Aldosterone production is determined by input from each loop. ACE: angiotensin-converting enzyme.

2.2. The mineralocorticoid receptor

2.2.1. A member of the nuclear receptor family

The classical way of action of aldosterone on target cells to regulate electrolyte and fluid balance is through binding to the mineralocorticoid receptor (MR). MR belongs to the nuclear receptor (NR) superfamily, which also includes receptors for thyroid and steroid hormones, vitamin D3, and retinoic acids, as well as numerous orphan receptors for which no ligands are known (5-8). Within the NR superfamily, MR belongs to the steroid receptor subfamily, together with the glucocorticoid receptor (GR), the androgen receptor (AR), the progesterone receptor (PR) and the estrogen receptor (ER).

NRs are ligand-activated transcription factors that modulate target gene transcription and contain five characteristic major domains. The amino-terminal domain (also called A/B region), which is of variable length and sequence in the different NR family members, contains several functional domains responsible for ligand-independent activation. The central highly conserved DNA-binding domain (DBD) (or C region) is reponsible for DNA binding and receptor dimerization. The hydrophilic hinge (D region) between the DBD and the carboxy-terminal domain contains the nuclear localization signal (NLS). The carboxy-terminal domain (E region) mediates numerous functions, including ligand binding, interaction with heat-shock proteins and

transcriptional coactivators, dimerization, nuclear targeting, and hormone-dependent activation. It contains the ligand-binding domain (LBD), which is well conserved between the various NR family members but diverges sufficiently to guarantee selective ligand recognition (5-9). The mouse MR gene (NR3C2), localized to chromosome 4, spans over approximately 450 kb and contains ten exons (10). The two first exons 1, referred to 1α and 1β, are untranslated, whereas the eight other exons (exon 2 - 9) encode the protein with the five domains (from A to E) characteristic for the NRs **(Figure 2)**. MR and GR show 15% of homology for the amino-terminal A/B region, 94% for the DBD and 57% for the LBD.

Ligand-dependent MR activation resulting in regulation of gene transcription is a multistep process characteristic for NRs. Binding of the ligand to MR causes a conformational change within the LBD that leads to the dissociation of the associated heat shock proteins from the receptor, thus unmasking the NLS sequence responsible for nuclear translocation (11, 12). The ligand-activated receptor then binds as a dimer to a palindromic sequence (CGZACAANNTGTYCTK) located in the promoter region of MR target genes, and activates or represses their transcription (13). When MR is activated by aldosterone, the MR target genes are called aldosterone-induced or aldosterone-repressed transcripts (AITs and ARTs, respectively) (11, 14, 15). The palindromic sequence is recognized not only by MR but also by GR and AR and is called glucocorticoid response element (GRE) as it was first detected as the target sequence for the GR.

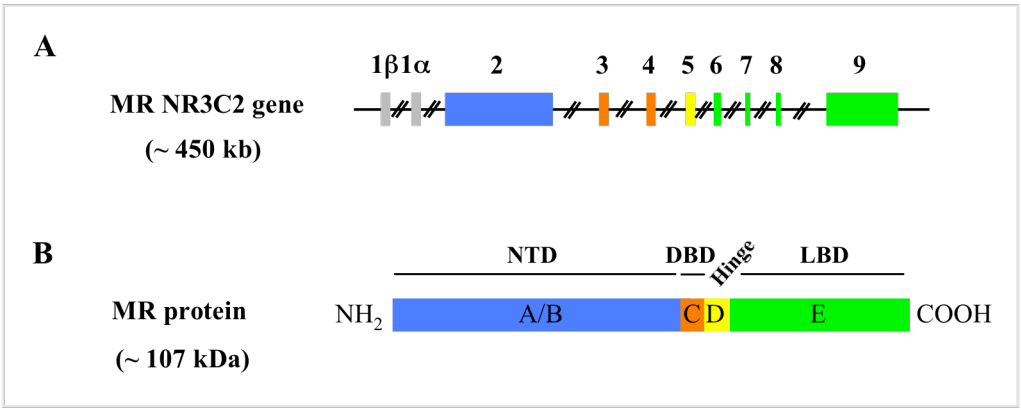

Figure 2. Schematic representation of the MR gene (A) and the structural organization of the encoded protein (B) with the five functional regions. Exons and the corresponding encoded protein domains (domains A-E) are indicated by colours boxes. NTD: N-terminal domain; DBD: DNA-binding domain; LBD: ligand-binding domain.

2.2.2. Ligand binding specificity

The cloning of GR (16) as well as of MR (17) allowed an unequivocal comparison of their expression patterns as well as of their affinities to gluco- and mineralocorticoids. In contrast to GR, which is expressed in most if not all cells, MR expression is restricted to the limbic system of the brain, to the heart, and to epithelial cells that line the distal part of the nephron, the distal colon, and the ducts of several exocrine glands (18-20). An important finding that issued from the cloning of the MR cDNA and expression of the MR protein is that the receptor is not selective for aldosterone. The MR binds the glucocorticoid cortisol (corticosterone in rodents) with a 10-fold higher affinity (dissociation constant: K_d = 0.5–2 nM) than the GR (K_d = 10-60 nM) and, in addition, the mineralocorticoid aldosterone with equal affinity (21). Since the concentration of corticosterone in the plasma is 100- to 1000-fold higher than that of aldosterone, and since MR has the same affinity for cortisol as for aldosterone, corticosterone should permanently occupy MR, precluding any regulatory role of aldosterone. It was shown that the specificity of aldosterone for MR in aldosterone target cells *in vivo* is given by a prereceptor mechanism, which converts corticosterone into receptor-inactive 11-dehydrocorticosterone (22, 23). The prereceptor mechanism found to protect MR from corticosterone, thus enabling aldosterone to interact with MR, is mediated by the enzyme 11β-hydroxysteroid dehydrogenase type 2 (11β-HSD2). Thus, in cells coexpressing MR and 11β-HSD2, namely epithelial cells from the distal nephron, the distal colon, and the ducts of sweat and salivary glands (24-26), permanent occupancy of MR by glucocorticoid hormones is largely prevented, allowing concentration-dependent binding of aldosterone to MR. The important role of 11β-HSD2 in MR binding selectivity is highlighted by the loss-of-function mutations in the 11β-HSD2 locus, identified in the syndrome of apparent mineralocorticoid excess (AME). Patients suffering from AME display severe hypertension, sodium retention and urinary potassium loss but very low levels of plasma aldosterone (27).

2.2.3. MR mutations and MR knockout mice

In humans, different MR loss-of-function mutations like missense, frameshift and nonsense mutations have been identified, which are localized in all exons of the MR gene. These mutations either change the conformation of the ligand-binding pocket and impair ligand binding, or generate premature termination codons and truncated proteins. All these MR mutations result in a syndrome of mineralocorticoid resistance called autosomal

pseudohypoaldosteronism type 1 (PHA1), characterized by renal salt wasting, dehydration, high plasma aldosterone levels and severe hyperkalemic acidosis (28).

To gain new insights into MR function *in vivo*, mice with a null mutation in the MR gene were generated (29). MR knockout mice died in the second week after birth due to severe loss of sodium and water, and showed symptoms similar to PHA1 (28). The effect of amiloride on renal sodium excretion and colonic transpithelial voltage showed that the activity of the amiloride-sensitive epithelial sodium channel (ENaC) and thereby sodium reabsorption was strongly impaired in kidney and colon in MR knockout mice. These mutant mice could be rescued by daily injection of an isotonic sodium-chloride solution, showing that the loss of sodium and water is the cause of lethality (30, 31). The severe salt-wasting phenotype of MR knockout mice demonstrates the central role of MR in the control of sodium and volume balance. In addition, the impaired renal sodium reabsorption in these mice suggests that the main site of MR action to control sodium balance is located in the aldosterone-sensitive part of the kidney.

2.3. Renal control of sodium and water balance

2.3.1. The kidney

The kidney plays a major role in the homeostasis of body fluid compartments in mammals (32). Despite the large quantitative variations in dietary intake of solutes and water, the kidneys are able to maintain within a narrow range the composition and volume of extracellular and intracellular fluid compartments. The kidney is made of three distinct regions: the pelvis, the medulla and the cortex. The renal pelvis is a large urine-collecting space formed from the expanded upper portion of the ureter. The renal medulla is the middle portion of the kidney. It contains 8 to 18 renal pyramids, which consist of tubules and collecting ducts (CDs) and which end in the renal pelvis. Urine passes from CDs in the pyramids to the renal pelvis, then into the ureter and is transported to the urinary bladder. The renal cortex is the outermost portion of the kidney and contains capillaries and glomeruli of the nephrons, the functional units of the kidney. The cortical tissue that penetrates the renal medulla between the renal pyramids forms the medullary rays, which contains the thick descending limb, the Henle loop, the distal nephron tubules and the CDs.

The nephron consists of a U-shaped tubular component and an associated vascular component. The tubular component starts with the glomerular (Bowman´s) capsule and includes the excretory tubules, which are the proximal convoluted tubule, the thick descending limb, the

Henle loop, the thick ascending limb (TAL), the distal convoluted tubule (DCT) and the connecting tubule (CNT). Each excretory tubules leads into a large collecting duct (CD) (whose cortical part only belongs to the nephron) that transports the resulting renal filtrate **(Figures 3A and 3B)**. Each kidney contains about one million of nephrons.

The kidney separates the molecules that will be excreted from the body as urine (through the ureter to the bladder) from those that will be returned to the circulating blood (through the renal vein) via three different processes: filtration, reabsorption, and secretion. The blood filtered by the kidney flows from the afferent arteriole into the glomerulus under a high pressure. This pressure forces some of the blood plasma into the glomerular capsule, but the blood cells and large proteins remain within the blood circulation, unable to pass through the endothelial capsular membrane. This process is called glomerular filtration and forms the initial urine called glomerular filtrate. As the glomerular filtrate passes through the length of the nephron tubule, useful substances like water, sodium ions, glucose and amino acids that were initially lost from the blood during filtration are returned to the blood by active and passive transport. This process is called tubular reabsorption. Some unwanted ions and substances may be transported from the blood in the peritubular capillaries into the glomerular filtrate as it passes through the nephron tubules. In this way, products such as potassium ions, hydrogen ions, certain drugs, and organic compounds may be excreted. This process is called tubular secretion and occurs in a direction opposite to that of tubular reabsorption. Finally, the glomerular filtrate moves to the medulla of the kidney, where it is now called urine, and passes to the bladder through the ureter.

2.3.2. The aldosterone-sensitive distal nephron (ASDN)

Aldosterone regulation of sodium reabsorption in kidney is restricted to a part of the distal nephron called the aldosterone-sensitive distal nephron (ASDN). The distal nephron of the mammalian kidney, which reabsorbs in humans 5% to 10% (0.5% to 1% in mice) of the filtered sodium under normal conditions, is defined as the nephron segment interposed between the macula densa region, a portion of the renal distal tubule in contact with the afferent arterioles, and the end part of the cortical CD upstream its confluence with another nephron. The distal nephron can be divided into successive portions, which are formed to adapt to the function of fine adjustments of sodium balance and which is reflected by an axial heterogeneity in protein expression (33, 34). The distal nephron comprises the TAL, the DCT, the CNT and the cortical CD. The ASDN is restricted to the segments of the distal nephron where MR and 11β-HSD2 are coexpressed: the late DCT, the CNT and the cortical CD **(Figure 3C)**.

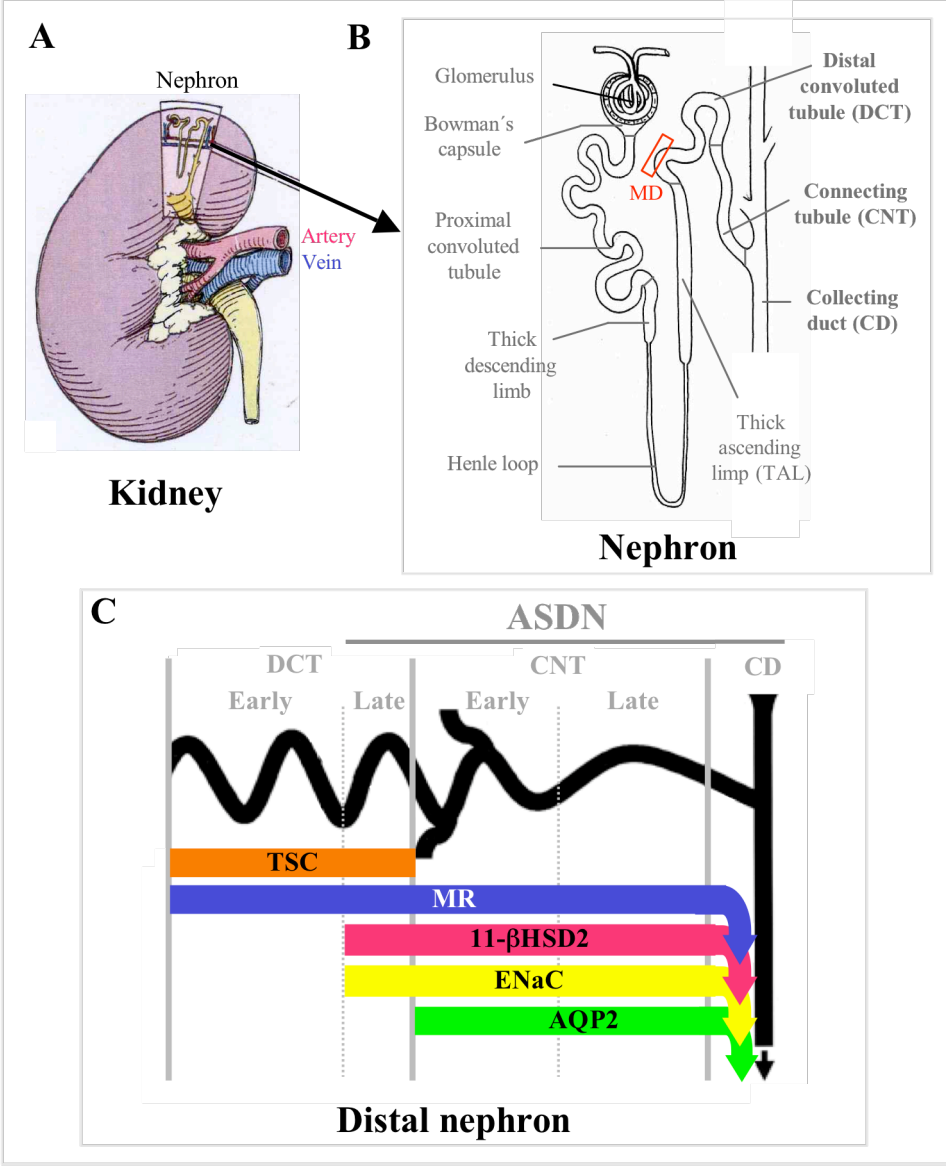

Figure 3. The kidney and the nephron. A: Entire kidney. **B:** Structure of the nephron and nomenclature of the different tubular segments. The red rectangle indicates the localization of the macula densa (MD) region. **C:** Schematic distribution of AQP2, ENaC, 11β-HSD2, MR and TSC protein expression along the different segments of the distal nephron in mice. AQP2: water channel aquaporin 2; ASDN: aldosterone-sensitive distal nephron; ENaC: epithelial sodium channel; MR: mineralocorticoid receptor; TSC: thiazide-sensitive sodium-chloride cotransporter; 11β-HSD2: 11β-hydroxysteroid dehydrogenase type 2.

Whereas the DCT and CNT are composed mainly of one type of epithelial cells, the CD consists of two different cell types, principal cells and intercalated cells, which exhibit profound morphological differences and serve markedly different functions (35, 36). The principal cells mediate sodium and water reabsorption, whereas the intercalated cells are responsible for proton transport (25). The CD and the different segments of the distal nephron have been defined according to the expression of specific transport proteins responsible for transepithelial ion movement from the tubular lumen to the interstitium (37). The DCT is characterized by the expression of the thiazide-sensitive sodium-chloride cotransporter (TSC, also termed NCC),

which is expressed in the more proximal part (early DCT) as well as in the distal part (late DCT) of the DCT. In the late DCT, the TSC is colocalized with the amiloride-sensitive epithelial sodium channel (ENaC). In the principal cells of the CNT and CD, ENaC is colocalized with MR and the apical water channel aquaporin 2 (AQP2) (29, 38-41) **(Figure 3C).**

2.4. Regulation of renal transepithelial sodium reabsorption by aldosterone

2.4.1. The epithelial sodium channel (ENaC)

Aldosterone controls the fine adjustments of sodium balance by acting on MR expressed in the ASDN (42). The main target for aldosterone action is the epithelial sodium channel (ENaC) responsible for apical sodium entry.

ENaC is a heteromultimeric ion channel located in the apical membrane of sodium-transporting epithelial cells. In addition to principal cells of the distal nephron, ENaC is also expressed in other aldosterone-responsive sites like the distal colon, the ducts of the sweat and the salivary glands. ENaC is also expressed in the airway epithelium from the nose to distal bronchiolar epithelium and in alveolar epithelial cells where its regulation is mediated by glucocorticoids (43). The activity of ENaC is the rate-limiting step for epithelial sodium reabsorption and is inhibited by the diuretic amiloride at submicromolar concentrations (44).

ENaC is composed of three different subunits (α, β and γENaC) in the ratio 2:1:1, which are encoded by three different genes (45). All the three subunits are necessary for maximal ENaC activity (45-47). However, heterologous expression of single ENaC subunits in Xenopus oocytes revealed that expression of αENaC is sufficient to generate a sodium current (48), but that βENaC and γENaC greatly potentiate sodium current when coexpressed with αENaC (49).

The importance of ENaC function in sodium homeostasis is highlighted by human genetic diseases caused by spontaneous mutations in the genes encoding the ENaC subunits. Gain-of-function mutations of βENaC or γENaC lead to increased ENaC activity and cause Liddle's syndrome, characterized by volume expansion and hypokalemic alkalosis (50, 51). Homozygous loss-of-function mutations of αENaC, βENaC and γENaC lead to PHA1 (52, 53). Gene targeting in mice confirmed the crucial role of the three ENaC subunits for sodium homeostasis (54). In addition, the strongly impaired renal ENaC activity together with the loss of sodium and water

observed in MR knockout mice suggest the importance of principal cell MR in the control of ENaC-mediated sodium reabsorption.

2.4.2. Regulation of ENaC-mediated renal sodium reabsorption by aldosterone

Epithelial cell layers separate compartments of distinct compositions. In order to maintain a constant ionic equilibrium, epithelial cells regulate transfer of water and solutes between them with extreme precision (55). The interstitium compartment, in equilibrium with the blood, is characterized by the constancy of its composition. In contrast, the composition of the luminal compartment varies greatly from one epithelium to another and with time. Epithelial cells are characterized by their functional polarization, since their apical membrane facing the luminal compartment has receptors as well as transport and permeability properties distinct from their basolateral membrane bathed in the interstitium compartment. Sodium as well as potassium and chloride transport is accompanied by a parallel movement of water.

In aldosterone-sensitive renal principal cells, aldosterone modulates the reabsorption of sodium by regulating sodium entry via ENaC across the apical membrane, the primary determinant of the intracellular sodium concentration in these cells. In turn, the intracellular sodium concentration directly controls the activity of the sodium-potassium-ATPase (Na^+-K^+-ATPase) responsible for sodium extrusion across the basolateral membrane (56) **(Figure 4)**. Therefore, apical ENaC-mediated sodium entry is limiting for transepithelial sodium and fluid transport, and any change in the quantity and/or activity of ENaC are important steps in the regulation of sodium reabsorption by aldosterone (57).

Several studies using candidate gene approaches (58, 59) or unbiased screens (60-64) have been undertaken to detect the mechanistic basis of aldosterone action on ENaC-mediated sodium reabsorption. As with other steroid hormone-regulated processes (65), two major classes of target genes have been identified: early and late. Early regulated genes appear to be required for initiation of the aldosterone response, whereas the late regulated genes are believed to participate in consolidation of the response (66). The latter include components of the ion transport machinery itself (for example, ENaC and Na^+-K^+-ATPase subunits) and genes that encode regulatory proteins that likely act to limit the extent of the aldosterone response (67). The former category (early aldosterone-regulated genes) encodes primarily signaling molecules, implicated in pathways that control ENaC activity and/or trafficking (57). The best characterized of these targets is the serum- and glucocorticoid-induced kinase 1 (SGK1) (57), which acts to increase

apical membrane ENaC, at least in part, by inhibiting the ubiquitin ligase Nedd4-2 by recruiting the 14-3-3 proteins and thus leading to modulation of ENaC trafficking and degradation (68, 69). Recently, several lines of evidence argue that aldosterone-regulated mediators other than SGK1 are also required for early ENaC activation (57). Most notably, although SGK1 knockout mice have aldosterone resistance, their phenotype is substantially less severe than that of either MR or ENaC knockout mice (57, 70) or of adrenalectomized wild-type animals (71), suggesting that renal ENaC function and renal mineralocorticoid action are only partially dependent on SGK1 and that aldosterone may act through multiple pathways to stimulate ENaC-mediated sodium reabsorption.

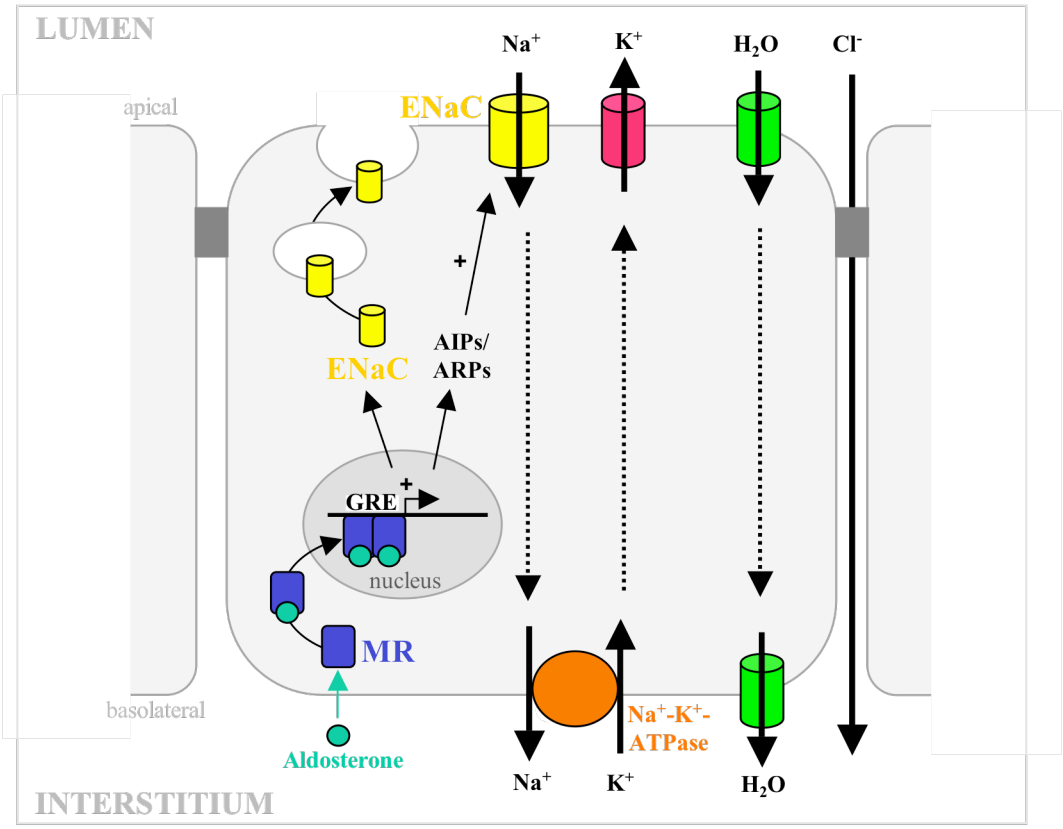

Figure 4. Cellular mechanism of transepithelial sodium and water transport in renal principal cells of the collecting duct. Sodium reabsorption in principal cells is mediated by Na^+-K^+-ATPase at the basolateral membrane and by ENaC at the apical membrane. Aldosterone binds to MR, which then translocates into the nucleus, regulates the transcription of target genes and leads to increased ENaC-mediated sodium reabsorption. Arrows indicate net fluxes of ions and water. AIP: aldosterone-induced proteins; ARP: aldosterone-repressed proteins; ENaC: epithelial sodium channel; GRE: glucocorticoid response element; MR: mineralocorticoid receptor.

In renal principal cells, potassium, chloride and water transport is coupled with sodium reabsorption **(Figure 4)**. The apical sodium entry leads to a depolarization of the apical membrane and apical extrusion of potassium is therefore favoured in order to achieve repolarization (72). In addition, the stoichiometry of the basolateral Na^+-K^+-ATPase-mediated

sodium and potassium transport (entry of 3 sodium cations and exit of 2 potassium cations) generates a cation desequilibrium. Electroneutral transepithelial sodium reabsorption in the collecting duct principal cells is achieved through a passive diffusion of chloride anions via a paracellular pathway across the tight-junctions from the tubular lumen to the interstitium, and via reabsorption through transporters or exchangers in the intercalated cells (73). The net movement of sodium-chloride drives water flow, which is mediated by water channels, aquaporin 2 in the apical membrane and aquaporins 3 and 4 in the basolateral membrane (74).

2.5. Conditional somatic mutagenesis in mice using the Cre-loxP recombination system

Gene targeting is one of the most powerful techniques to investigate the *in vivo* function of a gene product (75). However, knockouts may have disadvantages, e.g. the mutations may give rise to an embryonic or early postnatal lethal phenotype, thus precluding analysis of gene function in adult mice, and the problem of possible compensatory effects during development in mice containing the mutation. Furthermore, interpretation of a phenotype can be complicated by pleiotropic effects in many organs or tissues. To circumvent these problems, a strategy for conditional gene inactivation in a tissue-specific manner was developed using the Cre-loxP recombination system in mice (76). The Cre recombinase, encoded by the *Cre* gene of the bacteriophage P1, efficiently excises intervening DNA sequences located between two loxP sites in the same orientation (77, 78). For the application of gene targeting in mice, two transgenic mouse lines are necessary: one line expressing the Cre recombinase as a transgene under the control of a cell- or tissue-specific promoter (Cre line), and one line in which an essential exon of the gene of interest is flanked by two loxP sites (floxed allele). In mutant mice that are homozygous for the floxed allele and heterozygous for the Cre transgene, the gene of interest is inactivated **(Figure 5)**.

Since some promoters give already expression during pre- and postnatal development, the gene of interest will be inactivated before adulthood, and this could result in early lethality. To overcome this problem, an inducible ligand-activated recombination system has been established that can be used to induce recombination in adulthood (79-81). This system is based on the fusion of the Cre recombinase with a mutated ligand-binding domain (LBD) of the human estrogen receptor ER ($CreER^{T2}$). The ER-LBD contains a nuclear localization signal that is unmasked upon ligand binding. Two point mutations in the ER-LBD allow binding of the

synthetic ligand tamoxifen and prevent activation of the CreER^{T2} by the endogenous estradiol. Therefore, the unliganded form of the CreER^{T2} fusion protein resides in the cytoplasm and translocates to the nucleus only upon tamoxifen binding, thus mediating site-specific recombination resulting in the tamoxifen-dependent gene inactivation.

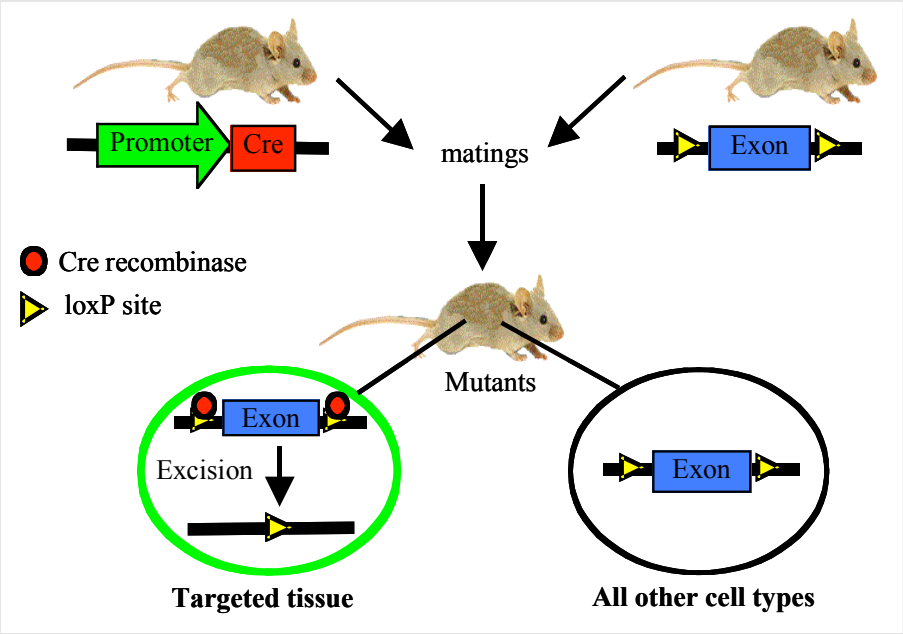

Figure 5. Constitutive tissue-specific gene inactivation in the mouse using the Cre-loxP recombination system. Breeding of a mouse expressing the Cre recombinase under the control of a tissue-specific promoter with a mouse harbouring a loxP-flanked exon of the gene to inactivate results in mice carrying both genetic modifications. Active Cre recombinase will excise the loxP-flanked DNA sequence in the cells of the targeted tissue, thereby inactivating the gene in these cells.

2.6. Aims of the present study

The severe salt-wasting phenotype of MR knockout mice demonstrated the importance of MR in the control of sodium balance. In addition, the impaired renal ENaC activity in these mice suggested that the main site of MR action to control sodium balance is located in the renal ENaC-expressing principal cells (29). To further investigate this hypothesis, the main aim of the present study was the

"Analysis of the role of MR in renal principal cell ENaC-mediated sodium reabsorption in vivo".

To this end, mice lacking MR in renal principal cells were generated using the Cre-loxP recombination system. To drive the expression of the Cre recombinase, a PAC-derived large

genomic DNA fragment containing the regulatory elements of the mouse AQP2 gene was used, since AQP2 is coexpressed with ENaC in principal cells of the collecting duct and connecting tubule already during development (40). AQP2Cre transgenic mice were bred with mice carrying a conditional MR allele (82) to generate mutant ($MR^{AQP2Cre}$) mice.

Since the prenatal constitutive inactivation of renal principal cell MR could result in a very strong phenotype that may even lead to lethality, an inducible renal principal cell-specific gene inactivation system was established in parallel in order to induce MR inactivation in adulthood only.

To identify MR-regulated genes involved in the control of ENaC-mediated sodium reabsorption in collecting duct principal cells upon aldosterone induction, gene expression profiling using microarrays was performed on a mouse collecting duct principal cell line treated with aldosterone or vehicle. The expression of aldosterone-regulated genes potentially involved in ENaC regulation was analyzed in microdissected collecting ducts from control and $MR^{AQP2Cre}$ mice.

3. RESULTS

3.1. Renal principal cell-specific MR inactivation in the mouse

Mice deficient for MR in renal principal cells were generated using the Cre-loxP recombination system. Transgenic mice expressing the Cre recombinase under the control of the regulatory elements of the mouse AQP2 gene (AQP2Cre mice) were generated and crossed with mice harboring a conditional MR allele generated previously (82), in which exon 3 encoding the first zinc finger of the MR DNA-binding domain was flanked by two loxP sites. For inactivation of MR-regulated sodium reabsorption mediated by ENaC in principal cells, the AQP2 promoter was chosen to drive the expression of the Cre recombinase in principal cells of the CD and CNT **(Figure 6)**.

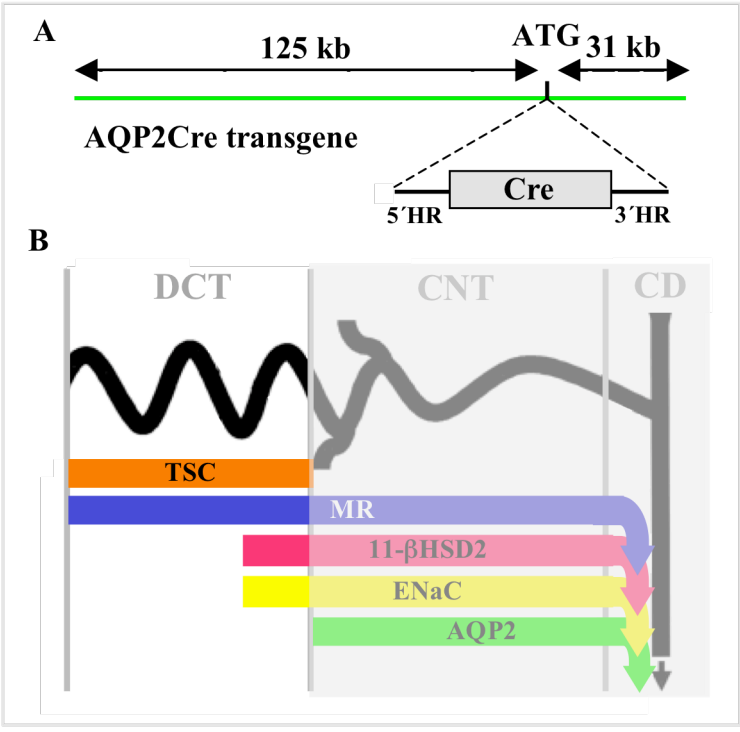

Figure 6. The regulatory elements of the mouse AQP2 gene were used to drive the expression of the Cre recombinase in ENaC-expressing principal cells of the connecting tubule (CNT) and collecting duct (CD). A: AQP2Cre transgene: a PAC harboring 125 kb of the 5´upstream region and 31 kb of the 3´upstream region of the mouse AQP2 gene was modified by homologous recombination in bacteria to insert a cassette encoding Cre recombinase at the ATG of the AQP2 gene. HR: homology region. **B:** Schematic distribution of AQP2, ENaC, 11β-HSD2, MR and TSC protein expression along the distal tubular segments of the nephron. The regulatory elements of the mouse AQP2 gene were used to drive Cre recombinase expression in ENaC-expressing principal cells of the CNT and CD. AQP2: water channel aquaporin 2; CD: collecting duct; CNT: connecting tubule; DCT: distal convoluted tubule; ENaC: epithelial sodium channel; MR: mineralocorticoid receptor; TSC: thiazide-sensitive sodium-chloride cotransporter; 11β-HSD2: 11β-hydroxysteroid dehydrogenase type 2.

3.1.1. Generation of mice lacking MR in renal principal cells

3.1.1.1. Generation of AQP2Cre transgenic mice

A mouse genomic PAC library (RPCI21, RZPD, Germany) was screened with a probe for the AQP2 gene as described in the Materials and Methods part. Three PACs containing a genomic DNA fragment of 156 kb, 118 kb and 97 kb respectively were isolated and characterized by sequencing the ends of the genomic insert. The respective sequences were then blasted to the mouse genome (www.ensembl.org) to determine the position of the start codon of the AQP2 locus on the PACs, the position of exons and introns, and the length of the 5′ and 3′ regions. A PAC with a 5′ region bigger than the 3′ region, namely the 156-kb PAC harbouring a 125-kb 5′ upstream region and a 31-kb 3′ downstream region of the AQP2 gene, was chosen for modification by homologous recombination in bacteria, also called ET-cloning (83).

To introduce the Cre recombinase coding sequence in the genomic insert by homologous recombination in bacteria, a plasmid (pConst) containing the sequence encoding the Cre recombinase (84) and an ampicillin resistance cassette flanked by two FRT sites was used. The cloning steps are described in the Material and Methods part. Briefly, a 319-bp 5′ homology region of the AQP2 gene (5′ homology arm) containing the ATG at the 3′ end was amplified by PCR and cloned in front of the Cre recombinase coding sequence. The open reading frame of the Cre recombinase will therefore be inserted at the ATG of the AQP2 locus in the PAC after homologous recombination. A 372-bp 3′ homology region of the AQP2 gene (3′ homology arm) was amplified by PCR and cloned behind the ampicillin resistance cassette. The construct was released and electroporated into DH10B bacteria harbouring the PAC and a plasmid expressing the *rec*E and *rec*T proteins mediating the homologous recombination in bacteria (83). After induction of the recombination and selection with ampicillin and chloramphenicol, the positive clones were electroporated with a plasmid expressing the Flp recombinase to remove the ampicillin resistance cassette (83). Clones with the recombined PACs were identified by restriction site analysis with Xho1 digestion. Xho1 digestion of the wild-type PAC generates eight bands, one with a length of 3.8 kb. The introduction by homologous recombination in bacteria of the Cre recombinase coding sequence and the ampicillin resistance cassette introduces a new Xho1 site leading to the decrease of the 3.8-kb band to 2.5 kb, and to the generation of an additional band of 3.9 kb, characteristic for the modified PAC containing the resistance cassette. After removal of the ampicillin resistance cassette, the size of the previously 3.9-kb band decreased to 2.8 kb, characteristic for the finaly modified PAC **(Figure 7)**.

The modified genomic fragment of 156 kb containing the Cre knock-in at the ATG of the AQP2 locus (abbreviated as AQP2Cre transgene) was released by digestion with Not I and separated from the PAC backbone by subsequent preparative pulsed field gel electrophoresis. The integrity of the homology regions and of the Cre recombinase coding sequence was checked by sequence analysis. The large genomic DNA fragment was purified from the gel slice by agarase digestion and microdialysis, and then microinjected into the pronucleus of FVB/N mouse oocytes to obtain AQP2Cre transgenic mice.

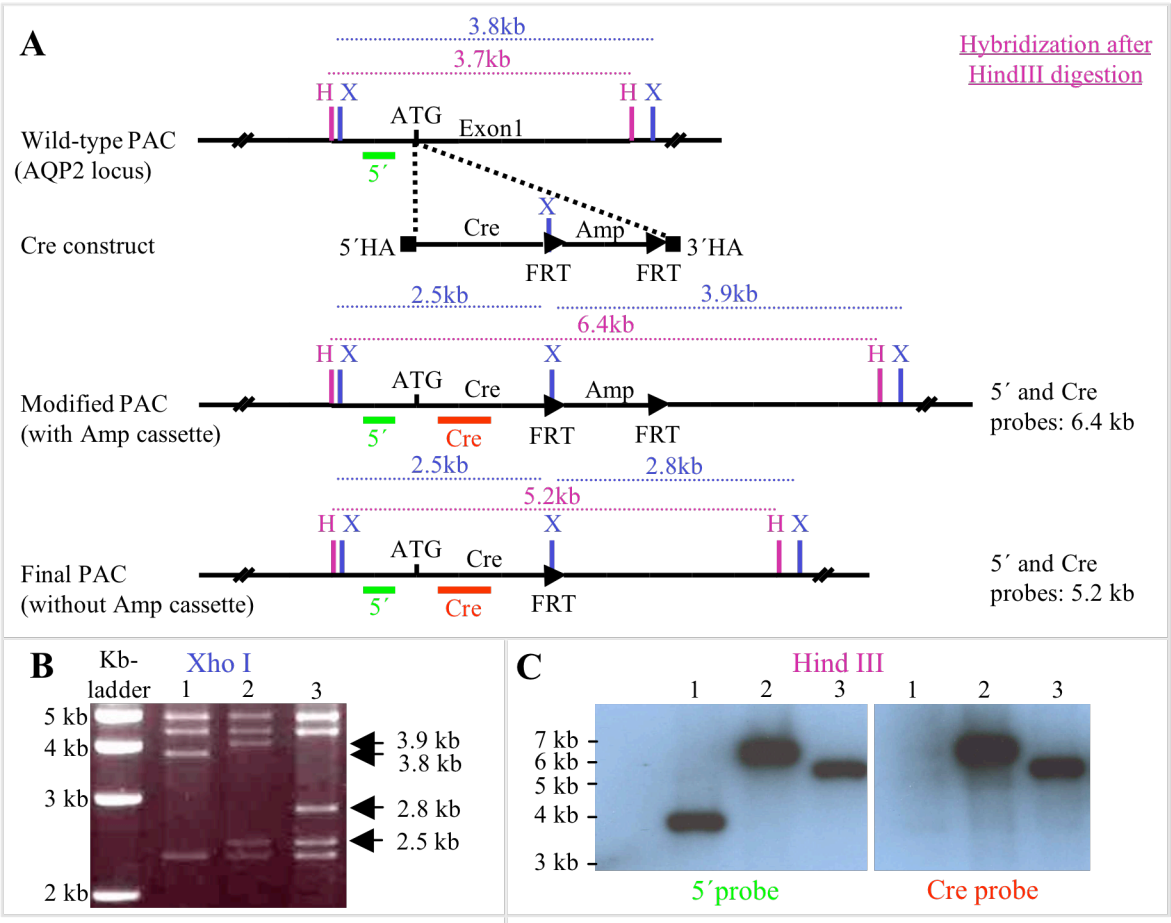

Figure 7. Identification of the wild-type and modified AQP2Cre PACs by enzymatic digestion and hybridization with DNA probes. **A:** Schematic map of the wild-type and modified PACs showing the size of the DNA fragments generated after HindIII (H) or Xho1 (X) digestion and the size of the bands identified after hybridization with the 5´ or Cre probes. Amp: ampicillin resistance cassette. HA: homology arm. FRT: Flp recombinase recognition sequences orientated in the same direction resulting in removal of the flanked sequence upon Flp expression. **B:** Picture of an agarose gel showing the DNA fragments obtained after Xho1 digestion of the wild-type PAC (line 1), the recombined PAC containing the Amp cassette (line 2) and the recombined PAC after removal of the Amp cassette (line 3). **C**: Picture of a Southern blot membrane showing the DNA fragments obtained after HindIII digestion of the PACs, and identified by hybridization with the 5´ and Cre probes (lines 1: wild type PAC, lines 2: modified PAC with the Amp cassette, lines 3: final PAC without the Amp cassette).

3.1.1.2. Analysis of AQP2Cre transgenic mice

Transgenic offsprings were identified by dot blot analysis of genomic tail DNA hybridized to a probe recognizing the Cre recombinase sequences **(Figure 8A)**. Twelve independent dot blot-positive mice were obtained from two successive oocyte injections of the AQP2Cre transgene and bred to C57Bl/6 mice to establish several transgenic mouse lines. Seven out of the twelve dot blot-positive mice showed germline transmission of the transgene to the first offspring generation (F1 generation). From them, three transgenic lines could be established and used for further analysis. For determining the transgene copy number, Southern blots were performed on genomic DNA from F1 mice digested with the restriction enzyme HindIII and hybridized to a probe recognizing the 5´ region of the AQP2 gene (5´ probe). Hybridization of the HindIII-digested genomic DNA with the 5´ probe revealed a DNA fragment of 3.7 kb for the endogenous AQP2 locus (wild-type band) and of 6.4 kb for the AQP2Cre transgene integrated into the genome (transgenic band) **(Figure 7C)**. The ratio of the intensities of these two bands was quantified by a Phospho-Imager for several blots, with the band for the endogenous AQP2 locus calculated as two copies (two alleles in the diploid genome). The transgene copy number for the three lines was determined as 1 copy, 2 copies and 4 copies, respectively **(Figure 8B)**. The AQP2Cre transgenic lines were continuously backcrossed into C57Bl/6 genetic background.

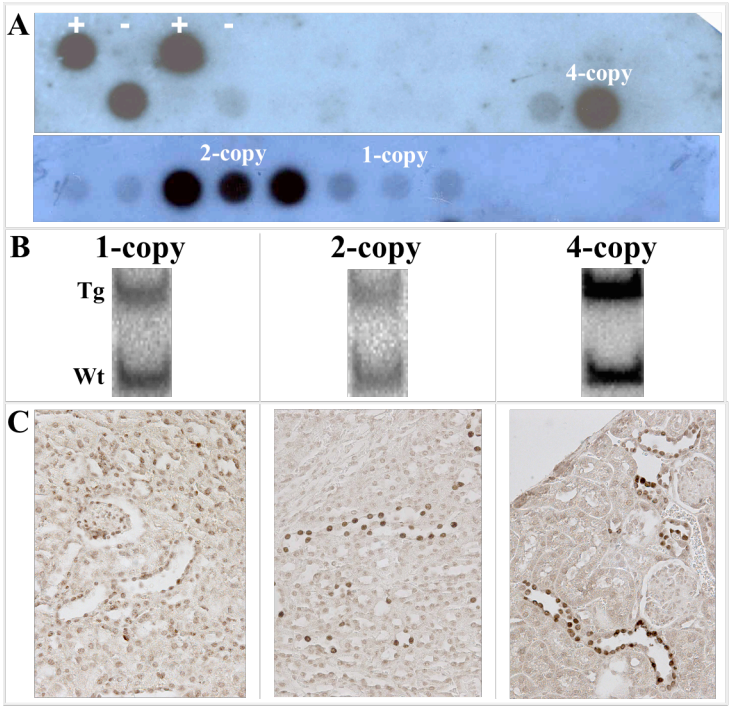

Figure 8. Identification and charaterization of the AQP2Cre mouse transgenic lines. A: Picture of dot blot membranes probed for the presence of the AQP2Cre transgene in offsprings obtained after oocyte injection. Positive signals for the founders of the 1-copy, 2-copy and 4-copy lines are indicated; +: positive control; -: negative control. **B:** Copy number Southern blot of HindIII-digested genomic DNA hybridized with the 5´ probe. Wt: wild-type band; Tg: transgenic band. **C:** Immunohistochemistry for Cre recombinase on kidney paraffin sections from the 1-copy, 2-copy and 4-copy lines, respectively.

To investigate Cre expression at the cellular level, kidneys were taken from F1 mice from the three transgenic lines and analyzed for Cre recombinase protein expression using immunohistochemistry. An intense nuclear staining was observed in cells from CDs and distal tubules, identified on account of their epithelial thickness and their localization in medullary rays and in the cortical labyrinth adjacent to cortical radial vessels, respectively. All three lines exhibited a similar pattern of Cre expression in the kidney, resembling the expression of the endogenous AQP2 gene, and only showed transgene copy number-dependent quantitative differences in Cre expression levels **(Figure 8C)**.

3.1.1.3. Generation of $MR^{AQP2Cre}$ mutant mice

Transgenic AQP2Cre mice from both lines showing the highest Cre expression level, namely the 2-copy and 4-copy lines, were crossed with mice harbouring a conditional MR allele ($MR^{flox/flox}$ abbreviated as MR^{flox}) to generate $MR^{flox/flox}$//AQP2Cre (abbreviated as $MR^{AQP2Cre}$) mutant mice. Due to limited fertility of the 4-copy line, the $MR^{AQP2Cre}$ mutant mice, which were analyzed were obtained from the 2-copy line only. Control mice used for analysis were the MR^{flox} littermates.

3.1.2. Analysis of $MR^{AQP2Cre}$ mutant mice

3.1.2.1. $MR^{AQP2Cre}$ mice are able to maintain sodium balance under standard diet

Colocalization of AQP2 and Cre expression in renal principal cells was confirmed by immunohistochemical costaining and resulted in loss of MR in AQP2-positive cells of $MR^{AQP2Cre}$ mice, but not in control mice **(Figure 9).** In contrast to MR inactivation in the germline (29), which results in inactivation of MR in all cells, inactivation of the MR gene restricted to renal principal cells did not impair survival, since at 4 weeks after birth a Mendelian distribution of the genotypes was observed. When fed with a standard diet (0.18% of sodium), control and $MR^{AQP2Cre}$ mice grew and developed normally, and exhibited similar bodyweight (controls: 21.8 ± 1.9 g, n = 15; mutants: 21.7 ± 2.0 g, n = 15, P = 0.90). No change in plasma sodium (controls: 144.8 ± 3.4 mmol/l, n = 6; mutants: 147.7 ± 1.2 mmol/l, n = 9, P = 0.45) and potassium levels (controls: 5.28 ± 0.27 mmol/l, n = 6; mutants: 5.24 ± 0.06 mmol/l, n = 9, P = 0.88) as well as in daily urine volume (controls: 0.05 ± 0.01 ml/g bodyweight/24h, n = 15; mutants: 0.06 ± 0.01 ml/g bodyweight/24h, n = 16, P = 0.29) and urinary sodium concentration (controls: 139 ± 6 mmol/l, n = 15; mutants: 127 ± 4 mmol/l, n = 16, P = 0.10) was observed in $MR^{AQP2Cre}$ mice

compared to controls. Therefore, absolute sodium excretion, as calculated from urine volume and urinary sodium concentration, was not changed **(Figure 10A)**, indicating that $MR^{AQP2Cre}$ mice are able to maintain sodium balance under standard conditions.

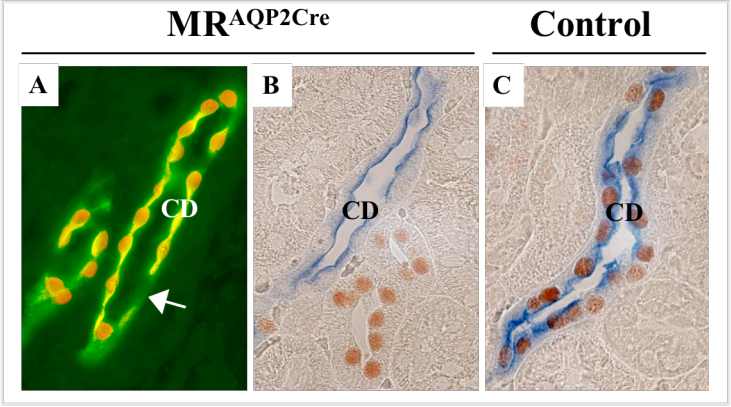

Figure 9. Analysis of AQP2, Cre and MR protein expression. A: Double immunofluorescence labeling for AQP2 (green) and Cre (red) on kidney paraffin sections. Overlap of AQP2 and Cre labeling results in a yellow signal. The arrow indicates an AQP2-negative intercalated cell of the CD with no Cre expression. **B and C:** Double immunohistochemical staining for AQP2 (blue) and MR (brown) on kidney paraffin sections of $MR^{AQP2Cre}$ (B) and control (C) mice. CD: collecting duct.

3.1.2.2. $MR^{AQP2Cre}$ mice show increased renal loss of sodium and water

Two-month old mice were challenged with a low-sodium diet (<0.01% sodium) for up to 10 days. Both control and $MR^{AQP2Cre}$ mice significantly decreased the absolute sodium excretion in comparison to standard diet conditions **(Figure 10A)**. This indicates that the low-sodium diet was effective and that the animals attempted to conserve sodium by enhancing renal sodium reabsorption. However, this attempt was only partially successful in the mutants, as their absolute sodium excretion was 70% higher after 10 days of low-sodium diet compared to controls. $MR^{AQP2Cre}$ mice showed an increase in the urine volume produced per day, but unchanged urinary sodium concentration compared to controls after 10 days of low-sodium diet. There was no significant difference in food consumption and therefore in sodium intake, as well as in water consumption, between both genotypes **(Figures 10B-10E)**. Under low-sodium diet, also a hyperkalemia was observed in mutants (controls: 6.48 ± 0.18 mmol/l, n = 9; mutants: 7.62 ± 0.25 mmol/l, n = 7, $P < 0.05$). Interestingly, mutants showed a continuous loss of bodyweight in the homecages **(Figure 10F)**.

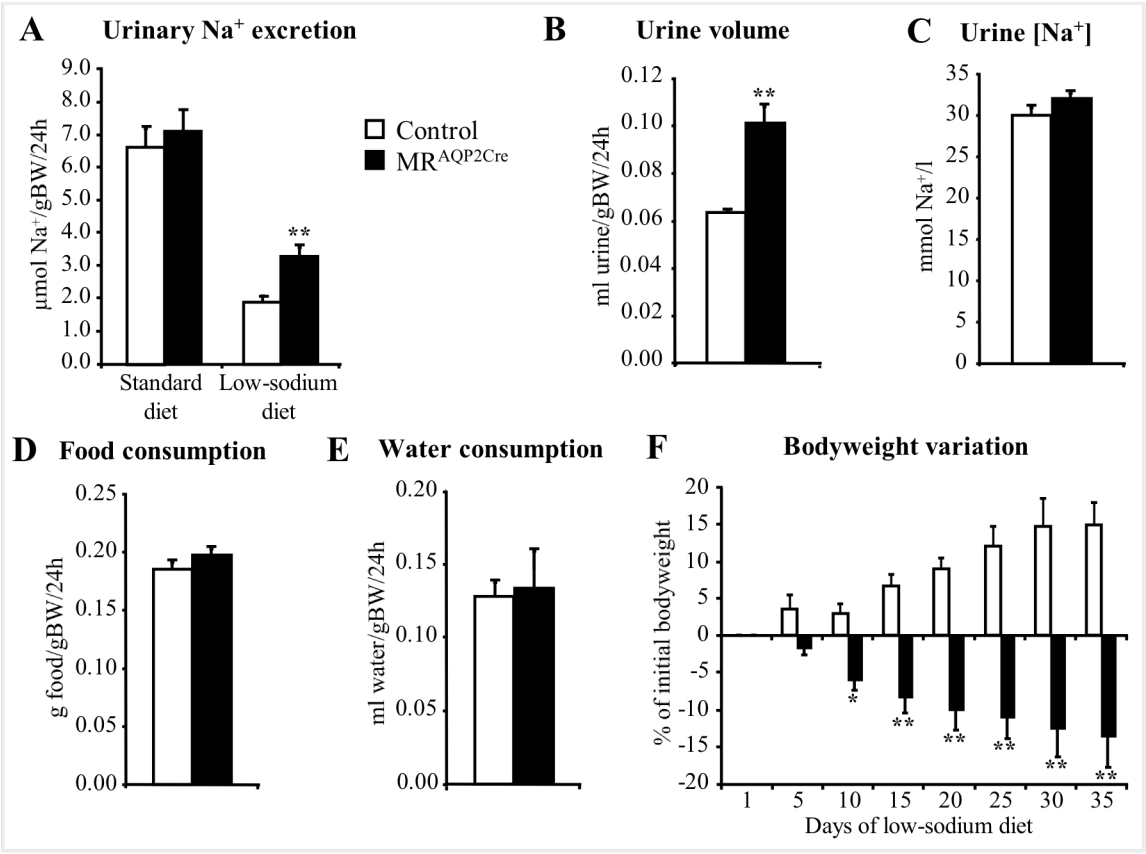

Figure 10. Analysis of urinary sodium excretion, urine volume, urine sodium concentration, food and water consumption over 24 hours, and bodyweight variation after 10 days of low-sodium diet. Mice were maintained for the first 9 days of low-sodium diet in their homecages and placed in metabolic cages on day 10 for urine collection. *P<0.05, **P<0.005. n = 10-15. BW: bodyweight.

A detailed time-course analysis of the first 5 days under low-sodium diet revealed that, from day 2 on, $MR^{AQP2Cre}$ mice show increased renal sodium excretion compared to controls, whereas within the first 24 hours no genotype effect was detected **(Figure 11A)**. Whereas the urinary sodium concentration was unchanged in mutant mice compared to control mice over the whole salt-restriction period, $MR^{AQP2Cre}$ mice showed increased urine volume production resulting in increased renal sodium excretion **(Figure 11B)**. Both genotypes showed no significant difference in food and water consumption over time (data not shown).

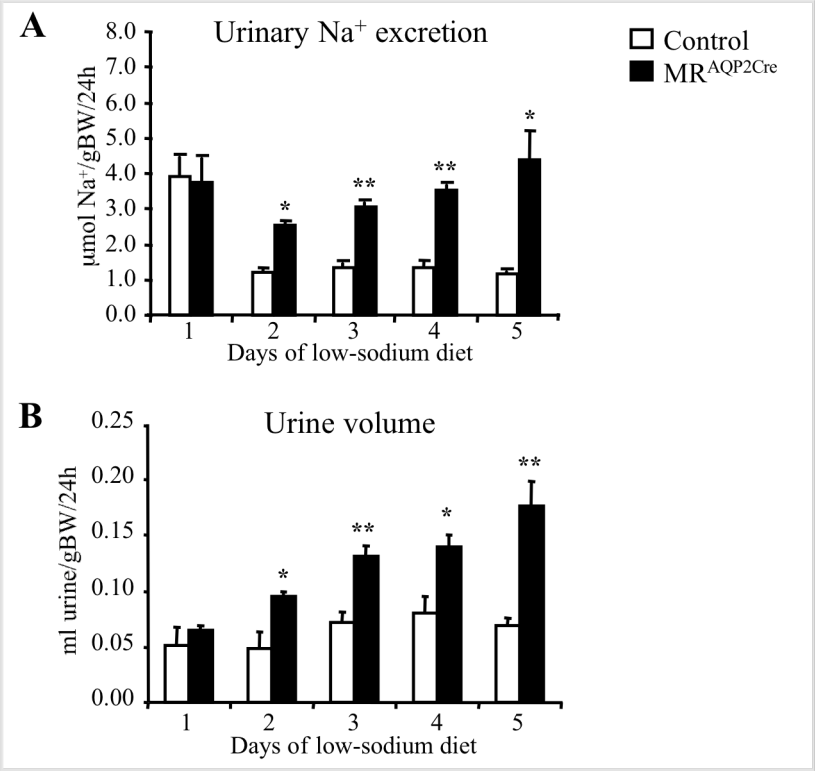

Figure 11. Time-course analysis of urinary sodium excretion (A) and urine volume (B) over 24 hours during 5 days of low-sodium diet. Mice were placed in metabolic cages for 5 days for urine collection. *P<0.05, **P<0.005. n = 5 per group. BW: bodyweight.

Histological examination of the kidneys of two-month old mice did not reveal any tubular or interstitial abnormalities, except for focal enlargement of the juxtaglomerular apparatus, the site of renin production, in $MR^{AQP2Cre}$ mice, indicating an activation of the renin-angiotensin-aldosterone system (RAAS) **(Figure 12A)**. Indeed, determination of plasma aldosterone levels revealed a dramatic increase in $MR^{AQP2Cre}$ mice. After 3 days of low-sodium diet, as expected, plasma aldosterone increased in controls compared to standard diet conditions. However, an increase was also detected in mutants to the same extent. Under both diets, mutants exhibit 10-fold elevated plasma aldosterone levels compared to controls. After 10 days of low-sodium diet, plasma aldosterone increased further in both genotypes and mutants still exhibited 6-fold increased levels **(Figure 12B)**.

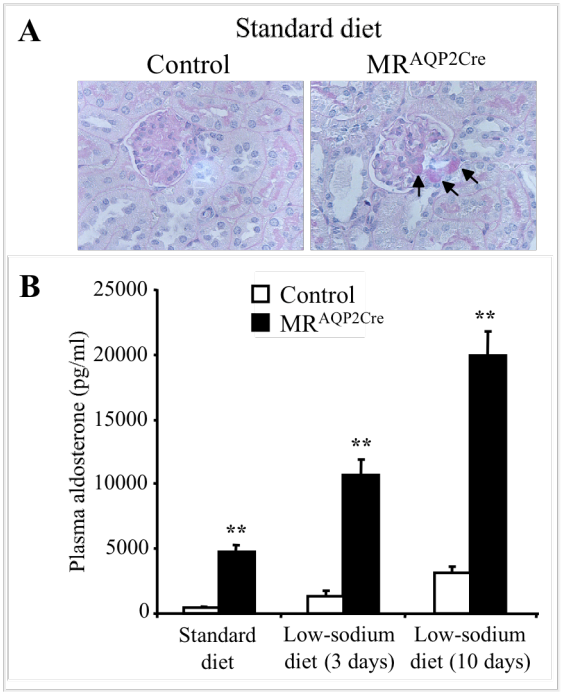

Figure 12. Analysis of the renin-angiotensin-aldosterone system (RAAS) activation. **A:** Hematoxylin-eosin histological staining of kidney paraffin sections from control and $MR^{AQP2Cre}$ mice under standard diet. Arrows indicate focal enlargement of juxtaglomerular renin-producing granular cells. **B:** Plasma aldosterone levels measured in control and $MR^{AQP2Cre}$ mice under standard diet (n = 15) or after 3 days (n = 15) or 10 days (n = 5) of low-sodium diet. **P<0.005.

3.1.2.3. $MR^{AQP2Cre}$ mice show preserved ENaC activity

To examine whether ENaC-mediated renal sodium reabsorption was affected in $MR^{AQP2Cre}$ mice, the effect of amiloride, a specific blocker of ENaC, on the excreted part of the sodium filtered by the kidney (fractional excretion of sodium, abbreviated as $FE(Na^+)$) was determined. Since after 10 days of low-sodium diet $MR^{AQP2Cre}$ and control mice show a similar glomerular filtration rate (GFR) determined by measuring the creatinine clearance within 24 hours (controls: 6.63 ± 0.32 µl/g bodyweight/min, n = 15; mutants: 6.17 ± 0.49 µl/g bodyweight/min, n = 15, P = 0.45), the direct comparison of $FE(Na^+)$ between controls and mutants is possible. In the absence of amiloride, $FE(Na^+)$ tended to be higher in $MR^{AQP2Cre}$ mice than in controls, suggesting salt wasting. However, the difference between both genotypes did not reach significance within the 2-hour sampling period (controls: 0.17 ± 0.04%, n = 5; mutants: 0.24 ± 0.04%, n = 6, P = 0.20), probably due to incomplete collection of the urine from the bladder and high variation and error in small urine volumes collected during a short period of time. As expected, amiloride strongly increased $FE(Na^+)$ in controls. Surprisingly, amiloride had a comparable effect on $FE(Na^+)$ in $MR^{AQP2Cre}$ mice, indicating preserved renal ENaC activity in the mutants **(Figure 13).**

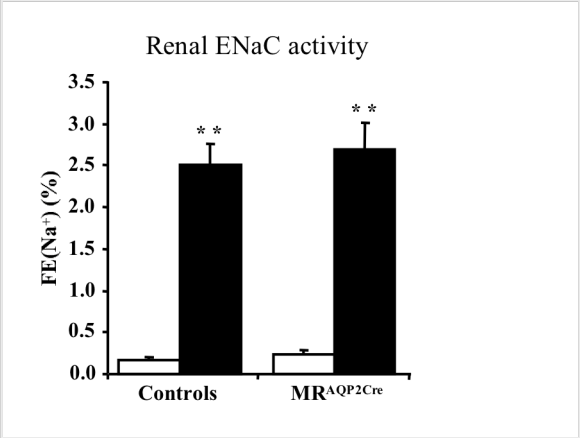

Figure 13. Analysis of renal ENaC activity. Determination of the effect of amiloride on the fractional excretion of sodium (FE(Na^+)) in untreated (white bars) and amiloride-treated (black bars) control and $MR^{AQP2Cre}$ mice after 10 days of low-sodium diet. The FE(Na^+) was calculated as ([urine sodium]/[plasma sodium])*([plasma creatinine]/[urine creatinine]). **P<0.005 (t-test treated versus untreated). Untreated groups: n = 5-6; amiloride-treated groups: n = 11-13.

3.1.2.4. $MR^{AQP2Cre}$ mice show loss of MR and apical αENaC in CD and late CNT

Since $MR^{AQP2Cre}$ mice showed preserved amiloride-sensitive renal sodium reabsorption, renal ENaC expression was assessed by immunohistochemistry in control and mutant mice after 10 days of low-sodium diet. As reported previously (85), the apical ENaC subunit α (αENaC) staining detected in controls was weaker in CD **(Figure 14A)** compared to CNT **(Figure 14C)**. In $MR^{AQP2Cre}$ mice, both MR and αENaC stainings were absent in all principal cells of cortical CD **(Figure 14B)** and in most principal cells of the CNT **(Figure 14D)**, demonstrating efficient targeting of MR in these tubular segments and the crucial role of MR expression for αENaC trafficking to the cell surface. However, some principal cells of the CNT retain MR and also apical αENaC expression **(Figure 14D, arrows)**. Closer inspection and co-immunostainings with antibodies against calbindin D28k and the thiazide-sensitive sodium-chloride cotransporter (TSC), established markers for the distal tubule subsegments (86), revealed strong expression of Cre in the CD and decreasing levels along the CNT towards the early CNT. In this subsegment, Cre expression was undetectable **(Figures 15A and 15B)**. Detailed analysis of MR and αENaC expression revealed that the cells retaining MR and apical αENaC expression are situated in the early CNT, adjacent to the transition from DCT to CNT, and in the late DCT **(Figure 15C)**. Thus, $MR^{AQP2Cre}$ mice exhibit targeting of the MR gene and loss of apical αENaC expression in CD and late CNT. The early CNT, however, is not targeted due to undetectable Cre expression. A gross survey revealed that about 30% of the CNT principal cells were not targeted.

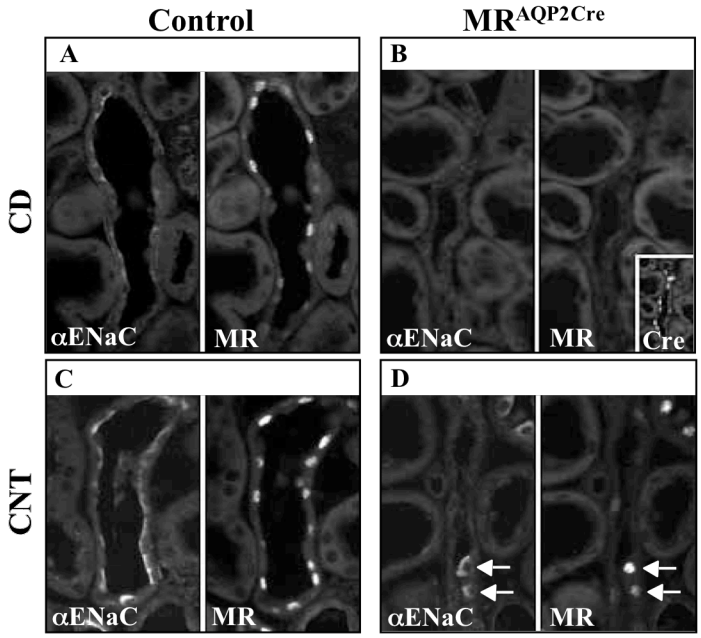

Figure 14. Analysis of MR and αENaC protein expression. Collecting duct (CD) and connecting tubule (CNT) from control (A and C) and $MR^{AQP2Cre}$ (B and D) mice kept for 10 days under low-sodium diet. Double immunofluorescence on the same cryosection with antibodies against αENaC and MR, respectively. **A and C:** In control, apical αENaC is well detectable in MR-expressing cells of CD (A) and CNT (C), with stronger expression in CNT cells. **B:** In $MR^{AQP2Cre}$, apical αENaC and MR immunostainings are absent from principal cells in CD, which express high levels of Cre as shown by immunofluorescence on a consecutive cryosection (low magnification insert). **D:** In CNT of $MR^{AQP2Cre}$, apical αENaC and MR are absent from most of the CNT cells. Only few CNT cells (arrows) retain MR and apical αENaC staining.

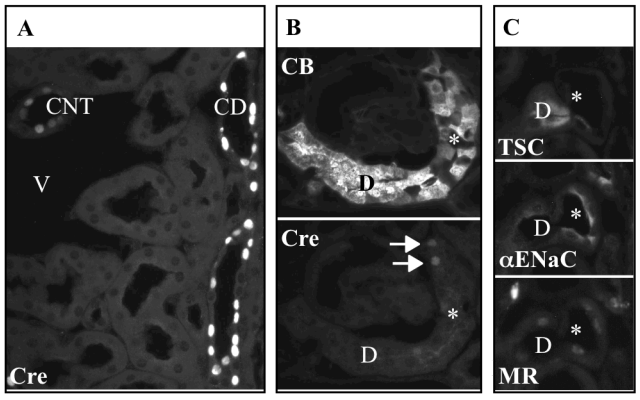

Figure 15. Detailed analysis of Cre expression along the distal nephron. Immunofluorescent labeling for Cre, calbindin D28k (CB), thiazide-sensitive sodium-chloride cotransporter (TSC), αENaC and MR on cryosections from a $MR^{AQP2Cre}$ mouse kept for 10 days under low-sodium diet. CD: collecting duct; CNT: connecting tubule; D: distal convoluted tubule; V: cortical radial vessel; *: early CNT; arrows: detectable low Cre staining.

3.1.2.5. $MR^{AQP2Cre}$ mice show unchanged TSC activity but increased colonic ENaC activity

To determine whether elevated plasma aldosterone observed in $MR^{AQP2Cre}$ mice could act on other sodium-reabsorbing MR-expressing epithelia than the early CNT, the activity of TSC in DCT and ENaC in colon were assessed. The activity of TSC, expressed in DCT and described to be activated by aldosterone (87), was determined by measuring FE(Na^+) under low-sodium diet before and after treament with thiazide, a specific TSC blocker. In both genotypes, no change in the thiazide-sensitive portion of the FE(Na^+) was observed **(Figure 16A)**. In contrast, the colon was responding to the elevated plasma aldosterone levels. $MR^{AQP2Cre}$ mice exhibit an 1.7-fold increased amiloride-sensitive transepithelial voltage compared to control mice under standard diet, and a 1.5-fold increase when challenged under low-sodium diet **(Figure 16B)**.

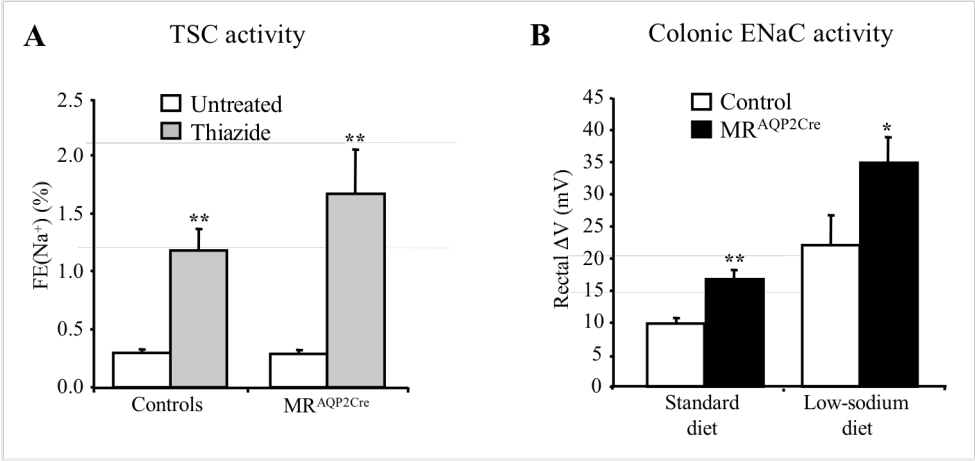

Figure 16. Analysis of TSC activity in the renal DCT and ENaC activity in the colon. A: Determination of the effect of thiazide on the fractional excretion of sodium (FE(Na^+)) in untreated and thiazide-treated control and $MR^{AQP2Cre}$ mice after 10 days of low-sodium diet. TSC: thiazide-sensitive sodium-chloride cotransporter. **P<0.005 (t-test treated versus untreated). Untreated groups: n = 5-6; thiazide-treated groups: n = 6-8. **B:** Difference in rectal transepithelial voltage measured before and after amiloride-treatment (ΔV) in controls and $MR^{AQP2Cre}$ mice under standard diet or after 10 days of low-sodium diet. ENaC: amiloride-sensitive epithelial sodium channel. *P<0.05, **P<0.005 (t-test $MR^{AQP2Cre}$ versus control). n = 6 per genotype.

3.2. Generation of an inducible renal principal cell-specific gene inactivation system

Principal cell MR-deficient ($MR^{AQP2Cre}$) mice were generated in order to determine the role of renal principal cell MR in the control of sodium reabsorption. However, before generating the $MR^{AQP2Cre}$ mice, the inactivation of MR in principal cells was expected to be the cause of lethality in MR knockout mice. Indeed, germline inactivation of the mouse MR gene results in

early postnatal lethality due to renal loss of sodium and water caused by strongly impaired ENaC activity in renal principal cells and colon. Since AQP2 is already expressed prenataly (88), it was expected that the early targeting of MR in all principal cells would mimic the early postnatal phenotype of the MR knockout mice. To be able to induce the MR mutation only in adulthood, an inducible renal principal cell-specific gene inactivation system was developped in parallel using the same genomic DNA fragment as for the construction of the constitutive transgene. The inducible recombination system that was used is based on a fusion protein consisting of the Cre recombinase and a mutated ligand-binding domain of the human estrogen receptor (89). The Cre fusion protein ($CreER^{T2}$) is not activated by endogenous estrogen but by the synthetic ligand tamoxifen. If expressed in the absence of tamoxifen, the inducible $CreER^{T2}$ remains in the cytoplasm. In the presence of tamoxifen, $CreER^{T2}$ is translocated to the nucleus where it can exert its enzymatic activity and therefore leads to recombination of floxed alleles (79, 81, 90).

3.2.1. Generation of AQP2CreER^{T2} mice

Transgenic mice expressing the $CreER^{T2}$ fusion protein under the control of the AQP2 gene (AQP2$CreER^{T2}$ mice) were generated as described for the constitutive AQP2Cre mice. Briefly, the PAC used for the generation of the constitutive AQP2Cre transgene, which was isolated from a mouse PAC library and contains a 156-kb genomic DNA fragment, was modified by homologous recombination in bacteria in order to introduce the $CreER^{T2}$ fusion protein coding sequence at the ATG of the AQP2 locus. The cloning of the construct was performed using the same strategy as for the constitutive approach, except that a plasmid (pIndu), containing the $CreER^{T2}$ fusion protein coding sequence and an ampicillin resistance cassette flanked by two FRT sites, was used instead of the pConst plasmid. After removal of the ampicillin resistance cassette and release from the PAC backbone, the modified fragment (AQP2$CreER^{T2}$ transgene) was purified and microinjected into FVB/N oocytes. Transgenic offsprings were identified by dot blot on genomic DNA using a DNA probe detecting the Cre recombinase sequences as described for the constitutive AQP2Cre transgenic mice **(Figure 17A)**. Seven dot blot-positive mice were obtained and bred to C57Bl/6 mice to establish different transgenic lines. All dot blot-positive mice showed germline transgene transmission to the F1 generation. From them, three transgenic lines could be established and used for further analysis. For determination of the transgene copy number, Southern blot was performed on HindIII-digested genomic DNA. Hybridization with a probe recognizing the 5´ region of the AQP2 gene (5´ probe) revealed a 3.7-kb DNA fragment for the endogenous AQP2 gene (wild-type band), and a 2.3-kb DNA

fragment for the AQP2CreER^{T2} transgene integrated into the genome (transgenic band) **(Figure 17B)**. The copy number of the three transgenic lines was determined as 1 copy, 4 copies and 9 copies, respectively.

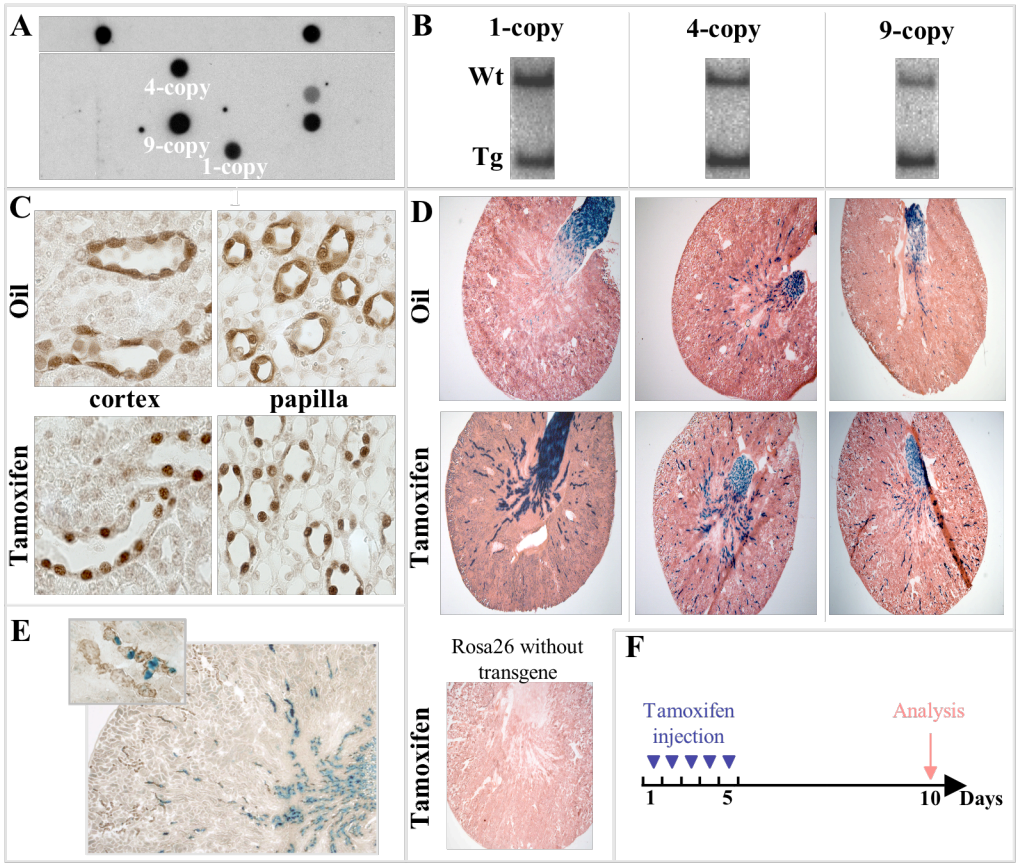

Figure 17. Identification and characterization of the AQP2CreER^{T2} mouse transgenic lines. A: Picture of the membranes of two dot blots probed for the presence of the AQP2CreER^{T2} transgene in offsprings obtained after oocyte injection. 1-copy, 4-copy and 9-copy: founders of the 1-copy line, 4-copy line and 9-copy line, respectively. **B:** Copy number Southern blot of HindIII-digested genomic DNA hybridized with the 5´probe detecting the AQP2 promoter sequence present in the transgene and in the endogenous locus, as illustrated in Figure 7. Wt: wild-type band; Tg: transgenic band. **C:** Immunohistochemical staining for Cre recombinase on paraffin sections from oil- or tamoxifen-injected AQP2CreER^{T2} mice. **D:** Kidney cryosections from oil- or tamoxifen-injected AQP2CreER^{T2}//Rosa26 mice stained for X-gal (blue staining) and counter-stained with eosin. A kidney cryosection from a tamoxifen-injected Rosa26 mouse stained for X-gal and counter-stained with eosin was used as control without transgene. **E:** Kidney cryosection from a tamoxifen-injected AQP2CreER^{T2}//Rosa26 mouse of the 1-copy line stained for X-gal (blue staining) and AQP2 expression (brown staining). The picture in the little pannel shows CDs from the cortical region at a higher magnification with AQP2-positive cells without recombination. **F:** Time-course of tamoxifen injection and analysis of recombination.

3.2.2. Analysis of AQP2CreER^{T2} mice

In order to assess the functionality of the CreER^{T2} fusion protein, the nuclear translocation of the fusion protein upon tamoxifen treatment was investigated by immunohistochemistry on cryosections from mice carrying the AQP2CreER^{T2} transgene, injected with vehicle (oil) or tamoxifen, and killed 1 hour after injection. In vehicle-injected mice, the CreER^{T2} fusion protein

was located in the cytoplasm and also in the nucleus of CD principal cells of the cortex and medulla. In tamoxifen-injected mice, a strong nuclear Cre staining was observed in principal cells, whereas no fusion protein was detected in the cytoplasm, reflecting the nuclear translocation upon tamoxifen induction **(Figure 17C)**. In addition, the 4-copy line showed stronger expression of the $CreER^{T2}$ fusion protein than the 2-copy line, which displayed a stronger $CreER^{T2}$ expression than the 1-copy line, indicating a copy number-dependent $CreER^{T2}$ protein expression (data not shown).

To determine the ability of the Cre recombinase to selectively recombine conditional alleles in renal principal cells *in vivo*, the $AQP2CreER^{T2}$ mice were bred to a Cre reporter line (Rosa26 mice) (91). The Cre reporter line carries at the ROSA26 locus a knock-in of a loxP-flanked STOP cassette in front of a LacZ coding sequence encoding the β-galactosidase. The β-galactosidase cannot be expressed from the Cre reporter allele unless the STOP cassette is excised after Cre-mediated recombination. Offsprings carrying both the $AQP2CreER^{T2}$ transgene and the Cre reporter allele (abbreviated as $AQP2CreER^{T2}$//Rosa26 mice), confirmed by PCR analysis on genomic DNA, received one i.p. injection of 1 mg tamoxifen per day for 5 consecutive days. Ten days after the last injection, mice were sacrificed and kidneys collected. Cryosections were X-gal stained to reveal expression of the β-galactosidase reporter gene indicating successful Cre-mediated recombination **(Figure 17D)**. As a control for recombination-independent β-galactosidase activity and for background of the X-gal staining procedure, Rosa26 mice carrying no $AQP2CreER^{T2}$ transgene were injected with tamoxifen. No blue signal was observed, indicating that the X-gal staining procedure does not produce any background and that the STOP cassette is tight **(Figure 17D)**. Vehicle (oil) injections were performed on $AQP2CreER^{T2}$//Rosa26 mice to serve as control for non-induced Cre-mediated recombination. These vehicle-treated mice showed blue staining in some tubular cells of the medullary rays of the outer and inner medulla, and very intense staining in tubular cells of the papilla, indicating constitutive recombination in these cells. Inducibility of the Cre-mediated recombination was assessed in $AQP2CreER^{T2}$//Rosa26 mice after tamoxifen injection. All three transgenic lines showed tamoxifen-induced β-galactosidase activity particularly in cortical CDs and much more intense β-galactosidase staining in the regions where the leakiness of the fusion protein was observed **(Figure 17D)**.

To determine whether Cre activity was specific for principal cells, colocalization of AQP2 protein expression and Cre-mediated recombination was assessed by immunohistochemistry for AQP2 on X-gal stained cryosections from $AQP2CreER^{T2}$//Rosa26 mice after tamoxifen induction. Since the 9-copy line could not be maintained because of low breeding efficiency,

further analysis was perfomed on the 1-copy and 4-copy lines only. In both lines, AQP2 protein expression and the recombination event were colocalized in every principal cells of the medulla. However, some AQP2-positive cells of the cortex did not show any blue signal **(Figure 17E)**.
Since the constitutive $MR^{AQP2Cre}$ mutant mice grew and developed normally and only upon low-sodium diet developed a salt-wasting phenotype, $AQP2CreER^{T2}$ mice were not used to generate inducible renal principal cell MR-deficient mice.

3.3. Identification of aldosterone-regulated genes possibly involved in the control of ENaC-mediated renal sodium reabsorption

As shown above, $MR^{AQP2Cre}$ mice show loss of apical αENaC expression in MR-deficient principal cells of CD and late CNT and impaired renal sodium reabsorption. In order to identify aldosterone-regulated genes involved in the control of ENaC-mediated sodium reabsorption in principal cells, gene expression profiling using microarrays was performed on a mouse kidney cortical CD principal cell line ($mpkCCD_{c14}$) in the presence or absence of aldosterone. *In vivo* validation of the aldosterone-regulated genes identified by gene expression profiling in the cell line was done on microdissected CDs of control mice kept under standard diet or challenged with low-sodium diet. The contribution of MR to the aldosterone response *in vivo* was assessed by comparing gene expression in microdissected CDs from principal cell MR-deficient ($MR^{AQP2Cre}$) mice and control mice.

3.3.1. Sodium transport in $mpkCCD_{c14}$ cells is mediated by ENaC and regulated by aldosterone via GR

The $mpkCCD_{c14}$ cell line established by Bens *et al.* has retained the sodium transport capacity as well as its regulation by aldosterone (92). In addition to the fact that the isolation of principal cells from native tissue is technically difficult, the use of the cell line allows easy hormone depletion, thereby increasing the fold change in gene expression between the untreated (baseline) and the aldosterone-treated state. In addition, the $mpkCCD_{c14}$ cell line allows easy measurement of the transepithelial sodium transport. Thus, this cell line provides an easy and powerful system to identify aldosterone-regulated genes involved in CD principal cell sodium reabsorption.

For determination of ion transport, mpkCCD$_{c14}$ cells were grown to confluence on permeable Transwell filters, which allow the formation of a tight epithelium. The short-circuit current (I_{sc}), which is a measure of the sodium flow across the epithelium from the apical to the basolateral compartment, was calculated from the measured transepithelial electrical resistance (R_T) and voltage (U_T) according to Ohm´s law ($I_{sc} = U_T / R_T$).

The effect of aldosterone on sodium transport was assessed by measuring I_{sc} in the presence or absence of aldosterone on cells incubated in hormone-free and steroid-free medium for 48 hours. Aldosterone was used at 10^{-6} M, a dose which was shown to lead to a strong elevation in I_{sc} in a time-dependent manner with a maximum increase observed after 4 hours of treatment (92). The rise in I_{sc} was due to a decrease in R_T and a increase in U_T, suggesting an effect of aldosterone on the ion transport. In the presence of amiloride, no induction by aldosterone could be observed, showing that it is the electrogenic amiloride-sensitive ENaC-mediated sodium transport that is stimulated by aldosterone **(Figure 18)**. Moreover, the I_{sc} levels measured after amiloride treatment were below the baseline levels measured in untreated cells, indicating the existence of a constitutive aldosterone-independent ENaC-mediated sodium transport.

In order to determine whether aldosterone regulation of sodium reabsorption in mpkCCD$_{c14}$ is mediated by MR or the glucocorticoid receptor (GR), the effect of aldosterone was measured with and without a 10-fold excess of the specific MR antagonist spironolactone, and with or without a 10-fold excess of the specific GR antagonist RU486. Spironolactone had no effect on I_{sc} in the presence of aldosterone, whereas RU486 prevented a rise in I_{sc} during aldosterone treatment, indicating that the aldosterone response is mediated by GR in mpkCCD$_{c14}$ cells **(Figure 18)**.

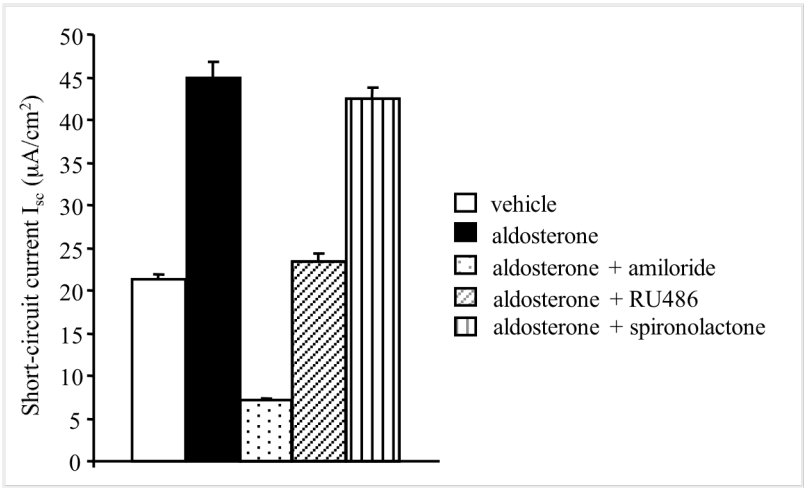

Figure 18. Sodium transport in mpkCCD$_{c14}$ cells is mediated by ENaC and regulated by aldosterone via GR. Transepithelial sodium transport was assessed by measuring the short-circuit current I_{sc} in the presence of vehicle or aldosterone (10^{-6} M), and with or without the ENaC blocker amiloride (5.10^{-6} M), the GR antagonist RU486 (10.10^{-6} M), or the MR antagonist spironolactone (10.10^{-6} M).

3.3.2. Gene expression profiling of mpkCCD$_{c14}$ cells

In order to identify aldosterone-regulated genes involved in the control of renal principal cell sodium reabsorption, microarrays analysis of gene expression was performed on mpkCCD$_{c14}$ cells in the presence or absence of aldosterone. Cells were grown on Transwell filters and incubated in hormone-free and steroid-free medium before and during treatment with vehicle (untreated control) or aldosterone for 1 hour, 2 hours or 4 hours. Determination of I_{sc} was performed at each time point to confirm the hormonal response. RNA samples prepared from lysed cells from two Transwell filters were pooled and used to generate probes for hybridization of the Affymetrix mouse expression MOE 430 2.0 A and B arrays. For each time point, three sets of untreated and aldosterone-treated RNA samples were independently prepared **(Figure 19A)**. Microarray data were controlled for quality, scaled, and normalized to correct for technical variations between arrays using the GC-RMA software of the Bio-Conductor Project. For each microarray, the GC-RMA software generates a signal value, which assigns a relative measure of abundance of the transcript. Additionally, a detection p-value is calculated, determining whether a transcript is reliably detected (present) or not detected (absent). For each time point (1 hour, 2 hours and 4 hours), a comparison analysis between arrays corresponding to untreated or aldosterone-treated cells was carried out to detect and quantify changes in gene expression. The software generates a quantitative estimate of the change in gene expression between the aldosterone-treated and untreated samples called fold-change (FC) and a corresponding p-value. A gene was considered as significantly changed when the FC of treated versus untreated cells was lower or higher than 1.4 and the p-value lower than 0.001 for at least one out of the three time points. The cut-off value for FC was chosen in order to obtain a reasonable number of genes. For the p-value, the cut-off value was chosen according to standard procedure. However, biologically relevant gene expression changes may or may not be effectively captured with a given statistical method, and the list of genes found to be significantly changed by one method may contain false positives and false negatives. In order to confirm the results obtained with the GC-RMA software and to narrow down the list of candidate genes by removing potential false positives and false negatives, microarray data were additionally analyzed with the SAS Microarray Solution software, and the lists of genes obtained with both methods were compared **(Figure 19B)**. For the analysis with the SAS Microarray Solution software, a FC lower or higher than 1.4 and a p-value lower than 0.002 were used as criteria for significantly changed genes. The cut-off value for the p-value was chosen in order to obtain a number of genes significantly changed in the range of that obtained with the GC-RMA software.

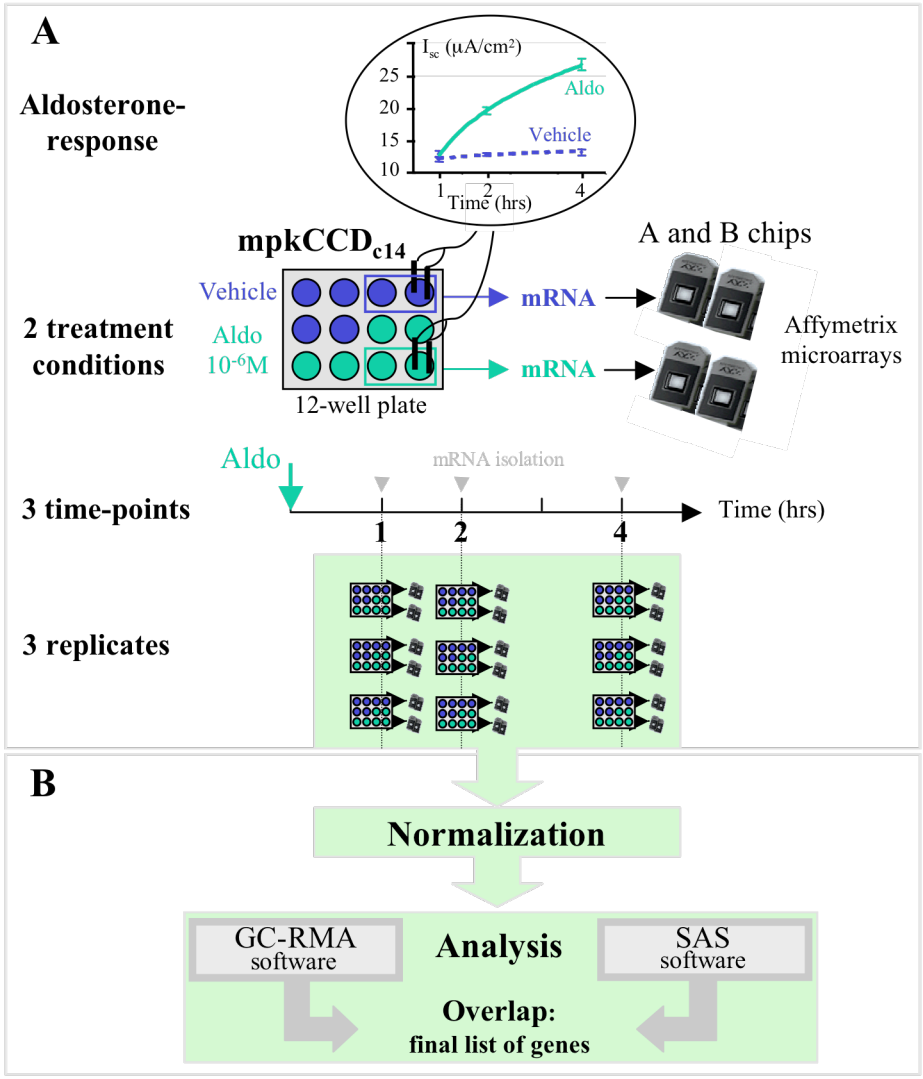

Figure 19. Gene expression profiling of mpkCCD$_{c14}$ cells. A: Experimental design: mpkCCD$_{c14}$ cells were grown on 12-well Transwell filter plates and treated with vehicle or aldosterone (10^{-6} M) for 1 hour, 2 hours or 4 hours. The aldosterone response was assessed by measuring the short-circuit current I_{sc}. For each treatment condition and each time-point, 3 replicates were independently prepared, mRNA was isolated from lyzed cells from two pooled Transwell filters and used for hybridization on Affymetrix MOE 430 2.0 A and B microarrays. **B:** Analysis of microarray data: microarray data were normalized and analyzed using the GC-RMA and SAS Microarray Solution softwares, and results obtained with both methods were compared to generate the final list of aldosterone-regulated genes.

Independent of the method used, no genes were identified as downregulated with the chosen cut-off values for FC and the p-value. To compare the lists of genes obtained with both methods, the significantly upregulated genes were ranked by decreasing FC for the three time points. There was a very good overlap between the two lists for the most highly induced genes. For the 1-hour aldosterone treatment, the same genes were found upregulated by both methods, except for one gene, which was not detected with the SAS Microarray Solution software. For the 2-hour time point, there was a 60% overlap between both lists, with almost 100% overlap for the 12 most strongly induced genes. At 4 hours, there was a 100% overlap for the 18 most strongly induced genes and 75% overlap for the 35 most induced genes with almost the same ranking (with decreasing FC). Mutual exclusion of the induced genes predicted with each software was

performed and only the genes, which were detected as aldosterone-upregulated by both methods, were further analyzed. The mutual exclusion allowed the identification of 10 induced genes at 1-hour aldosterone treatment, 30 induced genes at 2 hours and 47 upregulated genes at 4 hours **(Table 1)**. The serum- and glucocorticoid-regulated kinase 1 (SGK1) was identified as the most highly induced gene at each time point with both methods (GC-RMA estimated fold-changes: $FC_{1h} = 17.5$, $FC_{2h} = 26$, $FC_{4h} = 46$). The genes encoding the glucocorticoid-induced leucin zipper protein (GILZ, also called DSIP1), the serine/threonine-protein kinase 3 (PIM3) and the dual specificity phosphatase 6 (Dusp6) were found among the most induced transcripts at each time point with both methods.

1-hour aldosterone

GC-RMA		SAS	
Sgk	17,52	Sgk	3,71
Arfl4	3,43	Dsip1	1,77
Pim3	3,06	Pim3	1,62
Dsip1	3,05	Arfl4	1,52
Gadd45g	2,66	Ctgf	1,41
Per1	1,98	Per1	1,40
Dusp6	1,93	Dusp6	1,38
Trib1	1,90	Gadd45g	1,36
Klf6	1,69	Trib1	1,29
Ctgf	1,51	Klf6	1,23

2-hour aldosterone

GC-RMA		SAS	
Sgk	25,89	Sgk	4,30
Dsip1	3,90	Dsip1	2,13
Pim3	2,69	Pim3	1,56
Arfl4	2,61	1418469_at	1,54
Dnase1l2	2,57	Krt20	1,49
Usp2	2,38	Per1	1,49
Per1	2,33	Fkbp5	1,46
Fkbp5	2,31	Arfl4	1,46
AW011956	2,19	Usp2	1,37
4930422J18Rik	2,19	4930422J18Rik	1,36
Krt20	2,02	AW011956	1,36
1418469_at	1,99	Akap12	1,35
Gadd45g	1,86	1439163_at	1,33
2810474O19Rik	1,84	Ctgf	1,33
5730438N18Rik	1,76	Dnase1l2	1,32
Sh3md2	1,75	1454889_x_at	1,32
D5Ertd593e	1,72	Ehf	1,30
Gclc	1,69	Scnn1a	1,27
Rab17	1,63	5730438N18Rik	1,26
Ehf	1,58	Gclc	1,25
Scnn1a	1,56	D5Ertd593e	1,25
Herpud1	1,55	Ppl	1,24
Ppl	1,55	Gadd45g	1,23
Slc31a2	1,54	2810474O19Rik	1,23
Bcar3	1,49	Ccnd1	1,21
Ccnd1	1,47	Slc31a2	1,21
Ctgf	1,47	Herpud1	1,21
Akap12	1,46	Sh3md2	1,20
1439163_at	1,98	Bcar3	1,20
1454889_x_at	1,74	Rab17	1,19

4-hour aldosterone

GC-RMA		SAS	
Sgk	45,81	Sgk	5,76
Fkbp5	8,03	Dsip1	2,47
Sult1d1	7,73	1442025_a_at	2,15
Zfp145/Zbtb16	6,34	Zfp145/Zbtb16	2,06
Dsip1	5,58	Fkbp5	1,99
Dnase1l2	5,52	Sult1d1	1,96
Usp2	5,29	Dnase1l2	1,80
1442025_a_at	5,09	Krt20	1,76
Arg2	4,09	Arg2	1,69
Arfl4	3,90	Usp2	1,68
5730438N18Rik	3,71	Selenbp1	1,61
Pim3	3,38	Scnn1a	1,61
Selenbp1	3,37	Arfl4	1,60
Rhcg	3,17	AW011956	1,55
Mlph	3,10	Gclc	1,54
AW011956	3,07	5730438N18Rik	1,53
Scnn1a	2,87	Pim3	1,53
Gclc	2,85	Mlph	1,50
Rabl7	2,75	Akap12	1,45
Krt20	2,52	Rhcg	1,43
2810474O19Rik	2,29	Cited4	1,41
Sh3md2	2,22	Ehf	1,39
Gats	2,13	Sh3md2	1,34
Ehf	2,05	Man2a1	1,34
Kitl	2,00	Ppl	1,33
Man2a1	1,98	Per1	1,33
Bcat1	1,91	Kitl	1,33
Zfp91	1,88	Bcat1	1,32
Cntf///Zfp91	1,87	2810474O19Rik	1,32
Per1	1,78	Rabl7	1,31
Herpud1	1,77	1442026_at	1,28
Gadd45g	1,75	Herpud1	1,27
4930422J18Rik	1,74	Zfp91	1,27
Ppargc1a	1,73	4930422J18Rik	1,26
Ppl	1,69	Gats	1,25
Ngfb	1,69	1431213_a_at	1,24
Akap12	1,63	2610009E16Rik	1,24
D5Ertd593e	1,61	Cntf///Zfp91	1,24
Dock8	1,61	Gadd45g	1,23
1200016E24Rik	1,60	Ngfb	1,22
Cited4	1,59	D5Ertd593e	1,21
Slc39a14	1,58	1200016E24Rik	1,20
1442026_at	1,49	Ppargc1a	1,20
BC004853	1,47	Dock8	1,19
2610009E16Rik	1,47	Slc39a14	1,19
Elf3	1,43	BC004853	1,17
1431213_a_at	1,42	Elf3	1,11

Table 1. Lists of aldosterone-induced genes identified by gene expression profiling on mpkCCD$_{c14}$ cells after 1-hour, 2-hour or 4-hour aldosterone treatment. The fold changes in gene expression between aldosterone-treated and untreated cells, determined with the GC-RMA and the SAS Microarray Solution softwares, are indicated next to the gene name or Affymetrix ID for unknown genes. For each time-point of aldosterone treatment, genes are ranked by decreasing fold change. Genes chosen for further analysis *in vivo* are indicated with coloured rectangles.

The identified potential target genes that might be involved in the control of ENaC-mediated sodium reabsorption were checked for available functional information about the encoded proteins, using the Gene Ontology (GO) annotation of the mouse genome, and grouped by their possible mechanistic interaction with ENaC activity. Among the highly aldosterone-induced genes, genes encoding transcription factors (e.g. GILZ) were identified, as well as genes encoding proteins involved in post-translation modifications like kinases (e.g. SGK1, PIM3), ubiquitination proteins (e.g. the ubiquitin-specific protease 2 USP2), or proteins involved in protein transport (e.g. the GTPase RAB17). **Figure 20A** shows these potentially interesting genes as well as the pathways and protein functions used for classifying the aldosterone-regulated genes obtained in the microarray experiment.

The action of aldosterone on sodium transport can be operationally divided into two major phases: an early phase of sodium transport increase, and a late phase starting around 3 hours after hormone addition, during which a further increase in transport activity is observed. To distinguish the early aldosterone-regulated genes from the late aldosterone-regulated genes and to identify genes involved in the control of ENaC during both phases, a hierarchical cluster analysis of RNA expression data was used to group genes with similar expression profiles during the aldosterone treatment (1 hour, 2 hours and 4 hours) **(Figures 20B and 20C)**. SGK1, GILZ and PIM3 showed a clear increase in mRNA expression already after 1 hour of aldosterone treatment and remained highly induced during the 4 hours of treatment. USP2, RAB17, and interestingly also αENaC, were found to be upregulated after 2 hours and 4 hours of treatment.

Since aldosterone induction suggests a direct regulation under the transcriptional control of the hormone receptor, a search for glucocorticoid response elements (GREs) in the promoter region (10 kb upstream of the ATG) (13) was performed with the Possum program using the consensus sequence CGZACAANNTGTYCTK (93) provided as a weighted matrix in the TRANSFAC program (94). Apparent GRE sequences, matching the consensus sequence with a threshold value of at least 85%, were found in the promoter regions of PIM3 (87%), GILZ (86%) and SGK1 (85%).

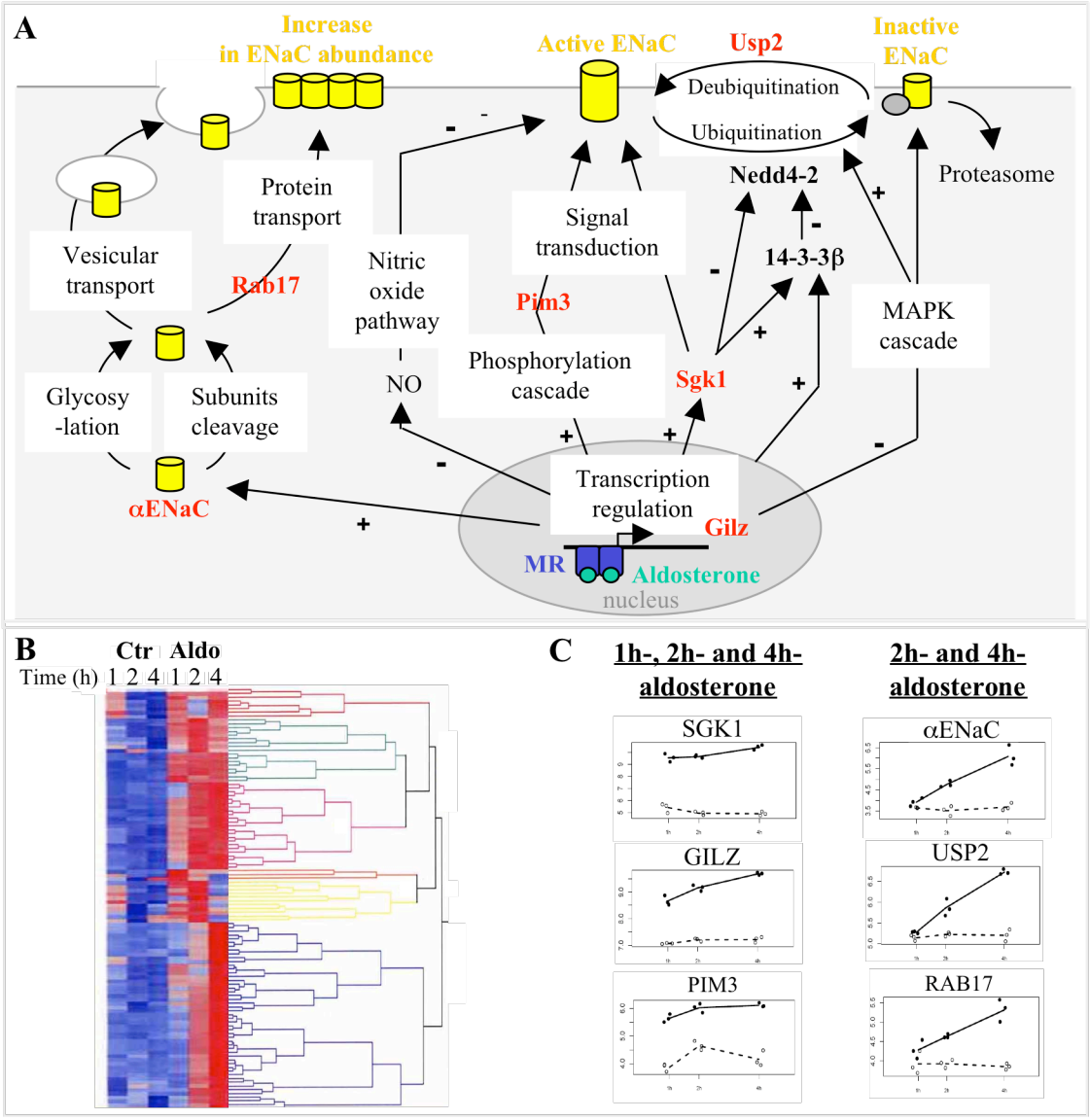

Figure 20. Identification of aldosterone-induced genes potentially involved in regulation of ENaC activity. A: Schematic representation of the different pathways potentially involved in the regulation of ENaC upon aldosterone stimulation, leading to increased sodium reabsorption in renal principal cells. The genes identified as aldosterone-induced by gene expression profiling in mpkCCD$_{c14}$ cells and potentially involved in the ENaC regulatory pathways are indicated in red. **B:** Hierarchical cluster analysis of transcripts significantly changed after 1-hour, 2-hour and 4-hour aldosterone treatment. Changes in expression ($\log_2$ ratio) are scaled by differences in colour for each transcript. The blue and red scales indicate decreases or increases in expression. **C:** Expression profiles of the serum- and glucocorticoid-regulated kinase 1 (SGK1), the glucocorticoid-induced leucin zipper protein (GILZ), the serine/threonine-protein kinase 3 (PIM3), the epithelial sodium channel subunit α (αENaC), the ubiquitin-specific protease 2 (USP2) and the GTPase Rab17 (RAB17) during aldosterone treatment. The graphs represent the $\log_2$ expression values at each time-point of aldosterone treatment. Open and filled circles represent estimated $\log_2$ expression values from untreated and aldosterone-treated cells, respectively. Broken and solid lines connect average of $\log_2$ expression values in untreated and aldosterone-treated cells, respectively.

3.3.3. Validation of aldosterone-induced genes in microdissected CDs

To validate the microarray experiment *in vivo*, the expression of selected genes (αENaC, SGK1, GILZ, PIM3, RAB17, 14-3-3β and USP2) was checked by quantitative real-time PCR (RT-PCR) in microdissected collecting ducts (CDs) of MR-expressing control mice fed with standard diet or low-sodium diet for 10 days that lead to a 7-fold elevation of plasma aldosterone levels in control mice. CDs were identified by the presence of branching connections, which define the end of the CNT and the start of the CD. The mRNA was isolated and RT-PCR carried out using HPRT as endogenous housekeeping gene for normalization. The analysis was focused on previously identified aldosterone-induced genes as positive controls, like αENaC, SGK1 and GILZ, and on candidates derived from the microarray experiment on mpkCCD$_{c14}$ cells, whose protein function could obviously be involved in ENaC regulation by aldosterone, like Rab17, a protein involved in protein transport, the kinase Pim3, which contains a GRE in its promoter region, and the ubiquitin-specific protease Usp2, which could activate ENaC by deubiquitination of the channel. The protein 14-3-3β was also analyzed since it was described to participate in the regulation of ENaC activity (95).

As shown in **Figure 21A**, SGK1 and USP2 gene expression underwent upregulation in CDs from control mice under low-sodium diet compared to standard diet, confirming the aldosterone response observed in the cell line. 14-3-3β was also induced under low-sodium diet. αENaC, GILZ and PIM3 showed a tendency to be upregulated under low-sodium diet, but the increase did not reach statistical significance. RAB17, which was found strongly induced in the cell line with a FC similar to the one for αENaC, did not show any induction under low-sodium diet in CDs of control mice.

3.3.4. Effect of MR deficiency on the aldosterone response *in vivo*

In order to investigate *in vivo* the role of MR in mediating the induction by aldosterone of genes potentially involved in the control of ENaC-mediated renal sodium reabsorption, quantitative RT-PCR was performed on mRNA isolated from microdissected CDs of principal cell MR-deficient (MR^{AQP2Cre}) and control mice challenged with low-sodium diet (10 days). As expected, despite strong plasma aldosterone elevation in MR^{AQP2Cre} mice (10-fold compared to control mice), expression levels of SGK1 and PIM3 were significantly reduced in the mutants, showing

that the aldosterone regulation of these genes, in response to the low-sodium diet, is mediated by MR in CDs **(Figure 21B)**. Gene expression levels of αENaC showed only a tendency to be reduced in the mutants, suggesting that MR might also mediate the upregulation of αENaC by aldosterone in CDs. In contrast, no change in gene expression was observed for GILZ, 14-3-3β and USP2, suggesting that the induction of GILZ, 14-3-3β and USP2 expression by aldosterone is not dependent on MR.

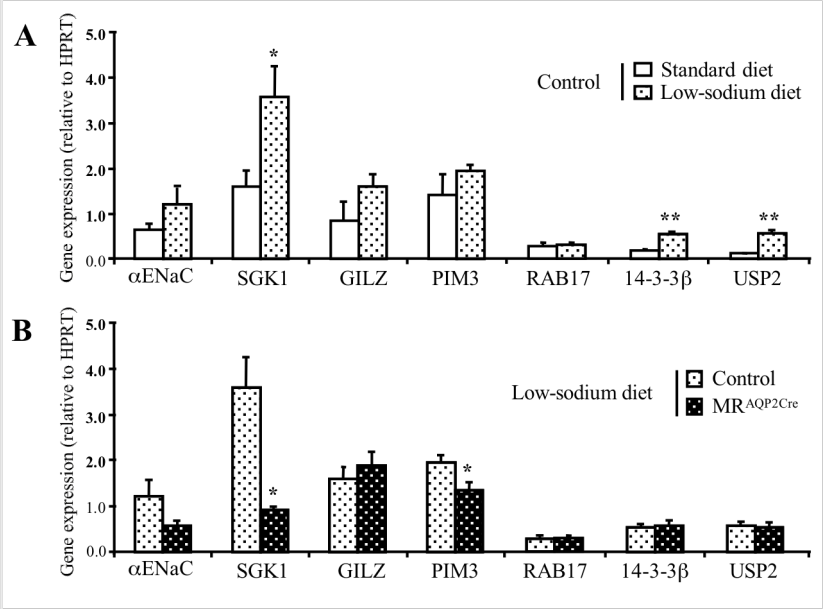

Figure 21. Gene expression analysis by real-time PCR on microdissected CDs from control (MR^{flox}) mice or principal cell MR-deficient ($MR^{AQP2Cre}$) mice. Relative expression of genes (versus HPRT) in microdissected collecting ducts (CDs) of control mice under standard or low-sodium diet (10 days) (**A**) or in microdissected CDs of control and $MR^{AQP2Cre}$ mice under low-sodium diet (10 days) (**B**). n = 5 per group. *P<0.05, **P<0.005 (t-test low-sodium diet versus standard diet, or $MR^{AQP2Cre}$ mice versus control mice).

4. DISCUSSION

4.1. Selective inactivation of MR in mouse renal principal cells

4.1.1. $MR^{AQP2Cre}$ mice are viable and show MR deficiency in all principal cells of the CD and late CNT

The present study reports the generation of mice with specific inactivation of the MR gene in renal principal cells ($MR^{AQP2Cre}$ mice). $MR^{AQP2Cre}$ mice were generated using the Cre-loxP recombination system by crossing mice harboring a conditional MR allele with transgenic mice expressing the Cre recombinase under the control of the regulatory elements of the mouse AQP2 gene, which is expressed in principal cells of the collecting duct (CD) and connecting tubule (CNT) (40). The AQP2 promoter was already used for Cre recombinase expression to target renal principal cells. However, both a 14-kb human and a 9.5-kb mouse AQP2 promoter fragments gave variegated patterns of transgene activity (96, 97). Therefore, a PAC-derived large genomic DNA fragment containing a 125-kb 5′ upstream region, thought to carry all elements required for high-fidelity tissue-specific and temporal regulation of the AQP2 gene activity (76), was used to generate the transgene. Furthermore, the use of a PAC-derived transgene should allow a copy number-dependent expression of the transgene (98).

Whereas the germline inactivation (knockout) of the mouse MR gene results in early postnatal lethality due to a massive renal loss of sodium and water (29), the renal principal cell-specific inactivation of MR did not impair survival. Therefore, $MR^{AQP2Cre}$ mice allowed the investigation of the role of principal cell MR in regulation of epithelial sodium channel (ENaC)-mediated sodium reabsorption. In contrast to the MR knockout mice, not all tight epithelia that are involved in sodium reabsorption were targeted in $MR^{AQP2Cre}$ mice. The use of the regulatory elements of the mouse AQP2 gene restricted the MR deficiency to the principal cells in kidney. The analysis of Cre, MR and αENaC expression by immunofluorescence revealed that the Cre expression of the PAC-derived transgene resembles the AQP2 expression pattern, with strong expression in CD and decreasing levels along the CNT towards the early CNT (40). The AQP2Cre transgene used in the present study therefore allowed the targeting of all ENaC-expressing principal cells of the CD and late CNT. The targeted cells were MR-negative and showed no apical αENaC expression. However, MR and apical αENaC expression was still

observed in the early CNT and late DCT, which were not targeted due to absence of Cre expression. These data demonstrate for the first time *in vivo* by genetic means that αENaC trafficking to the cell surface is strictly dependent on MR function.

4.1.2. The late CNT is an important site of MR-regulated ENaC-mediated sodium reabsorption

MR knockout mice die in the second week after birth, due to severe renal loss of sodium and water, and show decreased ENaC-mediated sodium reabsorption in kidney and colon (29). In contrast, $MR^{AQP2Cre}$ mice are viable, grow normally and show unaltered absolute sodium excretion when fed with a standard diet. When challenged with a low-sodium diet, $MR^{AQP2Cre}$ mice suffer from a continuous sodium wasting, as indicated by elevated absolute sodium excretion, and from a continuous water loss, as shown by the continuous increased urine volume associated with a loss of bodyweight.

To counterbalance the loss of MR in the principal cells of the CD and late CNT, the renin-angiotensin-aldosterone system (RAAS) was activated in $MR^{AQP2Cre}$ mice under standard as well as under low-sodium diet, as detected by the strongly elevated plasma aldosterone levels. Under standard diet, the aldosterone increase was apparently sufficient to achieve a complete compensation. However, when sodium supply was limited, the even stronger activation of the RAAS could no longer fully compensate the MR deficiency in $MR^{AQP2Cre}$ mice. It was previously reported that mice with αENaC deficiency in the CD ($\alpha ENaC^{Hoxb7Cre}$ mice) showed no change in renal sodium and water excretion (99). Compared to controls, the αENaC-deficient mice showed normal plasma aldosterone levels on both standard and low-sodium diet indicating that the αENaC loss in CD did not result in any impairement of sodium reabsorption. These results led to the conclusion that the increased renal sodium excretion and the observed elevation of plasma aldosterone levels measured in $MR^{AQP2Cre}$ mice result primarily from the loss of MR in the late CNT. The importance of the CNT in ENaC-mediated sodium reabsorption is highlighted by a recent patch-clamp study, which showed that ENaC-mediated sodium transport is several times higher in the CNT than in the CD in aldosterone-treated rats (100). This is consistent with a previous study on isolated perfused nephron segments, which showed that the rate of sodium reabsorption is much higher in the CNT than in the CD (101).

Since in MR knockout mice most of the amiloride effect on ENaC activity is abolished (29), ENaC activity in $MR^{AQP2Cre}$ mice was expected to be clearly reduced. Therefore, an increase in the fractional excretion of sodium ($FE(Na^+)$) and a reduced amiloride-sensitive portion of the

$FE(Na^+)$ were expected in the mutants. However, $MR^{AQP2Cre}$ mice showed, within an acute 2-hour sampling procedure, only a tendency to higher $FE(Na^+)$ as compared to controls. Morover, amiloride treatment led to a similar strong increase in $FE(Na^+)$ in both genotypes. Most likely, the early CNT and the late distal convoluted tubule (DCT) that were not targeted and consequently still express apical ENaC are responsible for the preserved amiloride action. Since in the untargeted colon of $MR^{AQP2Cre}$ mice ENaC activity is increased due to elevated plasma aldosterone levels, increased sodium transport in the early CNT and late DCT is also expected, which represents an intrinsic renal compensatory mechanism.

The unchanged acute $FE(Na^+)$ and preserved ENaC activity in $MR^{AQP2Cre}$ mice are not easy to reconcile with the salt-wasting syndrome leading to a continuous loss of bodyweight as it was observed at low sodium supply. A possible explanation is that the assessment of acute $FE(Na^+)$ is not sensitive enough as it only allows the detection of a 3-fold increase as measured in heterozygous MR knockout mice (29). Therefore, minor changes that still could account for the 70% increase observed in absolute sodium excretion over 24 hours, as well as minor changes in the amiloride-sensitive part of the $FE(Na^+)$, might have escaped from this type of analysis. To detect minimal changes in renal ENaC activity, more sophisticated quantitative analysis using patch-clamp of single cells or microperfusion of nephron segments are required. However, the visually indistinguishable boundary of the early and late CNT that can vary from animal to animal hampers these types of analysis.

4.1.3. Other possible compensatory actions triggered by increased plasma aldosterone levels

Besides activating MR in untargeted principal cells of the early CNT and late DCT, the elevated plasma aldosterone levels may also activate sodium reabsorption mediated by the thiazide-sensitive sodium-chloride cotransporter (TSC) in the DCT, as well as the ENaC-mediated sodium reabsorption in the colon. For the colon, measurement of the amiloride-sensitive rectal transepithelial voltage showed that $MR^{AQP2Cre}$ mice exhibit a 30% increase in colonic ENaC activity. However, the colon is known to reabsorb only about 5% of the total amount of reabsorbed sodium. Moreover, sodium transport in the colon is almost absent after weaning compared to the early life time (102). Thus, it is unlikely that colonic ENaC activity plays a major role in the compensation of MR loss in CD and late CNT. Since the renal principal cells were selectively targeted, the analysis of $MR^{AQP2Cre}$ mice was focused on ENaC-mediated renal sodium reabsorption. However, several studies had shown that the thiazide-sensitive sodium-chloride transport (103) and TSC abundance in DCT (87) are both induced by aldosterone via

MR (104). In order to determine whether the 10-fold increase in plasma aldosterone levels observed in $MR^{AQP2Cre}$ mice would also act on TSC, thus leading to increased sodium reabsorption, the activity of the sodium-chloride cotransporter was assessed by measuring renal $FE(Na^+)$ before and after application of thiazide. No gain of TSC function was observed in mutants compared to control mice. These results suggest that the DCT does not participate to the compensation for the loss of MR in CD and late CNT.

4.2. Generation of an inducible renal principal cell-specific gene inactivation system

Since germline inactivation of the mouse MR gene (MR knockout mice) results in early postnatal lethality due to massive loss of sodium and water caused by impaired ENaC activity in renal principal cells and colon (29), it was expected that the prenatal constitutive inactivation of MR in renal principal cells ($MR^{AQP2Cre}$ mice) would result in a similarly strong phenotype that may even lead to lethality. To be able to induce the MR gene inactivation in adulthood, an inducible renal principal cell-specific gene inactivation system was generated in parallel using the Cre-loxP recombination system in combination with the $CreER^{T2}$ fusion protein. The fusion protein consists of the Cre recombinase and a mutated ligand-binding domain of the human estrogen receptor, which allows the nuclear translocation of the fusion protein upon tamoxifen treatment, resulting in tamoxifen-dependent gene inactivation (89). Transgenic mice expressing the $CreER^{T2}$ under the control of the regulatory elements of the mouse AQP2 gene were generated and three transgenic lines with different copy numbers of the transgene (1, 4 and 9 copies) were established and analyzed. Induction of recombination was achieved by i.p. injection of 1 mg tamoxifen once a day for 5 days (105). The expression of the $AQP2CreER^{T2}$ transgene resembles that of the endogenous AQP2 gene and of the constitutive AQP2Cre transgene. In the different transgenic lines, the expression of the Cre recombinase shows only copy number-dependent quantitative differences but similar expression pattern. Nuclear translocation of the fusion protein upon tamoxifen treatment was observed 2 hours after tamoxifen injection in every line, indicating that the $CreER^{T2}$ fusion protein is functionning.

To determine the recombination efficiency, each line was crossed with a Cre reporter mouse line (Rosa26 mice) containing a loxP-flanked STOP cassette in front of a lacZ expression cassette within the ubiquitously expressed ROSA26 locus (91). Cre-mediated recombination in tamoxifen-injected $AQP2CreER^{T2}$//Rosa26 mice deleted the STOP cassette and thereby resulted

in β-galactosidase expression that was revealed by X-gal staining on cryosections. In all three transgenic lines, tamoxifen-independent recombination was observed in the papilla region and in some tubular cells of the medullary rays in the outer and inner medulla, indicating that the control of Cre activity exerted by the ER^{T2} domain was not tight. Since every recombination event results in an irreversible deletion of the STOP cassette, cells containing a recombined lacZ allele will accumulate overtime. Therefore, even low leakiness of the $CreER^{T2}$ fusion protein activity in the absence of tamoxifen can result in a high number of recombined cells. Moreover, the possible presence of tamoxifen-like molecules in the renal papilla, which could bind to the ER^{T2} domain, could lead to induction of the recombination in this region of the kidney. Nevertheless, analysis of β-galactosidase staining in tamoxifen-injected AQP2CreER^{T2}//Rosa26 mice revealed tamoxifen-induced recombination in most of the renal principal cells for all three transgenic lines. The pattern and degree of recombination were comparable to that observed in the constitutive AQP2Cre line. The two inducible lines with the highest transgene copy number (4 and 9 copies) showed a higher efficiency of the tamoxifen-induced β-galactosidase activity.

To determine whether Cre activity was restricted to principal cells, colocalization of AQP2 protein expression and Cre-mediated recombination was assessed by immunohistochemistry for AQP2 on X-gal stained cryosections from AQP2CreER^{T2}//Rosa26 mice after tamoxifen induction. In the medulla, AQP2 expression and the recombination event were colocalized. However, few AQP2-positive cells of the cortex did not show any blue signal, suggesting a lack of recombination in these cells. Since in the case of the inducible AQP2CreER^{T2} transgene, the Cre activity is only transiently activated during the period of tamoxifen application, the pattern of recombination reflects expression of the fusion protein at the time period of tamoxifen treatment, which might not be enough to induce recombination in every cell. Injection of a higher dose of tamoxifen or the same dose but twice a day could extend the number of recombined cells.

Since the constitutive $MR^{AQP2Cre}$ mutant mice did not show any lethality allowing a detailed functional analysis of the phenotype, inducible renal principal cell-specific MR gene inactivation ($MR^{AQP2CreERT2}$ mice) were not generated. However, these $MR^{AQP2CreERT2}$ mice could improve the description of the recombination efficiency by analyzing the loss of MR upon tamoxifen treatment.

4.3. Identification of MR-regulated genes potentially involved in the control of principal cell ENaC-mediated sodium reabsorption

4.3.1. Gene expression profiling of mpkCCD$_{c14}$ cells reveals aldosterone-induced genes potentially involved in ENaC regulation

To identify aldosterone-regulated genes involved in the control of ENaC-mediated sodium reabsorption in renal principal cells, microarray analysis was performed in a mouse kidney cortical collecting duct principal cell line (mpkCCD$_{c14}$) in the absence or presence of aldosterone. The effect of aldosterone on sodium transport was assessed by measuring the short-circuit current. The results of the amiloride treatment showed that sodium reabsorption in mpkCCD$_{c14}$ cells is mediated by ENaC. Kidney collecting ducts, like other targets for corticosteroid hormones, possess two types of corticosteroid receptors, which bind to the same palindromic DNA sequence (13): a receptor with a high affinity for aldosterone (MR) and a receptor with a low affinity for aldosterone (GR) (106),(107). The high concentration of aldosterone (10^{-6} M), necessary to stimulate maximal sodium reabsorption in mpkCCD$_{c14}$ cells, suggests that occupancy of GR by aldosterone is required. The question was therefore whether the increased sodium reabsorption elicited by aldosterone was mediated via the occupancy of MR and/or GR. The fact that the MR antagonist spironolactone had no effect on the short-circuit current in the presence of aldosterone, whereas the GR antagonist RU486 prevented completely the rise in the current induced by aldosterone, indicates that the ENaC-mediated sodium reabsorption in the mpkCCD$_{c14}$ cells is regulated by GR under high aldosterone concentrations, confirming previous binding assays (92). However, it was shown before that high doses of glucocorticoids in adult salt-rescued MR knockout mice normalized the urinary sodium excretion and could increase ENaC activity, showing that the role of MR in activation of ENaC activity can be taken over by GR (108). Therefore, the mpkCCD$_{c14}$ cell line should still allow the identification of the aldosterone-regulated genes that are important for ENaC regulation *in vivo*.

To identify aldosterone-regulated genes, RNA from mpkCCD$_{c14}$ cells was subjected to microarray analysis after treatment with aldosterone or vehicle. The action of aldosterone can be operationally divided into two phases: an early phase of sodium transport increase mediated by aldosterone-induced regulatory proteins acting on the preexisting transport machinery (66), and a

late phase during which a further increase in transport activity correlates with an increase in channels, pumps, and other elements of the transport machinery (109, 110). Therefore, cells were treated with aldosterone for 1 hour, 2 hours or 4 hours to distinguish between aldosterone-regulated genes contributing to the early phase of the hormone response and those contributing to the late phase. As data analysis performed with the GC-RMA (111) and the SAS Microarray Solution softwares gave consistent results for each time point, mutual exclusion of the upregulated genes predicted with both softwares was performed and only genes found in common were further analyzed. This resulted in the identification of 53 genes upregulated by aldosterone. Downregulated genes were not found. One of the genes induced by aldosterone was the ENaC subunit α (αENaC), but its time course of induction (starting after 2 hours) indicates that the transcriptional activation of this gene takes place during the late phase of aldosterone response. Candidate genes for the early activation of ENaC activity should be already regulated by aldosterone during its early phase of action (before 2 hours). Among the early and most induced genes, SGK1, GILZ, DUSP6 and PIM3 were identified. SGK1 showed the highest fold change at each time point, consistent with previous gene expression profiling studies (61, 112). In addition, several other genes not previously described as induced by aldosterone were also identified, extending the list of aldosterone-regulated transcripts.

The aldosterone-regulated genes obtained from the microarray analysis were grouped by function of the encoded proteins, in order to identify those genes that are potentially involved in the regulation of ENaC activity. ENaC activity has been shown to be regulated at different levels: channel protein synthesis, distribution of the channels between intracellular pools and transport to the apical membrane, channel open probability and stability (113-115). Control of channel surface density and channel degradation involves covalent modifications of the ENaC proteins themselves and/or interaction with other regulatory proteins. Sgk1, one of the best characterized aldosterone-induced proteins involved in the regulation of ENaC activity, was shown to increase apical membrane ENaC by inhibiting the ubiquitin ligase Nedd4-2 through recruitment of 14-3-3 proteins, which reduces the ability of Nedd4-2 to ubiquitinate ENaC (68), (116, 117). Gilz has recently been shown to contribute to the early aldosterone stimulation of ENaC-mediated sodium current through inhibition of ENaC ubiquitination by Nedd4-2 via the ERK cascade (112). In addition to αENaC, Sgk1 and Gilz, the present study revealed that the ubiquitin-specific protease Usp2 is also induced by aldosterone. Ubiquitination is reversed by a number of proteases that specifically recognize ubiquitinated proteins and remove the ubiquitin tag (118). By deubiquitination of ENaC, Usp2 could participate to the activation of the channel. Similarly, the GTPase Rab17 was also found as aldosterone-induced. Rab17, expressed only in

kidney, liver and intestine, has been shown to regulate membrane trafficking through apical recycling of endosomes in polarized epithelial cells (119, 120) and could therefore be involved in ENaC regulation by participating to the trafficking of the channel to the apical membrane. Finally, it has also been shown that ENaC activity is regulated by phosphorylation via serine/threonine kinases (121). In this context, the early (1 hour) and marked induction by aldosterone of the expression of the PIM3 gene and the presence of a GRE in its promoter region makes PIM3 a potential newly described MR target gene involved in the mediation of the aldosterone response in renal principal cells.

4.3.2. The regulation of SGK1 and PIM3 by aldosterone is mediated by MR in microdissected CDs

Because of their high induction upon aldosterone treatment in mpkCCD$_{c14}$ cells and of their encoded protein function, PIM3, RAB17 and USP2 were chosen for further mRNA expression analysis *in vivo*. αENaC, SGK1 and GILZ were also included in the analysis as genes already described to regulate ENaC activity. To verify that these genes are also regulated by aldosterone *in vivo*, mRNA expression was analyzed by quantitative RT-PCR on microdissected collecting ducts (CDs) from control mice kept under standard diet or after 10 days of low-sodium diet, which lead to 7-fold increase in plasma aldosterone levels. The mRNA expression of 14-3-3β was also analyzed, despite the fact that this transcript was not detected in the cell line. SGK1, 14-3-3β and USP2 mRNA expression levels were significantly elevated in CDs after 10 days of low-sodium diet. αENaC, GILZ and PIM3 expression levels only showed a tendency to be upregulated after salt restriction, but the increase did not reach statistical significance. RAB17 mRNA expression levels did not show any change between both diet conditions. The results of the RT-PCR confirmed the microarray data for SGK1 and USP2 and suggest that these two genes, as well as 14-3-3β, are potential targets for aldosterone regulation of ENaC activity in CD principal cells. For αENaC, GILZ, PIM3 and RAB17, the discrepancy between the results from the microarrays and the RT-PCR on microdissected CDs, in terms of FC and statistical significance of FC, is probably due to the low number of observations and the lack of sensitivity of the system used. Indeed, in contrast to the cell line, which possesses only one type of cells (principal cells), microdissected CDs contain also intercalated cells, which do not express ENaC and therefore miss the aldosterone regulation, thus diluting the aldosterone response of the principal cells. Moreover, the microdissected CDs from control mice under standard diet are not hormone-depleted. Changes in gene expression occuring after switch to low-sodium diet might

therefore escape from this type of analysis. The use of adrenalectomized mice infused with vehicle or aldosterone could increase the sensitivity of the system and allow a more complete identification of aldosterone-regulated transcripts.

To establish a correlation between the modulation of the mRNA levels of the genes induced by aldosterone via MR and potentially involved in ENaC regulation, and the physiological effects of the loss of MR in CD principal cells in $MR^{AQP2Cre}$ mice, quantitative RT-PCR was performed on microdissected CDs from control and $MR^{AQP2Cre}$ mice after 10 days of low-sodium diet. Despite strongly elevated plasma aldosterone levels in $MR^{AQP2Cre}$ mice, the expression levels of SGK1 and PIM3 were clearly reduced in mutant mice after 10 days of low-sodium diet. These results show for the first time *in vivo*, using a non-pharmacological approach, that MR is regulating the transcription of SGK1 and PIM3 in CDs. This suggests that SGK1 and PIM3 are involved in the impaired ENaC-mediated sodium reabsorption leading to salt wasting in $MR^{AQP2Cre}$ mice. However, the action of aldosterone to control renal sodium reabsorption is most likely pleiotropic and might therefore not be only dependent on SGK1 and PIM3. This was already concluded from the analysis of SGK1 knockout mice that showed, despite elevated plasma aldosterone levels, only a mild salt-wasting phenotype (70). The expression levels of αENaC showed a tendency to be reduced in $MR^{AQP2Cre}$ mice, but not significantly probably due to the lack of sensitivity of the system used, as discussed before. The regulation of αENaC by aldosterone might therefore be also mediated by MR. The expression levels of GILZ, 14-3-3β and USP2 were unchanged between control and mutant mice, suggesting that the regulation of these three genes by aldosterone is not dependent on MR.

5. CONCLUSION AND OUTLOOK

It is still widely accepted that "the collecting duct is the main nephron segment where sodium reabsorption is adjusted to maintain excretion at a level appropriate for dietary intake" (122). This statement reflects the emphasis that has been placed on the role of the collecting duct (CD) in the final control of sodium reabsorption. The recent generation of the CD αENaC-deficient mice has demonstrated that ENaC expression in the CD is not required for maintaining sodium balance (99). The present study reports that mice deficient for MR in principal cells of the whole CD and late connecting tubule (CNT) ($MR^{AQP2Cre}$ mice) grow and develop normally under standard diet. The switch to low-sodium diet results in continuous loss of bodyweight due to increased renal loss of sodium and water. The mutant mice show dramatically elevated plasma aldosterone levels on both standard and low-sodium diet. Under low-sodium diet, no apical αENaC expression was detectable in the late CNT and CD. These data show for the first time using a genetic approach the crucial role of MR for ENaC trafficking *in vivo*. In adition, the presented data show that the targeted inactivation of MR in CD and late CNT can be compensated on a standard diet by activation of the renin-angiotensin-aldosterone system, but that this compensation fails when sodium supply is limited. The preserved renal ENaC activity observed in the mutant mice indicates that the deficient ENaC-mediated sodium reabsorption in the late CNT and CD can be compensated to a large extent by the late distal convoluted tubule (DCT) and early CNT, demonstrating the pivotal role of these two distal nephron segments. Whether there is remaining ENaC-mediated sodium reabsorption in MR-deficient CD cells of $MR^{AQP2Cre}$ mice and to which extent ENaC-mediated sodium reabsorption is upregulated in MR-expressing cells of the late DCT and early CNT of $MR^{AQP2Cre}$ mice remains to be determined. This would require a more sophisticated quantitative assessment of the renal ENaC activity using patch-clamp analysis of single cells and/or microperfusion of distinct tubular segments, and analysis of sodium reabsorption using micropuncture.

The present study also reports the establishment of a tamoxifen-inducible renal principal cell-specific gene inactivation system in mice using the Cre-loxP recombination system. Cre reporter mice revealed induction of gene inactivation but also some leakiness of the fusion protein. The generation of inducible renal principal cell-specific MR-deficient mice will allow, by analyzing the loss of MR, a better assessment of the recombination efficiency.

Finally, the present work describes additional aldosterone-regulated genes and shows that SGK1 and USP2 are induced upon low-sodium diet in microdissected CDs. In addition, the present study shows for the first time *in vivo* by genetic means that the regulation of SGK1 and PIM3 by aldosterone in CDs is mediated by MR.

6. MATERIALS AND METHODS

6.1. Materials

6.1.2. Chemicals and radioactivity

The chemicals used were provided by Fluka (Germany), Roth (Germany), Sigma (Germany), and Merck (Germany).
DNA probe radiolabeling was performed with α-^{32}P-dCTP (3000 Ci/mmol, 10 mCi/ml) provided by Amersham (Germany).

6.1.3. Enzymes

Restriction enzymes were provided by Roche Molecular Biochemicals (Germany), New England Biolabs (Germany), or Promega (Germany). Taq Polymerase, Klenow-fragment, Shrimps alkaline phosphatase, T4 DNA ligase, and T4 polynucleotide kinase were provided by Roche Molecular Biochemicals (Germany), *Pfu* DNA polymerase by Promega (Germany), RNase A by Qiagen (Germany), and proteinase K by Roth (Germany). All enzymatic reactions were processed in the reaction buffer provided by the manufacturer.

6.1.4. Bacterial strains

DH10B:
The PAC library RPCI21 (RPZ, Germany) has been cloned in the DH10B bacterial strain. Therefore all steps for the modification of the PAC were done in DH10B bacteria.

NM554:
This bacterial strain was provided by Stratagene (Germany) and used for the cloning of plasmids. After preparation for transformation competency, bacteria were transformed with the plasmid by the heat-shock method.

6.1.5. Plasmids

pConst and pIndu:
Both plasmids, used as expression- and cloning-vectors for the generation of the constitutive and inducible transgenes respectively, were generated and provided by Dr. Erich Greiner (DKFZ, Heidelberg, Germany). These plasmids contain the human Cre recombinase (84) under the control of the CMV promoter. They also carry an ampicillin resistance cassette flanked by two FRT sites, which can therefore be removed by Flp recombination. The pIndu carries a fusion of the Cre recombinase with a mutated ligand-binding domain of the human estrogen receptor alpha, whose activity is induced by tamoxifen (89).

pBADR6K$\alpha\beta\gamma$tet^R (ET-plasmid) and p705-Flp:
Both plasmids, used to modify the PAC by homologous recombination in bacteria (ET-cloning), were provided by Dr. A. Francis Stewart (EMBL, Heidelberg, Germany).

6.1.6. DNA microarrays

The GeneChip Mouse Expression Arrays MOE 430 2.0 A and B were purchased from Affymetrix (USA). These two oligonucleotide arrays contain over 45000 probe sets representing more than 39000 transcripts and variants, including over 34000 well-characterized mouse genes.

6.1.7. Buffers and solutions

6.1.7.1. Isolation and storage of DNA

Plasmid DNA: TE buffer, pH 8.0: 10 mM Tris-HCl, pH 8.0
1 mM EDTA, pH 8.0

Genomic DNA: TE buffer, pH 7.4: 10 mM Tris-HCl, pH 7.4
1 mM EDTA, pH 8.0

Minipreps: STET buffer: 50 mM Tris-HCl, pH 8.0
50 mM EDTA
5% Triton X-100
8% saccharose

PAC DNA Mini and Midipreps: P1 buffer (Qiagen): 100 μg/ml RNase A
50 mM Tris-HCl, pH 8.0
10 mM EDTA, pH 8.0

P2 buffer (Qiagen): 200 mM NaOH
1% SDS

P3 buffer (Qiagen): 3 M potassium acetate, pH 5.5

DNA preparation from mouse tail: NID buffer: 50 mM KCl
10 mM Tris-HCl, pH 8.3
2 mM $MgCl_2$
0.1 mg/ml gelatine
0.45% NP40
0.45% Tween 20

Tail buffer: 50 mM Tris-HCl
100 mM EDTA
100 mM NaCl
20% SDS

6.1.7.2. DNA electrophoresis

50X Tris-acetate buffer (TAE) : 2M Tris
250 mM sodium acetate
50 mM EDTA, pH 8.0
pH 7.8 (adjusted with HCl)

Diluted 1X TAE was used as running buffer for gel electrophoresis.

6X loading buffer: 0.25% bromophenol blue
0.25% xylene cyanol FF
15% Ficoll 400

The marker Smart Ladder (Stratagene) was used as DNA size marker by loading 10 μl in one well.

6.1.7.3. DNA probe radiolabeling

5X OLB-C: 100 μl Solution A
250 μl 2 M HEPES, pH 6.6
150 μl Random Hexamers pd$(N)_6$ (50 $O.D._{260}$ dissolved in 550 μl TE)

Solution A: 1 ml Solution B
18 μl β-mercaptoethanol
5 μl each 100 mM dATP, dGTP, dTTP

Solution B: 1.25 M Tris-HCl, pH 8.0
125 mM $MgCl_2$

6.1.7.4. Southern blot

Denaturation buffer: 0.5 M NaOH
1.5 M NaCl

Neutralization buffer: 0.5 M Tris-HCl, pH 7.0
1.5 M NaCl

Blot buffer (20X SCC): 0.3 M sodium acetate
3 M NaCl
pH 7.0 (adjusted with NaOH)

6.1.7.5. Dot blot

Denaturation buffer: 0.5 M NaOH
1.5 M NaCl

Neutralization buffer: 0.5 M Tris-HCl, pH 8.0
1.5 M NaCl

Equilibration buffer: 0.2 M Tris-HCl, pH 8.0
2X SCC

6.1.7.6. DNA hybridization

Hybridization buffer: 0.5 M $NaHPO_4$, pH 7.2
(Church buffer) 1 mM EDTA, pH 8.0
7% SDS

Washing buffer I: 40 mM $NaHPO_4$, pH 7.2
1 mM EDTA, pH 8.0
5% SDS

Washing buffer II: 0.5 M $NaHPO_4$, pH 7.2
1 mM EDTA, pH 8.0
1% SDS

6.1.7.7. Bacteria culture media

LB medium: 10 g Bacto-trypton (Difco)
5 g yeast extract (Difco)
5 g NaCl
for 1 l final volume, pH 7.2 (adjusted with NaOH), autoclaved

LB Agar: 1X LB medium
1.5% (mass/volume) bacto-agar (Difco)

6.1.7.8. mpkCCD$_{c14}$ cell culture (92)

Standard culture medium (150 ml) : 75 ml HAMF´12 (Gibco)
75 ml DMEM (Gibco)
5 μg/ml insulin (Sigma)
5.10^{-8} M dexamethasone (Sigma)
60 nM selenium (Sigma)
5 μg/ml transferrin (Sigma)
5.10^{-8} M triodothyronine (Sigma)
10 ng/ml EGF (Sigma)
20 mM HEPES (Gibco)
2 mM glutamine (Gibco)
2% FCS (Seromad)
3.36 ml D-glucose (Sigma)

Hormone-free medium:
This medium has the same composition as the standard culture medium, but without insulin, dexamethasone, triodothyronine and EGF, and contains 2% CTS (Seromad) instead of FCS.

Hormone-free and serum-free medium:
This medium has the same composition as the hormone-free medium, but without CTS.

Cells were treated with aldosterone, amiloride, RU486 or spironolactone provided by Sigma (Germany).

6.1.7.9. DNA microarrays

5X first strand cDNA buffer: 50 mM Tris-HCl, pH 8.3
75 mM KCl
3 mM $MgCl_2$

5X second strand cDNA buffer: 25 mM Tris-HCl, pH 7.5
100 mM KCl
5 mM $MgCl_2$
10 mM $(NH_4)SO_4$
0.15 mM b-NAD^+

5X fragmentation buffer: 4 ml 1 M Tris-acetate, pH 8.1
0.64 g MgOAc
0.98 g KOAc
DEPC-water to 20 ml, filtered through 0.28-μm vacuum filter unit

6.1.7.10. DNA microinjection into mouse oocytes

Agarase buffer: 10 mM Tris-HCl, pH 6.5
1 mM EDTA, pH 8.0
100 mM NaCl
30 μM spermine
70 μM spermidine

Microinjection buffer: 10 mM Tris-HCl, pH 7.5
0.1 mM EDTA, pH 8.0
100 mM NaCl

The composition of the M2- and M16-media is decribed in (123).
Mice were superovulated by injection of PMS-gonadotropin and chorion-gonadotropin provided by Sigma.

6.1.7.11. Rosa26 mouse reporter assays

Fixation solution: 0.1 M PBS, pH 7.3
5 mM EGTA
2 mM $MgCl_2$
0.2% glutaraldehyde

Washing solution: 0.1 M PBS, pH 7.3
5 mM EGTA
2 mM $MgCl_2$
0.01% sodium-deoxycholat
0.02% NP40

Staining solution: 0.1 M PBS, pH 7.3
5 mM EGTA
2 mM $MgCl_2$
0.01% sodium-deoxycholat
0.02% NP40
10 mM $K_3[Fe(CN)_6]$[e] III (329.25 g/mol)
10 mM $K_4[Fe(CN)_6]$[f] II (422.4 g/mol)
0.5 mg/ml X-Gal in DMF

6.1.8. Genomic PAC library

The genomic PAC library RPCI21 (RZPD, Germany) constructed by K. Osoegawa (Rosewell Park Cancer Institute) was screened for PACs containing the AQP2 gene. The library represents 12.6 times the genome of a female 129/SvevTACfBr mouse. The genomic fragments of 147 kb are cloned in the P1-derived artificial chromosome (PAC) pPAC4. DNA clones are fixed on high-density filters, which were hybridized with a DNA probe recognizing the AQP2 gene. The positive clones were provided as transformed bacteria in agar with 0.025 mg/ml kanamycin.

6.1.9. mpkCCD$_{c14}$ cell line

The mpkCCD$_{c14}$ cell line was provided by Prof. Alain Vandewalle (INSERM Unité 478, Paris, France). This cell line is a clonal immortalized cell line derived from mouse cortical collecting

duct (92). In the present study, cells of passage number 5-20 were used (passage nuber 1 corresponds to the first passage after recieving the cell line from Paris).

6.1.10. Mouse strains

C57Bl/6:
This strain was used for the backcrossing of transgenic mice. Per definition, transgenic mice have 100% of C57Bl/6 genetic background after 10 generations of backcrossing with C57Bl/6 mice.

FVB/N:
This strain is an inbred mouse strain, which was used for transgenesis (oocytes microinjection).

6.1.11. Probes and primers

6.1.11.1. Primers for PCR

All primers used for PCR were ordered by MWG-Biotech AG (Munich, Germany).

Primers for analytic genotyping PCRs:

MR floxed allele:

MR flox-7	Forward	5´-CTGGAGATCTGAACTCCAGGCT-3´
MR flox-8	Reverse	5´-CCTAGAGTTCCTGAGCTGCTGA-3´
MR flox-10	Reverse	5´-TAGAAACACTTCGTAAAGTAGAGCT-3´

AQP2Cre and AQP2Cre-ER^{T2} transgenes:

AQP2-12	Forward	5´-AAGTGCCCACAGTCTAGCCTCT-3´
AQP2-13	Reverse	5´-GGAGAACGCTATGGACCGGAGT-3´
CAMK-2	Reverse	5´-CCTGTTGTTCAGCTTGCACCAG-3´

ROSA26 reporter:

ROSA-1	Forward	5´-TCTGCTGCCTCCTGGCTTCTGA-3´
ROSA-2	Reverse	5´-CCAGATGACTACCTATCCTCCCA-3´
ROSA-3	Reverse	5´-AAGCGCATGCTCCAGACTGCCT-3´

Primers for preparative PCR for amplification of homology arms:

5´homology arm:

AQP2-5´hom-1	Forward	5´-ATCGTTTAAACAGAGACGTCAATCCTTATCTG-3´
AQP2-5´hom-2	Reverse	5´-CATGCTGCTCGGCCTTCTGAG-3´

3´homology arm:

AQP2-3´hom-1	Forward	5´-GCTCTAGATGGGAACTCCGGTCCATAGCG-3´
AQP2-3´hom-2	Reverse	5´GATGCTAGCGTTTAAACTCGGGCTACTCACAGCATT-3´

6.1.11.2. Probes and primers for RT-PCR

Probes and primers for TaqMan reactions were ordered by Applied Biosystems (Germany) and provided within an Assay kit for each gene tested.

Gene name	Applied Biosystems Assay ID
αENaC	Mm00803386_m1
GILZ	Mm00726417_s1
HPRT	Mm00446968_m1
PIM3	Mm00446876_m1
RAB17	Mm00436205_m1
SGK1	Mm00441380_m1
USP2	Mm00497460_g1
14-3-3β	Mm00457545_m1

6.2. Methods

6.2.1. Standard technics of molecular biology

6.2.1.1. DNA isolation

6.2.1.1.1. Miniprep of plasmid DNA from bacteria

This method was adapted from (124) and is suitable for preparation of small amount of DNA for screening of bacterial clones. 1 ml of an overnight bacterial culture was centrifuged (14000 rpm) and resuspended in 400 µl of STET buffer. After addition of 32 µl of a lysozyme solution (10 mg/ml), the preparation was heated for 2 min at 95°C, then cooled down for 30 min at 4°C and centrifugated (14000 rpm, 15 min, 4°C). The pellet was removed and 800 µl of 100% ethanol were added to the supernatant. After 10 min at RT, the preparation was centrifuged (10 min, 4°C), the supernatant removed and the pellet washed once with 80% ethanol. After centrifugation (5 min, 4°C), the pellet was air-dried and then resuspended in 100 µl of TE.

6.2.1.1.2. Midiprep of plasmid DNA from bacteria

Preparation of big quantities of plasmid DNA was performed using the QiaFilter Plasmid Midi/Maxi Kit (Qiagen, Germany) according to the manufacturer´s instructions. In the present study, only Midipreps were performed from 25 ml of overnight bacterial cultures using the tip-50 Qiafilter cartridges (Qiagen). The concentration of the DNA preparation (diluted in TE pH 8.0) was determined by UV-photometry by measuring the extinction at 260 nm and 280 nm.

6.2.1.1.3. Miniprep of PAC DNA

The size of the PAC (140-150 kb circular supercoiled DNA) and its low quantity in a bacterial culture (1-2 copies/bacteria) require a different preparation method than the one used for plasmid DNA. The bacterial colonies identified as PAC-positive were inoculated in 2-ml LB medium containing Kanamycin (0.025 mg/ml). After centrifugation (4000 rpm, 10 min, 4°C), the cultures were resuspended and lyzed by alkaline lysis (125) using P1-, P2-, and P3-buffers from Qiagen. The neutralized lysate was then centrifuged (14000 rpm, 10 min, 4°C). The DNA contained in the supernatant was precipitated by addition of 600 µl of isopropanol and centrifugated (14000 rpm, 10 min, 4°C). The pellet was washed with 70% ethanol, centrifuged for 5 min at 4°C, dried and resuspended in 40 µl of TE pH 8.0. The concentration and quality of the DNA was checked by gel electrophoresis.

6.2.1.1.4. Midiprep of PAC DNA

Midiprep of PAC DNA was performed using Q20-columns and reagents from Qiagen. The bacterial colonies identified as PAC-positive were inoculated in 50-ml LB medium containing kanamycin (0.025 mg/ml). After centrifugation, the cultures were resuspended and lyzed by alkaline lysis. The neutralized lysate was then centrifuged (4000 rpm, 20 min, 4°C). After

filtering on cheesecloth filter, the DNA contained in the supernatant was precipitated by addition of 10 ml of isopropanol and centrifugation (4000 rpm, 20 min, 4°C). The pellet was resuspended in 1 ml of QBT buffer. After equilibration of the Q20-column with 1 ml of QBT buffer, the resuspended pellet was applied on the column for 5 min. After 3 washing steps with 2 ml of QC buffer and centrifugation at 4°C, the DNA was eluted 2 times with 800 µl of hot (70°C) QF buffer, precipitated with 560 µl isopropanol and centrifuged for 15 min at 4°C. The pellet was then washed with cold 70% ethanol, centrifuged (14000 rpm, 10 min, 4°C), dried and resuspended in 25 µl TE pH 8.0. The concentration and quality of the DNA were checked by gel electrophoresis. For Midiprep of PAC DNA for microinjection, the resuspension was done in 10 µl of TE only and exonuclease activity was inactivated by incubation at RT for 10 min and then at 65°C for 15 min.

6.2.1.1.5. DNA preparation from mouse tail

For DNA preparation for PCR, a 2-mm long piece of mouse tail was incubated at 56°C overnight in 0.2 ml of NID buffer with 2 µl of proteinase K (10 mg/ml). After heat inactivation of the proteinase K for 10 min at 96°C, 2 µl of the DNA preparation were used for genotyping PCR.
For DNA preparation for dot blot, the piece of tail was incubated at 56°C overnight in 0.72 ml of tail buffer with 40 µl of proteinase K (10 mg/ml).

6.2.1.1.6. Preparative gel electrophoresis of linear DNA fragment

DNA fragments from preparative restriction digestion or PCR reactions were separated from other DNA fragments or oligodeoxynucleotides by agarose gel electrophoresis as described previously. After staining with ethidium bromide, DNA fragments were visualized under long-wavelength UV light (the short-wavelength UV light damages the DNA). The piece of gel containing the DNA fragment with the desired size was cut out from the gel and placed in 2 ml of reaction buffer. The DNA was prepared from the gel piece according to the QIAquick Gel Extraction Kit protocol (Qiagen, Germany) and resuspended in 40 µl of water. The concentration and quality of the DNA preparation were checked by agarose gel electrophoresis.

6.2.1.1.7. Preparative PFGE of linear PAC DNA fragments

Pulsed field gel electrophoresis (PFGE) is a technique used to separate especially long fragments of DNA by length. It operates by alternating electric fields to run DNA through a flat gel matrix of agarose. In the present study, 100 µg of digested PAC DNA were resolved on a 1% Sea-Plug low-melting point agarose (Sigma) gel in 0.5X TAE running buffer using the Electrophoresis Cell device connected to the CHEF-DR III system (Biorad) according to the manufacturer´s instructions. The following parameters were used: initial $t_{switch} = 0.2$ s, final $t_{switch} = 12$ s, included angle $\alpha = 106°$, $|E| = 6$ V/cm, $I \cong 140$ mA, total time $T = 14$ h. For the detection of the DNA fragments, only the gel parts containing the ladder (cut out from the rest of the gel) were stained with ethidium bromide. The gel piece containing the linear digested PAC was cut out and the agarose was digested with β-agarase at 40°C for 2 h. Non-digested agarose was removed by centrifugation and the DNA was purified using ultracentrifugation cartridges. For microinjection of the PAC DNA into mouse oocytes, the DNA was further purified by dialysis with microinjection buffer for 2-3 h using dialysis membrane. The concentration of the PAC DNA preparation was estimated on a normal 0.8% agarose gel and the integrity of the DNA sample was checked by analytical PFGE as described in part 6.2.1.2.3 of Materials and Methods.

6.2.1.2. DNA characterization

6.2.1.2.1. Restriction digestion

The conditions (buffer, temperature) for the digestion reaction were depending on the restriction enzyme used and were given by the manufacturer. The reactions were incubated 30 min minimum, overnight if preparative. Depending on the final volume of the reaction, 0.5-4 µl of enzyme with 10 U/µl were added to the reaction.

For an analytic digestion reaction of plasmid DNA prepared with the Miniprep protocol as described previously, 5 µl of DNA were used in a final volume of 10 µl in the presence of RNase A (50 µg/ml). For a Midi or Maxi DNA preparation, 500 ng of DNA were used in a final volume of 20 µl (water). For an analytic restriction digestion (Southern blot) of PAC DNA, 3-10 µl of DNA (depending on the concentration) were digested overnight. For genomic DNA, 20 µg of DNA were digested overnight.

For a preparative restriction digestion, 2-5 µg of plasmid DNA (or 20-30 µl from a Mini-preparation) were digested overnight in a final volume of 40-50 µl. Double-digestion reactions with two enzymes were performed in the same digestion buffer allowing the digestion of both enzymes according to the manufacturer´s instructions.

6.2.1.2.2. Analytical agarose gel electrophoresis

The analytic and preparative separation of DNA molecules according to their size was performed on an agarose gel electrophoresis (126). The agarose concentration of the gel (from 0.7% to 2%) depends on the size of the expected DNA fragments. The electrophoresis was run in 1X TAE buffer. DNA was then vizualized under UV-light when stained with ethidium bromide (0.5 µg/ml).

6.2.1.2.3. Analytical PFGE

The analytical PFGE was performed as described previously for the preparative PFGE, except that the gel could be stained with ethidium bromide in order to detect the DNA fragments.

6.2.1.2.4. Southern blot

After restriction digestion and resolution by gel electrophoresis, the digested DNA was transfered on a positively charged nylon membrane and characterized by hybridization with a radiolabeled DNA probe. The gel was first depurinated by incubation for 10 min in 0.25 M HCl. To denature the DNA in order to get single stranded DNA for the hybridization, the gel was incubated 3 times 15 min under shaking in 0.4 M NaOH. At the same time the nylon membrane was equilibrated in 20X SCC. The gel was placed on the membrane covered with a dried Whatman filter paper and air bubles were removed. Four filter papers previously wet in 20X SCC were placed on the gel. Both extremities of the two last filter papers were soaked into a cuve containing 20X SCC. The first dried filter paper was soaking up the buffer and at the same time the DNA from the gel to the membrane. The buffer was then soaked up by the four upper filter papers (downward-blotting). The transfer time was lasting 2 h for plasmid DNA or overnight for PAC DNA. After transfer, the membrane was rinced in 1 M NaP buffer to avoid the formation of salt cristals. The DNA was then fixed covalently to the membrane by UV-cross linking (1200 mJ/cm^2) and could then be hybridized.

6.2.1.2.5. Hybridization

The radiolabeling of the probe (50 ng of a DNA fragment complementary to the sequence to recognize) was performed using the random prime labeling method (127). Distilled water was added to the DNA preparation to obtain a final volume of 31 µl. After incubation at 95°C for 5 min, the reagents were added as follows: 2 µl BSA (10 mg/ml), 10 µl 5X OLB-C, 5 µl α-^{32}P-

dCTP (10 µCi/µl), 2 µl Klenow polymerase (2 U/µl). The reaction was incubated at 37°C for 1 h. In order to check for the correct labeling of the probe, a gel chromatography was carried out to separate the radioactive labeled DNA from the non-incorporated radioactive dNTPs. NaH_2PO_4 pH 3.5 was used as running buffer. Before proceeding to the hybridization, the probe was denaturated by incubation at 95°C for 5 min.
The pre-hybridization was performed by incubation of the Southern blot membrane for 1 h at 65°C in a hybridization oven in glass cylinders containing some Church buffer. Before adding the radioactive probe, the Church buffer was exchanged with a defined volume of buffer (0.1 ml/cm^2 membrane surface) heated at the hybridization temperature. The radioactive probe was then added (10^7 cpm/10-20 ml - monitored with a Geiger counter - for Southern blot on genomic DNA, or 5.10^6-10^7 cpm/10-20 ml for Southern blots on PAC DNA) and hybridized overnight at the hybridization temperature.
After hybridization, the solution was removed and the membrane washed 4 times (2 times 5 min, then 2 times 20 min) with 65°C-heated washing buffer II and dried on a filter paper. The membrane was then exposed to autoradiography films (Kodak or Agfa/Fuji) at -80°C for an exposure time, which was depending on the signal strength (several hours or days). For determination of the transgene copy number by Southern blot, the membrane was exposed to Phospho-Imager plates at RT from several hours to overnight. Hybridization signals from the Phospho-Imager plates were detected with a FUJIFILM BAS-1800 Phosphor-Imager and quantified using the Aida V. 2.0 software, which allows manual baseline substraction of the intensity of the wiltd-type band.

6.2.1.2.6. DNA sequencing

Sequencing of plasmid DNA and PAC DNA was performed by the SeqLab company (Sequence Laboratories Göttingen GmbH, Germany). DNA was prepared according to the SeqLab´s instructions.

6.2.1.3. Clones screening

6.2.1.3.1. Screening of a genomic PAC library

A genomic PAC library is made of high-density gridded nylon filters ready for screening by hybridization. For the mouse genomic PAC library RPCI21 (RZPD, Germany), which was used in the present study and screened for the AQP2 gene, each filter contains 36864 colonies, which represent 18432 independent clones that have been spotted in duplicate. The filters were hybridized with a radiolabeled cDNA probe for the gene of interest, as described previously. After 16-18 h hybridization, the filters were rinced 6 times 10 min with the washing buffer I and 6 times 10 min with the washing buffer II and then dried. The hybridization signal was detected on a Röntgen film after 5 days of exposition. The interpretation of the position of the positive clones on the film was performed according to the manufacturer´s instructions and using the transparent overlay supplied with the filters as an orientation guide (http://bacpac.chori.org/download.htm).
All clones spotted on the filters were available as transformed bacterial agar cultures. To verify the positive clones identified in the genomic PAC library, DNA was isolated, the ends of the genomic insert were sequenced and the respective sequences were blasted to the mouse genome (www.ensembl.org).

6.2.1.3.2. Dot blot for screening of mouse transgenic founders

Dot blot allows large-scale identification of transgenic mice. The target DNA (30 µg prepared from mouse tail) was fixed to a nylon membrane by using a vacuum dot blot manifold system (Schleicher & Schüll, Germany) according to the manufacturer´s instructions. The dot blot chamber was assembled with two Whatman filter papers and the nylon membrane, previously

wet in water and then 2X SCC, on top. The DNA preparation (27 µl) diluted in 2M NaOH (3 µl) and 6X loading buffer (3 µl) was spoted on the membrane, followed by loading of 200 µl of 10X SCC for washing. The DNA was transfered to the membrane by the vaccum system. The membrane was rinced in 0.4 M NaP for 5 min, dried, and the DNA UV-crosslinked to the membrane. After washing of the membrane in 1 M NaP, the hybridization with the radiolabeled probe and detection were performed as described in part 6.2.1.2.5.

6.2.1.4. Generation and transformation of recombinant DNA

Molecules of recombinant DNA were generated by ligation of linear DNA fragments. The linear fragments were obtained from restriction digestion of DNA isolated by preparative agarose gel electrophoresis as described previously.

6.2.1.4.1. Vector dephosphorylation

To ligate a DNA fragment into a cloning vector, the vector was linearized by restriction digestion and dephosphorylated using the Shrimps alkaline phosphatase (Roche) to avoid any religation of the vector. The linearized dephosphorylated vector was purified by agarose gel electrophoresis.

6.2.1.4.2. Ligation

To obtain an efficient ligation reaction, the molar ratio vector:insert has to be 1:3 or 1:4, but can vary depending on the size of the insert. The concentrations of the vector and insert preparations were estimated according to the volumes and DNA amounts before isolation (using the band intensity on the agarose gel) and the ligation reaction processed accordingly. The ligation reaction was set up as following: 15 µl of vector + insert (with water if needed), 2 µl of 10 mM Li[ATP], 2 µl of 10X ligation buffer, 1 µl of T4 DNA ligase. The reaction was incubated at RT for 3-4 h or at 16°C overnight. For each newly prepared, linearized and dephosphorylated vector, a control ligation without insert was performed. Indeed, the number of resistant bacterial colonies, which grow after transformation in this control condition, gives an estimation of the non-linearized or non-dephosphorylated plasmid DNA in the vector preparation. The bacterial clones, which grow after transformation in the vector-insert ligation condition, contain the recombinant plasmid and not the original vector, only if the number of colonies obtained in the vector-insert ligation reaction is higher than that obtained in the control reaction.

6.2.1.4.3. Transformation

Bacteria, which contain an extragenous plasmid DNA and can replicate, are called competent (for a specific transformation method). For the transformation of a ligation reaction, heat-shock competent bacteria from the strain *E.coli* NM554 were used according to the protocol published in (126) and were transformed with DNA. Recombinant plasmid DNA was then isolated from the bacteria as described in part 6.2.1.1.1 of Materials and Methods.

6.2.2. Polymerase chain reaction (PCR)

6.2.2.1. Analytic genotyping PCR

To determine the genotype of a mouse, 2 µl of genomic DNA prepared from a piece of tail (as described previously) was processed for genotyping PCR on a thermocycler (MWG) using Taq polymerase (Roche) in 25 µl reaction volume according to the manufacturer´s instructions.

The conditions of the PCRs performed in the present study and the size of the expected amplified DNA fragments are presented in the table below:

PCR	Primers	Conditions	PCR products
MR floxed allele	MR flox-7 MR flox-10 MR flox-8	-95°C for 2 min -35 cycles {95°C for 30 s, 63°C for 2 min, 72°C for 2 min} -72°C for 5 min	-MR wild-type allele: 285 bp -MR floxed allele: 335 bp -MR null allele: 390 bp
AQP2Cre or AQP2Cre-ER^{T2} transgene	AQP2-12 CAMK-2 AQP2-13	Same conditions as for the MR floxed allele PCR except 1 min annealing and 1 min amplification	-AQP2 wild-type locus: 150 bp -Cre transgene: 310 bp
Rosa26 reporter	ROSA-1 ROSA-2 ROSA-3	Same conditions as for the AQP2Cre or AQP2CreER^{T2} transgene PCR	-Rosa26 wild-type locus: 270 bp -Rosa26 mutant: 420 bp

6.2.2.2. Preparative PCR for cloning

A preparative PCR (to isolate the amplificate) with plasmid DNA or first strand cDNA as template was set up on 1-50 ng plasmid DNA (or 2 µl first strand-cDNA) using the *Pfu* DNA polymerase in 50 µl reaction volume according to the manufacturer´s instructions. The PCR conditions were as follows: 94°C for 2 min, 20-30 cycles {94°C for 30 s, annealing temperature for 30 sec, 72°c for 2 min/kb amplificate length}, 72°C for 5 min.

6.2.3. Modification of a PAC by homologous recombination in E.coli (ET-cloning)

Recombinant DNA molecules can be generated by homologous recombination in *E.coli* using the ET-cloning method developped in the laboratory of A. Francis Stewart at EMBL (Heidelberg, Germany) (83). This method allows the integration of a linear DNA molecule flanked by sequences called homology arms into homologous regions in an acceptor vector. In the present study, the acceptor vector to recombine was a PAC containing the AQP2 gene and the linear DNA molecule to integrate into the PAC was a linear fragment containing the Cre recombinase coding sequence flanked by sequences homologous to the AQP2 gene (AQP2Cre linear fragment). The PAC was modified in the bacterial DH10B strain delivered by the genomic PAC library and containing the PAC. The bacteria were transformed with the ET-plasmid expressing the recombinase (128), the recombination induced and the linear fragment transformed.

6.2.3.1. Preparation of the linear fragment: PCR amplification of the homology arms and cloning into the Cre-containing plasmid

The homology arms were inserted in the linear DNA by PCR amplification. As described in (129), to obtain the best recombination efficiency, the primers for the PCR amplification have to be designed so that the homology arms on the linear DNA contain more than 50 bp overlap with the homologous regions in the acceptor vector. In the present study, in order to insert by homologous recombination in bacteria the sequence coding for the Cre recombinase into the PAC harbouring the AQP2 gene (acceptor vector), a 319-bp 5´ homology arm, homologous to the 5´ region of the AQP2 gene and containing the ATG at the 3´ end, and a 372-bp 3´ homology

arm, homologous to the 3′ region of the AQP2 gene, were amplified by PCR with the AQP2-5′hom forward and AQP2-5′hom reverse, and withz the AQP2-3′hom forward and AQP2-3′hom reverse primers, respectively. The primers were designed in order to introduce restriction sites needed for cloning and release of the linear fragment. Two half-restriction sites were introduced at the 5′ end of the 5′ homology arm: one EcoRV half-site for analysis of the insert orientation after cloning into the pConst plasmid (the second half-site is already present in the pConst plasmid) and one PmeI half-site for release of the final construct (the second half-site is present in the genomic AQP2 sequence). One XbaI site was introduced at the 5′ end of the 3′ homology arm to create after digestion a sticky end compatible with the NheI-digested end of the 5′ homology arm-containing pConst (abbreviated p5Const) and not digestable by NheI after ligation. At the 3′end of the 3′ homology arm, one NheI site was introduced for the cloning into the p5Const, and one PmeI site for the final release. The PCR products were then isolated on an agarose gel and purified using the Qiagen method as previously described. Both homology arms were then cloned in the Cre-containing plasmid (pConst for the constitutive construct or pIndu for the inducible construct) The 319-bp long 5′ homology arm containing the ATG at the 3′ end was cloned in front of the Cre coding sequence in the pConst plasmid previously digested with EcoRV and dephosphorylated. The 372-bp long 3′ homology arm was digested by XbaI and NheI and cloned after the ampicillin resistance cassette in the p5Const plasmid previously digested by NheI and dephosphorylated, to obtain the p5Const3 plasmid containing both homology arms upstream of the Cre coding sequence and downstream of the ampicillin resistance cassette, respectively. The final plasmid harbouring both homology arms (p5Const3 or p5Indu3) was linearized by PmeI digestion.

6.2.3.2. PAC modification by homologous recombination in bacteria

6.2.3.2.1. Preparation of competent bacteria containing the PAC and transformation with the ET-plasmid

A 500 ml kanamycin containing-LB medium culture was inoculated from a 2 ml culture of the DH10B clones containing the PAC and shaked at 37°C. When the O.D. reached 0.5, the culture was cooled down at 0°C for 10 min and centrifuged (3000g, 0°C). The bacterial pellet was resuspended in 50 ml of 10% glycerol and centrifuged again. This step was repeated once. The bacterial pellet was then resuspended in 300 µl of 10% glycerol, aliquoted in 50-µl aliquots and frozen in liquid nitrogen. The competent PAC-containing bacteria were defrozen on ice and added to 50-100 ng of ET-plasmid (pR6KBADαβγtet^R plasmid). The DNA was transformed in the bacteria by electroporation in cooled cuvettes using a Gene-Pulser (Biorad) at 2.30 kV, 25 µF and 200 Ω. The bacteria were resuspended in 1 ml of LB medium, shaked at 37°C for 90 min and plated on LB-agar plates containing 0.05 mg/ml of tetracyclin and 0.025 mg/ml of kanamycin.

6.2.3.2.2. Preparation of competent bacteria containing the PAC and the ET-plasmid and transformation with the linear Cre-containing fragment

The DH10B clones, which contained the modified PAC and the ET-plasmid, were prepared to be competent for electroporation as described previously, this time under recombinase (*rec*E) induction with arabinose: when the O.D. reached 0.2, 0.2% arabinose was added to the culture to induce the expression of *rec*E. Bacteria were then electroporated (2.3 kV, 25 µF, 200 Ω) with 0.3 µg of the linear Cre-containing fragment (PmeI-digested p5Const3 or PmeI-digested p5Indu3 plasmids) prepared as described in part 6.2.3.1 of Materials and Methods. After resuspension in 1 ml of LB-arabinose medium and shaking at 37°C for 90 min, the bacteria were plated on LB-kanamycin-ampicillin-agar plates and should therefore contain only the modified PAC and not the ET-plasmid. This was checked by analytic DNA Mini preparation, Southern blot and DNA sequencing.

6.2.3.2.3. Removal of the ampicillin resistance cassette

The linear DNA molecule contains an ampicillin resistance cassette to select efficient recombination event. After homologous recombination in bacteria, the modified PAC does not need to carry this resistance cassette, which is flanked by FRT sequences. To remove it, a plasmid expressing the Flp recombinase (p705-Flp plasmid) was transformed in the bacteria containing the modified PAC (128). This was performed by electroporation and by growing the bacteria at 30°C in the presence of kanamycin and chloramphenicol (p705-Flp carries a chloramphenicol resistance cassette and its replication is temperature-sensitive). The Flp expression was induced by growing bacteria in liquid culture at 37°C. The bacteria were then plated on LB-kanamycin-agar plates in order to get single clones, which lost the p705-Flp plasmid after the transient Flp expression.

6.2.4. RNA analysis

6.2.4.1. RNA isolation

6.2.4.1.1. From mpkCCD$_{c14}$

Total RNA was isolated from mpkCCD$_{c14}$ cells using the RNeasy Mini kit (Qiagen) essentially according to the manufacturer´s instructions with the following modifications. Cells were lysed directly in the Transwell filters, described in part 6.2.6, for 4 min at RT in β-mercaptoethanol-added RLT lysis buffer. Lyzed cells from 2 filters were pooled and either frozen at -80°C or processed to the next step. Lysed cells were homogenized by vortexing for 1 min. For the last step of the Qiagen RNeasy Mini protocol, the elution was done in 30 µl of DEPC-water. After 1 min at RT, the Qiagen column was centrifuged (13000 rpm, 1 min) and the eluate was used for a second elution step to increase the RNA isolation yield. The RNA amount was determined by measuring the O.D. at 260 nm and the quality of the RNA preparation was assessed by using a RNA 6000 Micro Labchip (Agilent). The RNA isolation yield reached 10-15 µg RNA for 2 Transwell filters.

6.2.4.1.2. From microdissected mouse renal tubules

Mice were deeply anesthetized by ketamine/xylazine (5 mg/kg bodyweight, i.p.). The abdominal aorta was exposed and clipped proximal to the renal arteries. A polyethylene catheter was inserted into the aorta and the kidneys were perfused by 1 ml supplemented Ringer-type solution at 37°C containing collagenase type II (225 U/mg) (Worthington) and protease type XIV (1 mg/ml) (Sigma), respectively. Ringer-type solution was supplemented with glycine (375 mg/l), trypsin inhibitor (48 mg/l), and DNase I (Roche) (25 mg/l). Perfused kidneys were immediately removed and sliced (300 µm). Four slices were further incubated for 10 min with gentle shaking at 37°C in 2 ml of the enzyme solution. The resulting tubule suspension was sedimented at 4°C, washed twice in ice-cold supplemented Ringer-type solution containing albumin (0,5 g/l). After resuspension, the tubules were dissected and sorted under a MZ16 stereo-microscope at dark field illumination (Leika) at 4°C. In the present study, 50 collecting ducts (cortex and outer medulla, ca. 25 µg wet weight) were identified and used for mRNA isolation and further processing. The method was adapted from (130). Total RNA was isolated from microdissected tubules using the Qiagen RNeasy Micro kit (Qiagen) essentially by the manufacturer´s instructions with the following modifications. Microdissected tubules were lysed by adding 5 µl of carrier RNA and the appropriate volume of β-mercaptoethanol-added RLT buffer to get a total volume of 350 µl. Lysed microdissected tubules were homogenized by vortexing for 1 min and RNA isolated as described in the Qiagen RNeasy Micro protocol. For the last step, elution was done in 14 µl DEPC-water.

6.2.5. Protein analysis

6.2.5.1. Extraction, fixation and embedding of mouse organs

6.2.5.1.1. Paraffin embedding

Mice were killed by CO_2, organs extracted and fixed overnight in 4% PFA at 4°C. Organs were washed 2 times 30 min in PBS at RT and then dehydrated through an increasing ethanol gradient: 2 times 30 min and 1 time 1 h in 70% ethanol, 1 h min in 85% ethanol, 1 h in 95% ethanol, and 3 times 1 h in 100% ethanol. The dehydrated organs were incubated in small glass cuvettes 2 times 30 min in xylol and overnight in fresh xylol. The organs were heated in xylol at 60°C for 30 min, xylol was then replaced with warm paraffin, which was exchanged every hour for 4 times. Organs were in this way impregnated with paraffin and could be embedded in small plastic cuvettes. After air-drying for 1 h, embedded organs were stored at 4°C.

6.2.5.1.2. Tissue-Tek embedding for cryosections

Mice were killed by CO_2, organs extracted, put in small plastic cuvettes containing Tissue-Tek and directly placed on a dried ice/ethanol bath for freezing before storage at -20°C.

6.2.5.2. Sectioning of mouse organs

Paraffin sections, of 6-µm thickness (equivalent to the thickness of a cell nucleus) for immunohistochemistry and immunofluorescence or of 3-µm thickness for histology, were obtained using a microtome (Leica). Sections were put on Superfrost Plus glass slides (Roth) coated with Tespa (Sigma), fixed to the slide by incubation overnight at 56°C and stored at RT.
For Rosa26 mouse reporter assays, cryosections of 10-µm thickness were obtained using a Cryostat (Leica), put on Superfrost Plus glass slides (Roth) and stored at -20°C.

6.2.5.3. Hematoxylin-Eosin staining

Paraffin sections were deparaffined 2 times 5 min in xylol and rehydrated through a decreasing ethanol gradient (100%, 95%, 85%, 70%, distilled water, eachtime 2 times 5 min). Sections were stained with Hemalin (Meyer), washed with distilled water and 25% HCl / 70% ethanol and differentiated in running tap water. Sections were then counter-stained with Eosin for 1 min, washed in distilled water and dehydrated through an increasing ethanol gradient. After a wash in xylol, sections were embedded in Eukitt (O. Kindler GmbH & Co, Germany).

6.2.5.4. Immunohistochemistry on paraffin sections

Paraffin sections were deparaffined 2 times 5 min in xylol and rehydrated through a decreasing ethanol gradient (100%, 95%, 85%, 70%, distilled water, eachtime 2 times 5 min). After blocking of endogenous peroxidase activity by incubation in 3% H_2O_2 for 10 min, sections were microwave-treated (800 W for 2 min, 360 W for 8 min) in Antigen-Retrieval buffer (DCS, Hamburg, Germany). After cooling-down at RT, sections were washed in PBS and incubated for 30 min with blocking solution (5% NSS in PBS). Sections were then incubated overnight at 4°C with the primary antibody diluted in PBS (or incubated with PBS as control). After washing in PBS, sections were incubated 30 min with the appropriated biotinylated secondary antibody. The avidin-biotin complex (ABC)-peroxidase system (Vectastain, Vector Laboratories) was used to detect the staining. The 3,3'-diaminobenzidine (DAB) substrate (Sigma Chemicals) was used to give a brown precipitate. Sections were then washed in distilled water. For single staining, sections were dehydrated through an increasing ethanol gradient, washed in xylol and embedded in Eukitt. For double staining, sections were incubated overnight with the second primary antibody, then with the corresponding secondary antibody and stained as described above for the first primary antibody.

Double immunohistochemistry for MR and AQP2 was performed with the following primary antibodies: a monoclonal MR antibody raised against the peptide comprising amino acids 1-18 of the rat MR N-terminus (131) diluted 1:20 and an affinity purified goat polyclonal antibody raised against the C-terminus of the human AQP2 (Santa Cruz Biotechnology, USA) diluted 1:100. A goat anti-mouse biotinylated antibody (Dianova-Jackson Laboratories, Germany) diluted 1:150 and a swine anti-goat biotinylated antibody (Cedarline Laboratories, Canada) diluted 1:80 were used as secondary antibodies. MR staining was revealed with a horseradish peroxidase-streptavidin complex (SA-5004, Vector Laboratories, USA) diluted 1:200 using 3-Amino-9-ethylcarbozole (SK-4200, Vector Laboratories) as substrate to give a brown substrate reaction. AQP2 staining was revealed with an alkaline phosphatase-streptavidin complex (Vector Laboratories) diluted 1:200 using the alkaline phosphatase substrate kit III (SV-5300, Vector Laboratories) to give a blue substrate reaction.

6.2.5.5. Immunofluorescence on paraffin sections

Paraffin sections were processed exactely as described for immunohistochemistry, except that all incubations were done at 4°C in the dark, that the secondary antibodies were conjugated to fluorophores and that sections were mounted in Fluoromount-G (Southern Biotechnology Associates, Burmingham, USA).
Double immunofluorescence for AQP2 and Cre was performed with the following antibodies: goat anti-AQP2 diluted 1:50 and rabbit anti-Cre (132) diluted 1:200 as primary antibodies, and Alexa 488-conjugated donkey anti-goat IgG and Alexa 594-conjugated goat anti-rabbit IgG (Molecular Probes, USA) both diluted 1:100 as secondary antibodies.

6.2.5.6. Immunofluorescence on cryosections

Cryosections were air-dried, hydrated in PBS and processed for immunofluorescence as described for paraffin sections.
Immunofluorescence labelings for MR, calbindin D28k, αENaC, TSC and Cre were performed as described in (99) on serial cryosections with the following primary antibodies: mouse anti-MR diluted 1:20, mouse anti-calbindin D28k (Swant, Switzerland) diluted 1:20000, rabbit anti-αENaC (99) diluted 1:500, rabbit anti-TSC (86) diluted 1:10000, rabbit anti-Cre and goat anti-AQP2 both diluted 1:1000. Binding sites of the primary antibody were detected using horseradish peroxidase (HRP)-conjugated sheep anti-mouse IgG (Amersham) revealed with a tyramide-signal amplification kit (PerkinElmer, Switzerland), FITC-conjugated goat anti-mouse IgG (Jackson ImmunoResearch, USA) diluted 1:40, Cy3-conjugated goat anti-rabbit IgG (Jackson ImmunoResearch) diluted 1:1000, and Cy3-conjugated donkey anti-goat IgG (Jackson ImmunoResearch) diluted 1:1000, respectively.

6.2.5.7. LacZ staining on cryosections for Rosa26 mouse reporter assays

Cryosections of organs from mice carrying the Rosa26 reporter allele were air-dried at RT for 5 min and at 37°C for 2-3 min, fixed at RT for 5 min in the fixation solution, washed 3 times 5 min in the washing solution on ice, and incubated in the staining solution at 37°C for 4-24 h (depending on staining intensity) in the dark. After staining, sections were rinced in PBS, dehydrated through an increasing ethanol gradient, washed in xylol and embedded in Eukitt (O. Kindler GmbH & Co, Germany).

6.2.6. mpkCCD$_{c14}$ cell culture

6.2.6.1. Cell culture and passage

Cells were routinely grown in 25-cm^2 culture flasks (Corning) at 37°C, 5% CO_2, 95% air atmosphere in standard culture medium. The medium was changed every 2 days. Confluent cells could be recognized by the appearing of domes observed under the microscope (92). To split the cells, culture medium was removed from the 25-cm^2 flask and cells were incubated with 3 ml of trypsine-EDTA for 20 min at 37°C. Trypsine action was stopped by adding 5 ml of fresh standard culture medium. Trypsinized cells were centrifuged in a Falcon tube (1000 rpm, 5 min), the supernatant was removed and the pellet resuspended in 7 ml of medium. For a 25-cm^2 flask, 0.5 ml of resuspended cells was diluted in 5 ml medium.

6.2.6.2. Cells freezing

Culture medium was removed from the 25-cm^2 flask and cells were incubated with 3 ml of trypsine-EDTA for 20 min at 37°C. Trypsine action was stopped by adding 5 ml of fresh standard culture medium. Trypsinized cells were centrifuged in a Falcon tube (1000 rpm, 5 min), the supernatant was removed and the pellet resuspended in 1.5 ml of FCS / 10% DMSO. Resuspended cells were transfered into cryovials and incubated at 4°C for 30-60 min, then at -80°C for 18-24 h before frozing in liquid nitrogen.

6.2.6.3. Cells defreezing

The day before defreezing, collagen-coated 25-cm^2 flasks were prepared with 400 µl of 2% collagen (in 60% ethanol) per flask, which was drying overnight under the hood. Cells were defrozen at RT under the hood and centrifuged (1000 rpm, 5 min). The supernatant was removed, the pellet resuspended in 5 ml of 10% FCS-containing standard culture medium and the resuspended cells plated in the collagen-coated 25-cm^2 flasks. The medium was replaced after 24 h and then after 48 h.

6.2.6.4. Cells treatment

Experiments were performed on confluent mpkCCD$_{c14}$ cells seeded on semi-permeable polycarbonate Transwell filters (0.4 µm pore size, 1-cm^2 growth area, Corning Costar, USA). For a 12-well Transwell filter plate used for the short-circuit current studies, 300 µl of resuspended cells were diluted in 300 µl of medium and plated on the Transwell membrane in the upper compartment of the insert. The lower compartment was filled with 1.5 ml of medium. Cells were grown in standard culture medium until confluence (day 6 after seeding), placed in hormone-free medium for 18 h, and then in hormone-free and serum-free medium for additional 18 h. Cells were then treated with vehicle or aldosterone (10^{-6} M) for 4 h in the presence or absence of amiloride (5.10^{-6} M), RU486 (10.10^{-6} M) or spironolactone (10.10^{-6} M) (added to both apical and basal sides of the filters). For the microarray experiment, cells were treated with vehicle or aldosterone (10^{-6} M) for varying times (1 h, 2 h or 4 h).

6.2.6.5. Short-circuit current studies

The sodium transport capacity of the mpkCCD$_{c14}$ cells was assessed by the short-circuit current (I_{sc}), calculated from the transepithelial votage U_T and resistance R_T using Ohm´s law. U_T and R_T were measured on cells grown on Transwell filters using dual Ag/AgCl electrodes connected to a Millicell-Electrical Resistance System (Millipore, Germany). Experiments were always performed on sets of untreated or treated cells from the same passage number to avoid interpassages variations.

6.2.7. Gene expression analysis

6.2.7.1. Microarray analysis on mpkCCD$_{c14}$ cells

6.2.7.1.1. RNA isolation

Total RNA was isolated from mpkCCD$_{c14}$ cells using the Qiagen RNeasy Mini kit as described in part 6.2.2.1.1. Ethanol precipitation was performed on 10 μg of RNA by adding 1/10 volume of 3 M NaOAc pH 5.2, 2.5 volumes of 100% ethanol, and 1.0 μl of Pellet Paint (Novagen). After precipitation at -20°C for 1 h, the reaction was centrifuged (>12000 g, 30 min, 4°C), the pellet washed twice with 80% ethanol and resuspended in 10 μl of DEPC-water.

6.2.7.1.2. Double-stranded cDNA synthesis

First and second cDNA strand synthesis was performed on 10 μg of total RNA from aldosterone- or vehicle-treated mpkCCD$_{c14}$ cells using Invitrogen reagents according to the protocol provided in the Affymetrix GeneChip Expression Analysis Manual with the following modifications. The first strand DNA synthesis reaction was pocessed for 1 h at 42°C using the SuperScript II reverse transcriptase (Invitrogen Life Technologies). The second strand cDNA synthesis was performed using 10 U of *E.coli* DNA ligase, 10 U of *E.coli* DNA polymerase I, and 2 U of *E.coli* RNase H in a reaction containing 5X second strand cDNA buffer and 10 mM dNTPs. The reaction was proceeded at 16°C for 2 h before 2 U of T4 DNA polymerase were added, the reaction allowed to proceed at 16°C for 5 min, and terminated by adding 0.5 M EDTA. Double stranded cDNA was then cleaned-up using Phase Lock Gel (PLG) tubes (Eppendorf) previously centrifuged (>12000 g, 20-30 s). An equal volume of phenol:chloroform:isoamyl alkohol (IAA) (25:24:1, saturated with 10 mM Tris-HCl pH 8.0, 1 mM EDTA) was added to the final cDNA preparation. After vortexing briefly, the entire cDNA / phenol:chloroform:IAA mixture was transfered to the PLG tube, centrifuged at full speed for 2 min, and the aqueous upper phase was transfered to a fresh 1.5 ml tube. The cleaned cDNA was then ethanol-precipitated by adding 0.5 volume of 7.5 M NH_4OAc and 2.5 volumes of 100% ethanol. After precipitation at -20°C for 1 h, the reaction was centrifuged (>12000 g, 30 min, 4°C), the pellet washed twice with 80% ethanol and resuspended in 12 μl of DEPC-water.

6.2.7.1.3. Biotin-labeled cRNA synthesis

The synthesized cDNA (5 μl) was *in vitro* transcribed (IVT) using the T7 RNA polymerase from the ENZO BioArray High Yield RNA Transcript Labeling Kit (Enzo, USA) according to the manufacturer´s instructions to obtain a biotin-labeled cRNA. Half of the IVT products was then cleaned-up using Qiagen RNeasy columns according to the manufacter´s instructions, except for the last step where the elution was done in 35 μl of DEPC-water, and the eluate re-used for a second elution step to increase the cRNA yield. Labeled cRNA quantification was performed by measure of the O.D. at 260 nm.

6.2.7.1.4. cRNA fragmentation

The random fragmentation of cRNA was performed on a minimum of 0.6 μg/μl of adjusted cRNA. The adjusted cRNA yield was calculated according to Affymetrix instructions as follows: adjusted cRNA yield = mRNA – (total RNA_i)(y), with mRNA = amount of cRNA measured after IVT (μg) (described in part 5.2.7.3.3), total RNA_i = starting amount of total RNA (5 μg), and y = fraction of cDNA used in IVT (5/12). The reaction was carried out at 95°C for 35 min with 8 μl of 5X fragmentation buffer in a final volume of 40 μl (adjusted with RNase-free water). Fragmented cRNA as well as unfragmented cRNA, cDNA and unpurified cRNA were checked for quality by gel electrophoresis (1% agarose gel) or using LabChips from Agilent.

6.2.7.1.5. Target hybridization on microarray

Hybridization, staining and scanning of the GeneChip Mouse Expression Arrays MOE 430 (Affymetrix) were performed on the Affymetrix platform at the Medical Research Center of the University Hospital Mannheim (Prof. Norbert Gretz) according to the GeneChip Expression Analysis Manual provided by Affymetrix.

6.2.7.1.6. Normalization and statistical analysis

Quality and normalization of the arrays were performed using the GC-RMA software (version 1.1.0) of the Bio-Conductor package (http://www.bioconductor.org) (133). The uniformity and the intensity of labeling were checked. Global scaling was applied to all arrays such that the mean intensity of each array was equivalent, and a quantitative assessment of signal-to-noise ratio and of the median intensity was also performed. Only those arrays having reasonable quality were used for further analysis. Statistical analysis of microarray data was performed using the GC-RMA and the SAS Microarray Solution (from SAS) softwares. Both factors "treatment" (aldosterone or vehicle) and "time of treatment" (1 h, 2 h or 4 h) were included in the analysis. For each array, gene expression values were determined for each gene. Comparison of the gene expression values between aldosterone-treated and untreated cells (used as baseline) resulted in a list of differentially expressed genes for each time-point and for each software. Mutual exclusion of the genes predicted by both GC-RMA and SAS Microarray Solution softwares was performed and only genes found as aldosterone-regulated by both softwares were further analyzed.

6.2.7.2. Quantitative real-time PCR on RNA isolated from microdissected mouse renal tubules

A reverse transcriptase reaction using the Superscript II enzyme (Invitrogen) and oligo$(dT)_{12-18}$ was carried out on 10 µl of total RNA prepared from microdissected mouse renal tubules to obtain a first strand cDNA according to the manufacturer´s instructions. Gene expression quantification was performed using the TaqMan Gene Expression Assays kit (Applied Biosystems) with the TaqMan Universal PCR Master Mix / No AmpErase UNG reagents (Applied Biosystems) according to the manufacturer´s instructions. Primers and TaqMan probes were designed and provided by Applied Biosciences. The HPRT gene, which is constitutively expressed in mouse kidney and whose expression was not influenced by the mutation in $MR^{AQP2Cre}$ mice, was used as endogenous control. For a given target gene, the gene expression relative to HPRT expression was determined as $2^{(\text{HPRT Ct} - \text{target gene Ct})}$, where Ct is the first cycle at which the reporter signal significantly exceeds the baseline signal. For each target gene, each PCR reaction was performed on RNA isolated from several mice and averaged to obtain a mean Ct value. Real time PCR reactions were performed on a CHROMO 4 Continuous Fluorescence detector (MJ Research) and data were analyzed using the Opticon Monitor 3 software (MJ Research).

6.2.8. Generation of transgenic mice

6.2.8.1. DNA preparation

Preparation of PAC DNA was performed according to (98) and as described in part 6.2.1.1.1 of Materials and Methods.

6.2.8.2. DNA microinjection in mouse oocytes

The microinjection of the DNA in oocytes was performed according to (123). Superovulated fertilized FVB/N females were used as source of oocytes. Females were bred with FVB/N males and checked for vaginal plug on the day before injection. To induce superovulation, females

were injected i.p. with PMS-gonadotropin (Sigma) 3 days before the experiment and with chorion-gonadotropin (Sigma) 1 day before the experiment. Females were killed by cervical dislocation, the oviducts were removed and transfered to 37°C-heated M2-medium. Oocytes were isolated and cumulus cells surrounding the oocytes removed by hyaluronidase treatment (100 mg/ml in M2-medium). Oocytes were then rinced with M2-medium in a glass pipette, transfered in M16-medium and stored at 37°C, 5% CO_2. To proceed to the microinjection, 30-50 oocytes were transfered in an injection seringe containing some M2-medium under the microscope with two micromanipulators setups connected to an hydrolic control system (Eppendorf femtoJet). Oocytes were held in place with a blunt holding pipette and the tip of the injection needle was filled with a solution containing the transgenic DNA (1-1.5 ng) prepared and purified as described in part 6.2.4.1. The DNA was injected into one of the pronuclei, usually the larger male one. After injection, oocytes were incubated in M16-medium for 2 h at 37°C, 5% CO_2 and checked for vitality under the microscope. The abdominal cavity of anesthezied pseudopregnant FVB/N females was opened and 20-30 transgenic oocytes were injected in the oviducts with a thin transfer canule. The lesion of the abdominal cavity was then closed with a clamp. Eighteen days after the surgery, FVB/N females give birth, and 10 to 30% of the born mice should be transgenic (hemizygous). They were checked for the presence of the transgene by genotyping PCR and dot blot on tail DNA.

6.2.8.3. Establishment of AQP2Cre and AQP2CreER^{T2} transgenic mouse lines and generation of MR^{AQP2Cre} mutant mice

AQP2Cre and AQP2CreER^{T2} transgenic founder mice were bred to C57Bl/6 mice to generate different constitutive or inducible Cre transgenic mouse lines, respectively. The constitutive renal principal cell-specific MR mutant (MR$^{flox/flox}$//AQP2Cre abbreviated as MR^{AQP2Cre}) mice and their control (MR$^{flox/flox}$) littermates were obtained by breeding MR$^{flox/flox}$ with MR$^{flox/wt}$//AQP2Cre mice. The MR^{flox} allele was generated as reported previously (82). The genetic background of the mice used in this study was a mixture of FVB/N and C57Bl/6.

6.2.9. Metabolic balance studies

6.2.9.1. Collection of urine and plasma samples and determination of food and water consumption

Two-month old mice were fed in their homecage either with a standard diet (0.18% sodium; ssniff GmbH, Soest, Germany) or with a low-sodium diet (<0.05% sodium; ssniff GmbH, Soest, Germany). Bodyweight measurement and blood and urine sampling were always performed in the morning between 9 a.m. and 11 a.m. Mice were placed in mouse metabolic cages for 24 hours to determine water and food consumption and to collect urine. For time-course analysis of renal sodium exretion under low-sodium diet, mice were placed in metabolic cages for 5 days. Urine volume, urinary sodium concentration, bodyweight and food and water consumption were determined every 24 hours. Blood samples were collected from the orbital venous plexus under anesthesia with CO_2 or decapitation. Blood was collected in sodium/EDTA-coated tubes for plasma aldosterone determination and in Li/heparin-coated tubes (Sarstedt AG & Co, Germany) for plasma electrolyte measurements.

6.2.9.2. Hormones and metabolites analysis

Plasma and urinary creatinine concentrations as well as plasma sodium and potassium concentrations were measured on a Hitachi 911 autoanalyser (Roche Diagnostics, Germany) at the Medical Research Center of the University Hospital Mannheim (Prof. Norbert Gretz). Urinary sodium was measured using the EML100 System 625 (Radiometer, Germany) at the

Medical Research Center, Mannheim. Aldosterone was measured by radioimmunoassay (Coat-a-Count; Diagnostics Products Inc., USA).

6.2.9.3. Determination of the glomerular filtration rate (GFR)

Renal creatinine clearance was measured over 24 hours and the GFR was calculated as: urine flow * [urine creatinine] / [plasma creatinine].

6.2.10. Determination of ENaC and TSC activity

6.2.10.1. Determination of ENaC activity in kidney

Mice were injected s.c. with amiloride 5 mg/kg bodyweight (29, 30) in 100 µl of isotonic saline during low-sodium diet. Urine was collected over 3 h before amiloride treatment and within 3 h after injection. Before each 3-h period, the bladder was emptied by forced voiding achieved through placing mice on a cold metalic plate. Blood samples were then collected as previously described.

6.2.10.2. Determination of ENaC activity in colon

Colonic transepithelial potential difference was measured *in vivo* in anesthetized mice (1.5% isoflurane). A perforated, double-barreled flexible polyethylene tube (O.D. 1 mm) was inserted into the rectum at a length of 12 mm and perfused with Ringer-type solution in the presence or absence of amiloride (50 µmol/l) at 37°C with a flow rate of 0.5 ml/min. The electrical potential of this tube was measured via Ag/AgCl electrodes using an UPG1 high input resistance differential amplifier (www.ad-elektronik.net). The reference electrode was inserted under the skin. The method was adapted from (136).

6.2.10.3. Determination of TSC activity

Mice were injected s.c. with thiazide 20 mg/kg bodyweight in 100 µl of isotonic saline during low-sodium diet. Urine and blood samples were collected as previously described.

6.2.11. Statistics

All measurements are presented as mean values ± SEM. The data were analyzed using unpaired two-tailed Student´s t-test, mutants versus controls if not stated otherwise.

7. REFERENCES

1. Connell, J.M., and Davies, E. 2005. The new biology of aldosterone. *J Endocrinol* 186:1-20.
2. Young, D.B. 1985. Analysis of long-term potassium regulation. *Endocr Rev* 6:24-44.
3. Hollenberg, N.K., Chenitz, W.R., Adams, D.F., and Williams, G.H. 1974. Reciprocal influence of salt intake on adrenal glomerulosa and renal vascular responses to angiotensin II in normal man. *J Clin Invest* 54:34-42.
4. Williams, G.H., and Hollenberg, N.K. 1985. "Sodium sensitive" essential hypertension: emerging insights into pathogenesis and therapeutic implications. In *Contemporary Nephrology*. S. Klahr, and S.G. Massry, editors. New York: Plenum. 303-331.
5. Evans, R.M. 1988. The steroid and thyroid hormone receptor superfamily. *Science* 240:889-895.
6. Tsai, M.J., and O'Malley, B.W. 1994. Molecular mechanisms of action of steroid/thyroid receptor superfamily members. *Annu Rev Biochem* 63:451-486.
7. Mangelsdorf, D.J., Thummel, C., Beato, M., Herrlich, P., Schutz, G., Umesono, K., Blumberg, B., Kastner, P., Mark, M., Chambon, P., et al. 1995. The nuclear receptor superfamily: the second decade. *Cell* 83:835-839.
8. Ribeiro, R.C., Kushner, P.J., and Baxter, J.D. 1995. The nuclear hormone receptor gene superfamily. *Annu Rev Med* 46:443-453.
9. Collingwood, T.N., Urnov, F.D., and Wolffe, A.P. 1999. Nuclear receptors: coactivators, corepressors and chromatin remodeling in the control of transcription. *J Mol Endocrinol* 23:255-275.
10. Zennaro, M.C., Keightley, M.C., Kotelevtsev, Y., Conway, G.S., Soubrier, F., and Fuller, P.J. 1995. Human mineralocorticoid receptor genomic structure and identification of expressed isoforms. *J Biol Chem* 270:21016-21020.
11. Trapp, T., and Holsboer, F. 1995. Ligand-induced conformational changes in the mineralocorticoid receptor analyzed by protease mapping. *Biochem Biophys Res Commun* 215:286-291.
12. Couette, B., Fagart, J., Jalaguier, S., Lombes, M., Souque, A., and Rafestin-Oblin, M.E. 1996. Ligand-induced conformational change in the human mineralocorticoid receptor occurs within its hetero-oligomeric structure. *Biochem J* 315 (Pt 2):421-427.
13. Jantzen, H.M., Strahle, U., Gloss, B., Stewart, F., Schmid, W., Boshart, M., Miksicek, R., and Schutz, G. 1987. Cooperativity of glucocorticoid response elements located far upstream of the tyrosine aminotransferase gene. *Cell* 49:29-38.
14. Lombes, M., Binart, N., Oblin, M.E., Joulin, V., and Baulieu, E.E. 1993. Characterization of the interaction of the human mineralocorticosteroid receptor with hormone response elements. *Biochem J* 292 (Pt 2):577-583.
15. Liu, W., Wang, J., Sauter, N.K., and Pearce, D. 1995. Steroid receptor heterodimerization demonstrated in vitro and in vivo. *Proc Natl Acad Sci U S A* 92:12480-12484.
16. Hollenberg, S.M., Weinberger, C., Ong, E.S., Cerelli, G., Oro, A., Lebo, R., Thompson, E.B., Rosenfeld, M.G., and Evans, R.M. 1985. Primary structure and expression of a functional human glucocorticoid receptor cDNA. *Nature* 318:635-641.
17. Arriza, J.L., Weinberger, C., Cerelli, G., Glaser, T.M., Handelin, B.L., Housman, D.E., and Evans, R.M. 1987. Cloning of human mineralocorticoid receptor complementary DNA: structural and functional kinship with the glucocorticoid receptor. *Science* 237:268-275.
18. Arriza, J.L., Simerly, R.B., Swanson, L.W., and Evans, R.M. 1988. The neuronal mineralocorticoid receptor as a mediator of glucocorticoid response. *Neuron* 1:887-900.

19. Lombes, M., Alfaidy, N., Eugene, E., Lessana, A., Farman, N., and Bonvalet, J.P. 1995. Prerequisite for cardiac aldosterone action. Mineralocorticoid receptor and 11 beta-hydroxysteroid dehydrogenase in the human heart. *Circulation* 92:175-182.
20. Zennaro, M.C., Farman, N., Bonvalet, J.P., and Lombes, M. 1997. Tissue-specific expression of alpha and beta messenger ribonucleic acid isoforms of the human mineralocorticoid receptor in normal and pathological states. *J Clin Endocrinol Metab* 82:1345-1352.
21. Funder, J.W. 1992. Glucocorticoid receptors. *J Steroid Biochem Mol Biol* 43:389-394.
22. Kyossev, Z., Walker, P.D., and Reeves, W.B. 1996. Immunolocalization of NAD-dependent 11 beta-hydroxysteroid dehydrogenase in human kidney and colon. *Kidney Int* 49:271-281.
23. Brown, R.W., Diaz, R., Robson, A.C., Kotelevtsev, Y.V., Mullins, J.J., Kaufman, M.H., and Seckl, J.R. 1996. The ontogeny of 11 beta-hydroxysteroid dehydrogenase type 2 and mineralocorticoid receptor gene expression reveal intricate control of glucocorticoid action in development. *Endocrinology* 137:794-797.
24. Bonvalet, J.P., Doignon, I., Blot-Chabaud, M., Pradelles, P., and Farman, N. 1990. Distribution of 11 beta-hydroxysteroid dehydrogenase along the rabbit nephron. *J Clin Invest* 86:832-837.
25. Todd-Turla, K.M., Schnermann, J., Fejes-Toth, G., Naray-Fejes-Toth, A., Smart, A., Killen, P.D., and Briggs, J.P. 1993. Distribution of mineralocorticoid and glucocorticoid receptor mRNA along the nephron. *Am J Physiol* 264:F781-791.
26. Rusvai, E., and Naray-Fejes-Toth, A. 1993. A new isoform of 11 beta-hydroxysteroid dehydrogenase in aldosterone target cells. *J Biol Chem* 268:10717-10720.
27. White, P.C., Mune, T., and Agarwal, A.K. 1997. 11 beta-Hydroxysteroid dehydrogenase and the syndrome of apparent mineralocorticoid excess. *Endocr Rev* 18:135-156.
28. Zennaro, M.C., and Lombes, M. 2004. Mineralocorticoid resistance. *Trends Endocrinol Metab* 15:264-270.
29. Berger, S., Bleich, M., Schmid, W., Cole, T.J., Peters, J., Watanabe, H., Kriz, W., Warth, R., Greger, R., and Schutz, G. 1998. Mineralocorticoid receptor knockout mice: pathophysiology of Na+ metabolism. *Proc Natl Acad Sci U S A* 95:9424-9429.
30. Bleich, M., Warth, R., Schmidt-Hieber, M., Schulz-Baldes, A., Hasselblatt, P., Fisch, D., Berger, S., Kunzelmann, K., Kriz, W., Schutz, G., et al. 1999. Rescue of the mineralocorticoid receptor knock-out mouse. *Pflugers Arch* 438:245-254.
31. Berger, S., Bleich, M., Schmid, W., Greger, R., and Schutz, G. 2000. Mineralocorticoid receptor knockout mice: lessons on Na+ metabolism. *Kidney Int* 57:1295-1298.
32. Guyton, A.C. 1991. Blood pressure control--special role of the kidneys and body fluids. *Science* 252:1813-1816.
33. Kriz, W. 2001. Structural organization of the mammalian kidney. In *The Kidney: Physiology and Pathophysiology*. D.W. Seldin, and G. Giebisch, editors. New York: Raven. 589.
34. Kaplan, M.R., Plotkin, M.D., Lee, W.S., Xu, Z.C., Lytton, J., and Hebert, S.C. 1996. Apical localization of the Na-K-Cl cotransporter, rBSC1, on rat thick ascending limbs. *Kidney Int* 49:40-47.
35. Kaissling, B., and Kriz, W. 1979. Structural analysis of the rabbit kidney. *Adv Anat Embryol Cell Biol* 56:1-123.
36. Madsen, K.M., and Tisher, C.C. 1986. Structural-functional relationship along the distal nephron. *Am J Physiol* 250:F1-15.
37. Bachmann, S., Bostanjoglo, M., Schmitt, R., and Ellison, D.H. 1999. Sodium transport-related proteins in the mammalian distal nephron - distribution, ontogeny and functional aspects. *Anat Embryol (Berl)* 200:447-468.

38. Bostanjoglo, M., Reeves, W.B., Reilly, R.F., Velazquez, H., Robertson, N., Litwack, G., Morsing, P., Dorup, J., Bachmann, S., and Ellison, D.H. 1998. 11Beta-hydroxysteroid dehydrogenase, mineralocorticoid receptor, and thiazide-sensitive Na-Cl cotransporter expression by distal tubules. *J Am Soc Nephrol* 9:1347-1358.
39. Schmitt, R., Ellison, D.H., Farman, N., Rossier, B.C., Reilly, R.F., Reeves, W.B., Oberbaumer, I., Tapp, R., and Bachmann, S. 1999. Developmental expression of sodium entry pathways in rat nephron. *Am J Physiol* 276:F367-381.
40. Loffing, J., and Kaissling, B. 2003. Sodium and calcium transport pathways along the mammalian distal nephron: from rabbit to human. *Am J Physiol Renal Physiol* 284:F628-643.
41. Obermuller, N., Bernstein, P., Velazquez, H., Reilly, R., Moser, D., Ellison, D.H., and Bachmann, S. 1995. Expression of the thiazide-sensitive Na-Cl cotransporter in rat and human kidney. *Am J Physiol* 269:F900-910.
42. Bonvalet, J.P. 1998. Regulation of sodium transport by steroid hormones. *Kidney Int Suppl* 65:S49-56.
43. Garty, H., and Palmer, L.G. 1997. Epithelial sodium channels: function, structure, and regulation. *Physiol Rev* 77:359-396.
44. Kleyman, T.R., and Cragoe, E.J., Jr. 1990. Cation transport probes: the amiloride series. *Methods Enzymol* 191:739-755.
45. Firsov, D., Gautschi, I., Merillat, A.M., Rossier, B.C., and Schild, L. 1998. The heterotetrameric architecture of the epithelial sodium channel (ENaC). *Embo J* 17:344-352.
46. Cheng, C., Prince, L.S., Snyder, P.M., and Welsh, M.J. 1998. Assembly of the epithelial Na+ channel evaluated using sucrose gradient sedimentation analysis. *J Biol Chem* 273:22693-22700.
47. Li, X.J., Xu, R.H., Guggino, W.B., and Snyder, S.H. 1995. Alternatively spliced forms of the alpha subunit of the epithelial sodium channel: distinct sites for amiloride binding and channel pore. *Mol Pharmacol* 47:1133-1140.
48. Bonny, O., Chraibi, A., Loffing, J., Jaeger, N.F., Grunder, S., Horisberger, J.D., and Rossier, B.C. 1999. Functional expression of a pseudohypoaldosteronism type I mutated epithelial Na+ channel lacking the pore-forming region of its alpha subunit. *J Clin Invest* 104:967-974.
49. Canessa, C.M., Schild, L., Buell, G., Thorens, B., Gautschi, I., Horisberger, J.D., and Rossier, B.C. 1994. Amiloride-sensitive epithelial Na+ channel is made of three homologous subunits. *Nature* 367:463-467.
50. Shimkets, R.A., Warnock, D.G., Bositis, C.M., Nelson-Williams, C., Hansson, J.H., Schambelan, M., Gill, J.R., Jr., Ulick, S., Milora, R.V., Findling, J.W., et al. 1994. Liddle's syndrome: heritable human hypertension caused by mutations in the beta subunit of the epithelial sodium channel. *Cell* 79:407-414.
51. Hansson, J.H., Nelson-Williams, C., Suzuki, H., Schild, L., Shimkets, R., Lu, Y., Canessa, C., Iwasaki, T., Rossier, B., and Lifton, R.P. 1995. Hypertension caused by a truncated epithelial sodium channel gamma subunit: genetic heterogeneity of Liddle syndrome. *Nat Genet* 11:76-82.
52. Chang, S.S., Grunder, S., Hanukoglu, A., Rosler, A., Mathew, P.M., Hanukoglu, I., Schild, L., Lu, Y., Shimkets, R.A., Nelson-Williams, C., et al. 1996. Mutations in subunits of the epithelial sodium channel cause salt wasting with hyperkalaemic acidosis, pseudohypoaldosteronism type 1. *Nat Genet* 12:248-253.
53. Strautnieks, S.S., Thompson, R.J., Gardiner, R.M., and Chung, E. 1996. A novel splice-site mutation in the gamma subunit of the epithelial sodium channel gene in three pseudohypoaldosteronism type 1 families. *Nat Genet* 13:248-250.

54. Hummler, E., and Vallon, V. 2005. Lessons from mouse mutants of epithelial sodium channel and its regulatory proteins. *J Am Soc Nephrol* 16:3160-3166.
55. Aperia, A.C. 1995. Regulation of sodium transport. *Curr Opin Nephrol Hypertens* 4:416-420.
56. Stanton, B.A., and Kaissling, B. 1989. Regulation of renal ion transport and cell growth by sodium. *Am J Physiol* 257:F1-10.
57. Bhargava, A., and Pearce, D. 2004. Mechanisms of mineralocorticoid action: determinants of receptor specificity and actions of regulated gene products. *Trends Endocrinol Metab* 15:147-153.
58. Verrey, F., Schaerer, E., Zoerkler, P., Paccolat, M.P., Geering, K., Kraehenbuhl, J.P., and Rossier, B.C. 1987. Regulation by aldosterone of Na+,K+-ATPase mRNAs, protein synthesis, and sodium transport in cultured kidney cells. *J Cell Biol* 104:1231-1237.
59. Asher, C., Wald, H., Rossier, B.C., and Garty, H. 1996. Aldosterone-induced increase in the abundance of Na+ channel subunits. *Am J Physiol* 271:C605-611.
60. Gumz, M.L., Popp, M.P., Wingo, C.S., and Cain, B.D. 2003. Early transcriptional effects of aldosterone in a mouse inner medullary collecting duct cell line. *Am J Physiol Renal Physiol* 285:F664-673.
61. Robert-Nicoud, M., Flahaut, M., Elalouf, J.M., Nicod, M., Salinas, M., Bens, M., Doucet, A., Wincker, P., Artiguenave, F., Horisberger, J.D., et al. 2001. Transcriptome of a mouse kidney cortical collecting duct cell line: effects of aldosterone and vasopressin. *Proc Natl Acad Sci U S A* 98:2712-2716.
62. Kellner, M., Peiter, A., Hafner, M., Feuring, M., Christ, M., Wehling, M., Falkenstein, E., and Losel, R. 2003. Early aldosterone up-regulated genes: new pathways for renal disease? *Kidney Int* 64:1199-1207.
63. Chen, S.Y., Bhargava, A., Mastroberardino, L., Meijer, O.C., Wang, J., Buse, P., Firestone, G.L., Verrey, F., and Pearce, D. 1999. Epithelial sodium channel regulated by aldosterone-induced protein sgk. *Proc Natl Acad Sci U S A* 96:2514-2519.
64. Attali, B., Latter, H., Rachamim, N., and Garty, H. 1995. A corticosteroid-induced gene expressing an "IsK-like" K+ channel activity in Xenopus oocytes. *Proc Natl Acad Sci U S A* 92:6092-6096.
65. King-Jones, K., and Thummel, C.S. 2005. Nuclear receptors--a perspective from Drosophila. *Nat Rev Genet* 6:311-323.
66. Verrey, F. 1999. Early aldosterone action: toward filling the gap between transcription and transport. *Am J Physiol* 277:F319-327.
67. Grossmann, C., Freudinger, R., Mildenberger, S., Krug, A.W., and Gekle, M. 2004. Evidence for epidermal growth factor receptor as negative-feedback control in aldosterone-induced Na+ reabsorption. *Am J Physiol Renal Physiol* 286:F1226-1231.
68. Snyder, P.M., Olson, D.R., and Thomas, B.C. 2002. Serum and glucocorticoid-regulated kinase modulates Nedd4-2-mediated inhibition of the epithelial Na+ channel. *J Biol Chem* 277:5-8.
69. Debonneville, C., Flores, S.Y., Kamynina, E., Plant, P.J., Tauxe, C., Thomas, M.A., Munster, C., Chraibi, A., Pratt, J.H., Horisberger, J.D., et al. 2001. Phosphorylation of Nedd4-2 by Sgk1 regulates epithelial Na(+) channel cell surface expression. *Embo J* 20:7052-7059.
70. Wulff, P., Vallon, V., Huang, D.Y., Volkl, H., Yu, F., Richter, K., Jansen, M., Schlunz, M., Klingel, K., Loffing, J., et al. 2002. Impaired renal Na(+) retention in the sgk1-knockout mouse. *J Clin Invest* 110:1263-1268.
71. Loffing, J., Zecevic, M., Feraille, E., Kaissling, B., Asher, C., Rossier, B.C., Firestone, G.L., Pearce, D., and Verrey, F. 2001. Aldosterone induces rapid apical translocation of ENaC in early portion of renal collecting system: possible role of SGK. *Am J Physiol Renal Physiol* 280:F675-682.

72. Wang, W., Hebert, S.C., and Giebisch, G. 1997. Renal K+ channels: structure and function. *Annu Rev Physiol* 59:413-436.
73. Veizis, I.E., and Cotton, C.U. 2006. Role of kidney chloride channels in health and disease. *Pediatr Nephrol*.
74. Nielsen, S., Frokiaer, J., Marples, D., Kwon, T.H., Agre, P., and Knepper, M.A. 2002. Aquaporins in the kidney: from molecules to medicine. *Physiol Rev* 82:205-244.
75. Thomas, K.R., and Capecchi, M.R. 1987. Site-directed mutagenesis by gene targeting in mouse embryo-derived stem cells. *Cell* 51:503-512.
76. Haseroth, K., Gerdes, D., Berger, S., Feuring, M., Gunther, A., Herbst, C., Christ, M., and Wehling, M. 1999. Rapid nongenomic effects of aldosterone in mineralocorticoid-receptor-knockout mice. *Biochem Biophys Res Commun* 266:257-261.
77. Sternberg, N. 1981. Bacteriophage P1 site-specific recombination. III. Strand exchange during recombination at lox sites. *J Mol Biol* 150:603-608.
78. Sternberg, N., Hamilton, D., and Hoess, R. 1981. Bacteriophage P1 site-specific recombination. II. Recombination between loxP and the bacterial chromosome. *J Mol Biol* 150:487-507.
79. Feil, R., Brocard, J., Mascrez, B., LeMeur, M., Metzger, D., and Chambon, P. 1996. Ligand-activated site-specific recombination in mice. *Proc Natl Acad Sci U S A* 93:10887-10890.
80. Schwenk, F., Kuhn, R., Angrand, P.O., Rajewsky, K., and Stewart, A.F. 1998. Temporally and spatially regulated somatic mutagenesis in mice. *Nucleic Acids Res* 26:1427-1432.
81. Metzger, D., and Chambon, P. 2001. Site- and time-specific gene targeting in the mouse. *Methods* 24:71-80.
82. Berger, S., Wolfer, D.P., Selbach, O., Alter, H., Erdmann, G., Reichardt, H.M., Chepkova, A.N., Welzl, H., Haas, H.L., Lipp, H.P., et al. 2006. Loss of the limbic mineralocorticoid receptor impairs behavioral plasticity. *Proc Natl Acad Sci U S A* 103:195-200.
83. Zhang, Y., Buchholz, F., Muyrers, J.P., and Stewart, A.F. 1998. A new logic for DNA engineering using recombination in Escherichia coli. *Nat Genet* 20:123-128.
84. Shimshek, D.R., Kim, J., Hubner, M.R., Spergel, D.J., Buchholz, F., Casanova, E., Stewart, A.F., Seeburg, P.H., and Sprengel, R. 2002. Codon-improved Cre recombinase (iCre) expression in the mouse. *Genesis* 32:19-26.
85. Loffing, J., Pietri, L., Aregger, F., Bloch-Faure, M., Ziegler, U., Meneton, P., Rossier, B.C., and Kaissling, B. 2000. Differential subcellular localization of ENaC subunits in mouse kidney in response to high- and low-Na diets. *Am J Physiol Renal Physiol* 279:F252-258.
86. Loffing, J., Vallon, V., Loffing-Cueni, D., Aregger, F., Richter, K., Pietri, L., Bloch-Faure, M., Hoenderop, J.G., Shull, G.E., Meneton, P., et al. 2004. Altered renal distal tubule structure and renal Na(+) and Ca(2+) handling in a mouse model for Gitelman's syndrome. *J Am Soc Nephrol* 15:2276-2288.
87. Kim, G.H., Masilamani, S., Turner, R., Mitchell, C., Wade, J.B., and Knepper, M.A. 1998. The thiazide-sensitive Na-Cl cotransporter is an aldosterone-induced protein. *Proc Natl Acad Sci U S A* 95:14552-14557.
88. Horster, M. 2000. Embryonic epithelial membrane transporters. *Am J Physiol Renal Physiol* 279:F982-996.
89. Indra, A.K., Warot, X., Brocard, J., Bornert, J.M., Xiao, J.H., Chambon, P., and Metzger, D. 1999. Temporally-controlled site-specific mutagenesis in the basal layer of the epidermis: comparison of the recombinase activity of the tamoxifen-inducible Cre-ER(T) and Cre-ER(T2) recombinases. *Nucleic Acids Res* 27:4324-4327.

90. Metzger, E., Muller, J.M., Ferrari, S., Buettner, R., and Schule, R. 2003. A novel inducible transactivation domain in the androgen receptor: implications for PRK in prostate cancer. *Embo J* 22:270-280.
91. Soriano, P. 1999. Generalized lacZ expression with the ROSA26 Cre reporter strain. *Nat Genet* 21:70-71.
92. Bens, M., Vallet, V., Cluzeaud, F., Pascual-Letallec, L., Kahn, A., Rafestin-Oblin, M.E., Rossier, B.C., and Vandewalle, A. 1999. Corticosteroid-dependent sodium transport in a novel immortalized mouse collecting duct principal cell line. *J Am Soc Nephrol* 10:923-934.
93. Jung, D., Fantin, A.C., Scheurer, U., Fried, M., and Kullak-Ublick, G.A. 2004. Human ileal bile acid transporter gene ASBT (SLC10A2) is transactivated by the glucocorticoid receptor. *Gut* 53:78-84.
94. Heinemeyer, T., Wingender, E., Reuter, I., Hermjakob, H., Kel, A.E., Kel, O.V., Ignatieva, E.V., Ananko, E.A., Podkolodnaya, O.A., Kolpakov, F.A., et al. 1998. Databases on transcriptional regulation: TRANSFAC, TRRD and COMPEL. *Nucleic Acids Res* 26:362-367.
95. Liang, X., Peters, K.W., Butterworth, M.B., and Frizzell, R.A. 2006. 14-3-3 isoforms are induced by aldosterone and participate in its regulation of epithelial sodium channels. *J Biol Chem* 281:16323-16332.
96. Nelson, R.D., Stricklett, P., Gustafson, C., Stevens, A., Ausiello, D., Brown, D., and Kohan, D.E. 1998. Expression of an AQP2 Cre recombinase transgene in kidney and male reproductive system of transgenic mice. *Am J Physiol* 275:C216-226.
97. Zharkikh, L., Zhu, X., Stricklett, P.K., Kohan, D.E., Chipman, G., Breton, S., Brown, D., and Nelson, R.D. 2002. Renal principal cell-specific expression of green fluorescent protein in transgenic mice. *Am J Physiol Renal Physiol* 283:F1351-1364.
98. Schedl, A., Montoliu, L., Kelsey, G., and Schutz, G. 1993. A yeast artificial chromosome covering the tyrosinase gene confers copy number-dependent expression in transgenic mice. *Nature* 362:258-261.
99. Rubera, I., Loffing, J., Palmer, L.G., Frindt, G., Fowler-Jaeger, N., Sauter, D., Carroll, T., McMahon, A., Hummler, E., and Rossier, B.C. 2003. Collecting duct-specific gene inactivation of alphaENaC in the mouse kidney does not impair sodium and potassium balance. *J Clin Invest* 112:554-565.
100. Frindt, G., and Palmer, L.G. 2004. Na channels in the rat connecting tubule. *Am J Physiol Renal Physiol* 286:F669-674.
101. Almeida, A.J., and Burg, M.B. 1982. Sodium transport in the rabbit connecting tubule. *Am J Physiol* 243:F330-334.
102. Pacha, J., Miksik, I., Mrnka, L., Zemanova, Z., Bryndova, J., Mazancova, K., and Kucka, M. 2004. Corticosteroid regulation of colonic ion transport during postnatal development: methods for corticosteroid analysis. *Physiol Res* 53 Suppl 1:S63-80.
103. Velazquez, H., Bartiss, A., Bernstein, P., and Ellison, D.H. 1996. Adrenal steroids stimulate thiazide-sensitive NaCl transport by rat renal distal tubules. *Am J Physiol* 270:F211-219.
104. Nielsen, J., Kwon, T.H., Masilamani, S., Beutler, K., Hager, H., Nielsen, S., and Knepper, M.A. 2002. Sodium transporter abundance profiling in kidney: effect of spironolactone. *Am J Physiol Renal Physiol* 283:F923-933.
105. Leone, D.P., Genoud, S., Atanasoski, S., Grausenburger, R., Berger, P., Metzger, D., Macklin, W.B., Chambon, P., and Suter, U. 2003. Tamoxifen-inducible glia-specific Cre mice for somatic mutagenesis in oligodendrocytes and Schwann cells. *Mol Cell Neurosci* 22:430-440.

106. Farman, N., Vandewalle, A., and Bonvalet, J.P. 1982. Aldosterone binding in isolated tubules II. An autoradiographic study of concentration dependency in the rabbit nephron. *Am J Physiol* 242:F69-77.
107. Claire, M., Machard, B., Lombes, M., Oblin, M.E., Bonvalet, J.P., and Farman, N. 1989. Aldosterone receptors in A6 cells: physicochemical characterization and autoradiographic study. *Am J Physiol* 257:C665-677.
108. Schulz-Baldes, A., Berger, S., Grahammer, F., Warth, R., Goldschmidt, I., Peters, J., Schutz, G., Greger, R., and Bleich, M. 2001. Induction of the epithelial Na+ channel via glucocorticoids in mineralocorticoid receptor knockout mice. *Pflugers Arch* 443:297-305.
109. Rachamim, N., Latter, H., Malinin, N., Asher, C., Wald, H., and Garty, H. 1995. Dexamethasone enhances expression of mitochondrial oxidative phosphorylation genes in rat distal colon. *Am J Physiol* 269:C1305-1310.
110. Verrey, F., Hummler, E., Schild, L., and Rossier, B. 2000. Control of Na+ transport by aldosterone. In *The Kidney: Physiology and Pathophysiology*. D.a.G. Seldin, G., editor. New York: Lippincott, Williams & Wilkins.
111. Irizarry, R.A., Hobbs, B., Collin, F., Beazer-Barclay, Y.D., Antonellis, K.J., Scherf, U., and Speed, T.P. 2003. Exploration, normalization, and summaries of high density oligonucleotide array probe level data. *Biostatistics* 4:249-264.
112. Soundararajan, R., Zhang, T.T., Wang, J., Vandewalle, A., and Pearce, D. 2005. A novel role for glucocorticoid-induced leucine zipper protein in epithelial sodium channel-mediated sodium transport. *J Biol Chem* 280:39970-39981.
113. Snyder, P.M. 2005. Minireview: regulation of epithelial Na+ channel trafficking. *Endocrinology* 146:5079-5085.
114. Thomas, C.P., and Itani, O.A. 2004. New insights into epithelial sodium channel function in the kidney: site of action, regulation by ubiquitin ligases, serum- and glucocorticoid-inducible kinase and proteolysis. *Curr Opin Nephrol Hypertens* 13:541-548.
115. Gormley, K., Dong, Y., and Sagnella, G.A. 2003. Regulation of the epithelial sodium channel by accessory proteins. *Biochem J* 371:1-14.
116. Bhalla, V., Daidie, D., Li, H., Pao, A.C., LaGrange, L.P., Wang, J., Vandewalle, A., Stockand, J.D., Staub, O., and Pearce, D. 2005. Serum- and glucocorticoid-regulated kinase 1 regulates ubiquitin ligase neural precursor cell-expressed, developmentally down-regulated protein 4-2 by inducing interaction with 14-3-3. *Mol Endocrinol* 19:3073-3084.
117. Ichimura, T., Yamamura, H., Sasamoto, K., Tominaga, Y., Taoka, M., Kakiuchi, K., Shinkawa, T., Takahashi, N., Shimada, S., and Isobe, T. 2005. 14-3-3 proteins modulate the expression of epithelial Na+ channels by phosphorylation-dependent interaction with Nedd4-2 ubiquitin ligase. *J Biol Chem* 280:13187-13194.
118. Renatus, M., Parrado, S.G., D'Arcy, A., Eidhoff, U., Gerhartz, B., Hassiepen, U., Pierrat, B., Riedl, R., Vinzenz, D., Worpenberg, S., et al. 2006. Structural basis of ubiquitin recognition by the deubiquitinating protease USP2. *Structure* 14:1293-1302.
119. Lutcke, A., Jansson, S., Parton, R.G., Chavrier, P., Valencia, A., Huber, L.A., Lehtonen, E., and Zerial, M. 1993. Rab17, a novel small GTPase, is specific for epithelial cells and is induced during cell polarization. *J Cell Biol* 121:553-564.
120. Lehtonen, S., Lehtonen, E., and Olkkonen, V.M. 1999. Vesicular transport and kidney development. *Int J Dev Biol* 43:425-433.
121. Shimkets, R.A., Lifton, R.P., and Canessa, C.M. 1997. The activity of the epithelial sodium channel is regulated by clathrin-mediated endocytosis. *J Biol Chem* 272:25537-25541.
122. Koeppen, B.M., and Stanton, B.A. 2000. In *Principles of Physiology*. MO, editor. St Louis: Mosby.

123. Hogan, B., Beddington, R., Constantini, F., and Lacy, E. 1986. *Manipulating the Mouse Embryo: a laboratory manual*. Plainview, NY: Cold Spring Harbor Laboratory Press.
124. Holmes, D.S., and Quigley, M. 1981. A rapid boiling method for the preparation of bacterial plasmids. *Anal Biochem* 114:193-197.
125. Birnboim, H.C., and Doly, J. 1979. A rapid alkaline extraction procedure for screening recombinant plasmid DNA. *Nucleic Acids Res* 7:1513-1523.
126. Sambrook, P., Fritsch, E.F., and Maniatis, T. 1989. *Molecular Cloning. A Laboratory Manual*. Cold Spring Harbor: Cold Spring Harbor Laboratory Press.
127. Feinberg, A.P., and Vogelstein, B. 1984. "A technique for radiolabeling DNA restriction endonuclease fragments to high specific activity". Addendum. *Anal Biochem* 137:266-267.
128. Muyrers, J.P., Zhang, Y., Testa, G., and Stewart, A.F. 1999. Rapid modification of bacterial artificial chromosomes by ET-recombination. *Nucleic Acids Res* 27:1555-1557.
129. Raymond, C.K., Pownder, T.A., and Sexson, S.L. 1999. General method for plasmid construction using homologous recombination. *Biotechniques* 26:134-138, 140-131.
130. Schafer, J.A., Watkins, M.L., Li, L., Herter, P., Haxelmans, S., and Schlatter, E. 1997. A simplified method for isolation of large numbers of defined nephron segments. *Am J Physiol* 273:F650-657.
131. Gomez-Sanchez, C.E., de Rodriguez, A.F., Romero, D.G., Estess, J., Warden, M.P., Gomez-Sanchez, M.T., and Gomez-Sanchez, E.P. 2006. Development of a panel of monoclonal antibodies against the mineralocorticoid receptor. *Endocrinology* 147:1343-1348.
132. Kellendonk, C., Tronche, F., Reichardt, H.M., and Schutz, G. 1999. Mutagenesis of the glucocorticoid receptor in mice. *J Steroid Biochem Mol Biol* 69:253-259.
133. Wu, Z., and Irizarry, R.A. 2004. Stochastic models inspired by hybridization theory for short oligonucleotide arrays. *Proc RECOMB*.
134. Irizarry, R.A., Bolstad, B.M., Collin, F., Cope, L.M., Hobbs, B., and Speed, T.P. 2003. Summaries of Affymetrix GeneChip probe level data. *Nucleic Acids Res* 31:e15.
135. Bolstad, B.M., Irizarry, R.A., Astrand, M., and Speed, T.P. 2003. A comparison of normalization methods for high density oligonucleotide array data based on variance and bias. *Bioinformatics* 19:185-193.
136. Skrabal, F., Aubock, J., Edwards, C.R., and Braunsteiner, H. 1978. Subtraction potential difference: In-vivo assay for mineralocorticoid activity. *Lancet* 1:298-302.

8. PUBLICATIONS

Ronzaud, C., Loffing, J., Bleich, M., Gretz, N., Gröne, H.J., Schütz, G., Berger, S. Impairment of sodium balance in mice deficient for renal principal cell mineralocorticoid receptor. Submitted to JASN and currently under revision.

9. ABBREVIATIONS

A	Ampere
ABC	avidin-biotin complex
ACE	angiotensin-converting enzyme
AIP	aldosterone-induced proteins
AIT	aldosterone-induced transcripts
AME	apparent mineralocorticoid excess
AQP2	aquaporin 2 water channel
AR	androgen receptor
ART	aldosterone-repressed transcripts
ASDN	aldosterone-sensitive distal nephron
ATP	adenosine triphosphate
bp	base pair
BSA	bovine serum albumine
BW	bodyweight
°C	Celcius degree
CD	collecting duct
CD28K	calbindin D28k
cDNA	complementary DNA
Ci	Curie
CNT	connecting tubule
Cpm	count(s) per minute
Cre-loxP	Cre recombinase-loxP site recombination system
DAB	3,3´diaminobenzidine
dATP	deoxyadenosine triphosphate
DBD	DNA-binding domain
DCT	distal convoluted tubule
dCTP	deoxycytidine triphosphate
DEPC	diethylpyrocarbonate
dGTP	deoxyguanosine triphosphate
DMEM	Dulbecco´s modified eagle medium
DMSO	dimethylsulfoxide
DNA	desoxyribonucleic acid
DNase	desoxyribonuclease
dNTP	desoxyribonucleotide triphosphate
DSIP1	delta sleep inducing peptide 1 (glucocorticoid-induced leucine zipper protein)
DTT	dithiothreitol
DUSP6	dual specificity phosphatase 6
EDTA	ethylenediaminetetraacetic acid
EGF	epidermal growth factor
ENaC	epithelial sodium channel
ER	estrogen receptor
ER^{T2}	estrogen receptor two point-mutated ligand-binding domain
ES	embryonic stem (cell)

FC	fold change
FCS	fetal calf serum
FITC	fluorescein isothiocyanate
Flp	FRT site-specific flippase recombinase
FRT	Flp recombination target
g	gram
g	acceleration of gravity
GC-RMA	GC content-based robust multi-array average
GILZ	glucocorticoid-induced leucin zipper protein
GR	glucocorticoid receptor
GRE	glucocorticoid response element
GTP	guanosine triphosphate
h	hour
Hoxb7	homeobox B7
HPRT	hypoxanthine guanine phosphoribosyl transferase
HRP	horseradish peroxidase
11β-HSD2	11β-hydroxysteroid dehydrogenase type 2
IAA	isoamyl alcohol
IgG	immunoglobulin G
i.p.	intra-peritoneal
I_{sc}	short-circuit current
IVT	*in vitro* transcription
JGC	juxtaglomerular cell
kb	kilobase
Kd	dissociation constant
kg	kilogram
kV	kilovolt
l	liter
LacZ	β-galactosidase gene
LB	Luria Bertani (medium)
LBD	ligand-binding domain
M	molar
mg	milligram
min	minute
mJ	millijoule
ml	milliliter
mmol	millimol
MOE	mouse expression (Affymetrix microarray)
$mpkCCD_{c14}$	mouse pyruvate kinase promoter cortical collecting duct cell line (clone 14)
MR	mineralocorticoid receptor
mRNA	messanger ribonucleic acid
μF	microfarad
μl	microliter

n	number
Na^+-K^+-ATPase	sodium-potassium-adenosine triphosphatase
Nedd4-2	neural precursor cell-expressed developmentally downregulated gene 4-2
ng	nanogram
NID	non ionic detergent (buffer)
NLS	nuclear localization signal
nm	nanometer
nM	nanomolar
NR	nuclear receptor
NSS	normal sheep serum
OD	optical density
Ω	Ohm
P	p-value (Student´s test)
PAC	P1-derived artificial chromosome
PBS	phosphate-buffered saline
PCR	polymerase chain reaction
PFA	paraformaldehyde
PFGE	pulsed field gel electrophoresis
PHA1	pseudohypoaldosteronism type 1
PIM3	proviral integration site 3 (serine/threonine-protein kinase 3)
PMS	pregnant mare serum
PR	progesterone receptor
RAAS	renin-angiotensin-aldosterone system
RNA	ribonucleic acid
RNase	ribonuclease
rpm	rotation(s) per minute
R_T	transepithelial electrical resistance
RT	room temperature
RT-PCR	real time polymerase chain reaction
s	second
SGK1	serum- and glucocorticoid-induced kinase 1
s.c.	sub-cutaneously
TAE	tris-acetate buffer
TAL	thick ascending limb
TE	tris-ethylenediaminetetraacetic acid
Tespa	3-aminopropyltriethoxysilane
TSC	thiazide-sensitive sodium chloride cotransporter
U	enzymatic unit
USP2	ubiquitin-specific protease 2
U_T	transepithelial voltage
UV	ultraviolet
V	volt

W	watt
Wt	wild-type
X-gal	5-bromo-4-chloro-3-indolyl-β-D-galactopyranoside (β-galactosidase substrate)

10. ACKNOWLEDGEMENTS

Bei allen, die zum Gelingen der vorliegenden Arbeit beigetragen haben, möchte ich mich an dieser Stelle herzlich bedanken.
Dieser Dank gilt an erster Stelle Herrn Professor Dr. Günther Schütz für die Überlassung des interessanten Projekts, für die Betreuung, die Unterstützung und die Möglichkeit, in seinem Labor im DKFZ zu arbeiten.
Frau Prof. Dr. Blanche Schwappach danke ich für ihre Bereitschaft, das Koreferat meiner Doktorarbeit zu übernehmen.
Mein besonderer Dank geht an Dr. Stefan Berger, der diese Arbeit mit wertvollen Anregungen, intensiven Diskussionen und konstruktive Kritik begleitet und unterstützt hat. Ich danke ihn auch für das Korrekturlesen der Arbeit.
Bedanken möchte ich mich auch bei den Professoren Dr. Markus Bleich, Institut für Physiologie der Universität Kiel, und Dr. Jan Loffing, Abteilung für Medizin und Anatomie der Universität Fribourg, für ihre Bereitschaft an den Projekt mitzuwirken, die gute Zusammenarbeit und die hilfreiche Diskussionen und Ratschläge.
Professoren Dr. Norbert Gretz, Universitäts-Klinik Mannheim, und Dr. Hermann-Josef Gröne, Abteilung für molekulare und zelluläre Pathologie des DKFZ, danke ich für die gute Zusammenarbeit und interessante Diskussionen, Rat und Hilfe.
Dr. Wolfgang Schmid danke ich für seine Ratschläge und das Korrekturlesen der Arbeit.
Für die gute und freundschaftliche Arbeitsatmosphäre bedanke ich mich bei allen Mitarbeitern und Mitarbeiterinnen der Abteilung für molekulare Biologie der Zelle I, besonders bei Heike Alter, die mich in die Techniken des Labors eingeführt hat, und bei Monika Bock, die mir bei allen administrativen Belangen sehr geholfen hat.

Besonders danke ich auch meinen Eltern und meiner Familie sowie allen meinen Freunden und Bekannten, die mich während meiner Zeit in Heidelberg begleitet und gefördert haben.